The Electrochemistry of Li-LiCl-Li$_2$O Molten Salt Systems and the Role of Moisture

A Thesis

Presented in Partial Fulfillment of the Requirements for the

Degree of Master of Science

with a

Major in Nuclear Engineering

in the

College of Graduate Studies

University of Idaho

by

Natalie J. Gese

Major Professor: Batric Pesic, Ph.D.

Committee Members: Indrajit Charit, Ph.D.; Wudneh Admassu, Ph.D.

Department Administrator: Eric Aston, Ph.D.

April 2015

Authorization to Submit Thesis

This thesis of Natalie J. Gese, submitted for the degree of Master of Science with a Major in Nuclear Engineering and titled "The Electrochemistry of Li-LiCl-Li$_2$O Molten Salt Systems and the Role of Moisture," has been reviewed in final form. Permission, as indicated by the signatures and dates below, is now granted to submit final copies to the College of Graduate Studies for approval.

Major Professor:　　　_____　　Date: _____

　　　　　　　　　　　Batric Pesic, Ph.D.

Committee
Members:　　　　　　 _____　　Date: _____

　　　　　　　　　　　Indrajit Charit, Ph.D.

　　　　　　　　　　 _____　　Date: _____

　　　　　　　　　　　Wudneh Admassu, Ph.D.

Department
Administrator:　　　　_____　　Date: _____

　　　　　　　　　　　Eric Aston, Ph.D.

Abstract

Uranium can be recovered from uranium-oxide (UO_2) spent fuel through the combination of oxide reduction and electrorefining processes. During oxide reduction, the spent fuel is introduced to molten $LiCl$-Li_2O salt at 650°C, and the UO_2 is reduced to uranium metal via two routes: (1) electrochemically, and (2) chemically by lithium metal ($Li°$) that is produced electrochemically. However, the hygroscopic nature of both $LiCl$ and Li_2O leads to the formation of $LiOH$, contributing hydroxyl anions (OH^-), the reduction of which interferes with the $Li°$ generation required for the chemical reduction of UO_2. In order for the oxide reduction process to be an effective method for the treatment of uranium-oxide fuel, the role of moisture in the $LiCl$-Li_2O system must be understood. The behavior of moisture in the $LiCl$-Li_2O molten-salt system was studied using cyclic voltammetry, chronopotentiometry, and chronoamperometry while reduction to hydrogen was confirmed with gas chromatography.

Acknowledgements

I would like to sincerely thank Dr. Batric Pesic for his support, guidance, and encouragement, and for his setting good examples of hard work ethic and devotion to research. It was a privilege to work in his laboratories and to have so many resources available for research and experimentation. Starting as an undergraduate working in his laboratories, a door of endless opportunities opened to me. Also, Dr. Pesic introduced me to researchers in the Pyroprocessing Technologies Department at Idaho National Laboratory, providing many networking opportunities, and helped to find an internship and later employment.

I would also like to thank Ken Marsden for mentoring and providing an amazing internship experience at Idaho National Laboratory. During my internship, I was introduced to molten salts and the pyroprocessing technologies.

Thanks to Dr. Mike Simpson for his support through the INL–LDRD programs and to Dr. Fred Gunnerson for providing a graduate-student assistantship through the University of Idaho.

Special thanks to the many mentors in the Pyroprocessing Technologies group within the Separations Department in the Nuclear Science and Technology Directorate of Idaho National Laboratory. Thanks especially to Dr. Guy Fredrickson, for mentoring and encouragement.

Dedication

To my husband Aaron and family.

Table of Contents

List of Figures

List of Tables

Chapter 1: Introduction

Oxide reduction is the key process used to convert spent oxide fuel to metal suitable for treatment in an electrorefiner.[1, 2, 3] During the reduction process, oxide fuel is converted to metal both electrolytically and chemically in a vessel containing electrolyte comprised of molten LiCl-Li$_2$O at 650°C.[4, 5] Conversion efficiencies of 99.7% (for the conversion of oxide to metal) and enhanced reduction rates (due to the fast kinetics of lithium reduction from Li$_2$O) have been reported.[3,6] In the electrorefining process, remaining fission products, transuranics, and minor actinides are separated to yield a high-purity uranium-metal product (>99.99%).[3,6] One of the major causes of lower current efficiencies in the oxide-reduction process is attributed to the recombination of lithium with oxygen in the cell and the decrease in oxide ion concentration from Li$_2$O degradation.[17] The contamination of moisture is another issue. The focus of this work is mainly on the events preceding the reduction of lithium, as indicated in Table 1. The results here will provide a fundamental understanding of the impact of moisture and the need and mechanism to purify the molten salt in order to achieve higher throughput for the oxide-reduction process.

Electrochemical stability, reaction kinetics, and high ionic conductivities are among the favorable properties of LiCl-based melts.[7, 8, 9] However, lithium chloride, as well as other lithium-based salts, will form hydrates.[10] LiCl crystallizes with water to form LiCl·H$_2$O and LiCl·1/2H$_2$O, which have been reported to thermally decompose at 98–110°C and 152–162°C, respectively.[11] Moisture in LiCl and LiCl-KCl melts has been observed, even following many different moisture removal treatment methods.[12,13] The choice of LiCl molten salt used for the oxide reduction process is due to the high solubility of Li$_2$O from which Li metal can be made in-situ for chemical reaction with UO$_2$. Counter-electrode degradation is prevented in LiCl containing greater the 0.5 wt% Li$_2$O.[14] Advantages for transition to LiCl-Li$_2$O system from the LiCl-Li and LiCl-KCl based systems for oxide reduction have been discussed in detail elsewhere.[15,16,17,18,19,20,21,22]

Table 1. Standard potential of pertinent redox reactions in this study.

Overall	ΔG (kcal)	Half-cell Reactions	Standard Potential E(V) vs. SHE
$LiCi = Li + \frac{1}{2}Cl_{2(g)}$	79.76	Cathode: $Li^+ + e = Li$ Anode: $Cl^- = \frac{1}{2}Cl_2 + e$	-3.46
$Li_2O_{(LiCl)} = 2Li + \frac{1}{2}O_{2(g)}$	113.70	Cathode: $2Li^+ + 2e = Li$ Anode: $O^{2-} = \frac{1}{2}O_2 = 4e$	-2.47
$UO_2 = U + O_{2(g)}$	79.76	Cathode: $U^{4+} + 4e = U$ Anode: $2O^{2-} = O_2 + 4e$	-2.40
$H_2O = H_{2(g)} + \frac{1}{2}O_{2(g)}$	36.57	Cathode: $2OH^- + 2e = H_2 + 2O^{2-}$ Anode: $O^{2-} = \frac{1}{2}O_2 + 2e$	-1.59

1.1 Reprocessing Spent Nuclear Fuel

A technological approach, with the near future in mind, for reducing high-level waste (HLW) from spent nuclear fuel (SNF) inventories, those which come from the burning of uranium-based fuel in a nuclear reactor, would be to implement pyroprocessing for recycling spent nuclear fuel. In this approach, a large percentage of HLW currently stored could be reduced when the uranium is separated from transuranics and fission products. In particular, pyroprocessing for recovery of actinides from spent oxide fuel has the advantage of a high recovery yield of fissile materials and inherent resistance to diversion[14] due to extremely high radiation fields produced and shielding required associated with handling. The pyroprocessing method of treatment was initially developed to treat spent metallic fuel and has, more recently, been extended to oxide fuel.[23] Pending the establishment of a geological repository able to accept HLW, reprocessing with the implementation of pyroprocessing is an appealing approach to the management of SNF and for other nuclear-waste-management strategies. Separation of uranium and low-level fission products from the HLW would free up a significant amount of space required for HLW storage. Additional value could be placed on the reprocessing route, although a closed fuel cycle, wherein uranium is recovered and reintroduced into the fuel cycle, is deemed less economical than the open (or once-through) fuel cycle wherein spent fuel, in an unaugmented state, is placed for long-term disposal in a repository. These calculations, however, do not include the cost of disposing of large volumes of HLW and the long-term site operations and maintenance of a repository in the overall cost.

After these considerations, reprocessing SNF may be more appealing from an economic standpoint. Additionally, reprocessing of LWR fuel from this perspective would be considered economical in that no additional dry storage and/or interim storage facilities would be necessary once the volume reduction associated with reprocessing is achieved. For example, depending on the burnup and the reactor-core design, approximately 95.5 wt% of the spent fuel is uranium, 1 wt% plutonium, and 3.2 wt% is fission products.[24] Thus, the separation of uranium could largely eliminate the storage burden.

Motivation for reprocessing HLW is based on the many challenges associated with handling. The main challenges are:

1. Storage
2. Management/safeguarding, and
3. Disposal.

Commercial nuclear utility companies in the United States are currently storing all HLW (spent fuel) generated from the nuclear reactors. In recent years there has been elevated concern related to the accumulation of high-level waste from commercial nuclear-power reactors. The onsite storage facilities for the reactor plants are onsite storage ponds, which in many cases have exceeded their material-storage limits. As a result, facilities have resorted to storing the HLW overflow in dry-storage casks.

Loss of water and loss of water circulation in storage ponds are main concerns for safeguarding against security threats, such as terrorist attacks, and natural disasters. The primary functions of storage ponds are to provide shielding and to remove decay heat from spent fuel. The spent fuel can overheat if either function is compromised. Zirconium in the fuel cladding reacts with steam to produce hydrogen. Zirconium fires would be a possibility and, in such an event, could potentially release radioactive materials into the environment.

Currently, there is no designated area for permanent disposal of civilian HLW in the United States. Under the Nuclear Waste Policy Act (NWPA) of 1982, a fee ($0.001/kWh) is charged to the nuclear utilities and consumers to be allocated to a Nuclear Waste Fund (NWF) to finance the United States Department of Energy (DOE) management of HLW. In 1987 the

NWPA was amended to designate Yucca Mountain, Nevada, as the repository site for disposal of HLW. In 2010, the Yucca Mountain project was halted, and a Blue Ribbon Commission (BRC) was established to evaluate U.S. nuclear waste management options.

After more than 23 years of studying the Yucca Mountain geological-repository location as the disposition site for HLW, a decade behind schedule, the work was stopped, and the DOE application for construction was withdrawn by the administration.[25,26] This decision imposes huge costs to taxpayers as a result of lawsuits that nuclear utility companies have filed against the government. Costs of DOE custody of HLW is estimated at $12.3 billion through 2020 and could eventually amount to over $500 million per year thereafter.[26] Alternative geological-repository and centralized storage facilities have been proposed;[25,26] however, it is necessary that a non-politicized organization be established to move forward such plans and developments. Meanwhile, many years could pass, and billions of taxpayer dollars could be spent.

Reprocessing used fuel can significantly condense the HLW inventory that would have been destined for disposal. Although Yucca Mountain is not currently an option for waste disposal, if it had been employed for HLW disposal, it would have been oversubscribed, and there would still be a need for a second repository. Reprocessing to separate major actinides from small concentrations of fission products would free space in storage ponds and drastically reduce the amount of waste destined for disposal. Reducing the used fuel inventory in storage ponds would remove the need for additional dry-storage casks and associated safeguarding demands. In addition, the need for HLW-disposal sites to provide space that would accommodate growing HLW inventories would be mitigated, and resources that may have otherwise been immobilized would be freed as high-level waste is retained for use in the reactor fleets of future generation.

Through reprocessing, uranium, which accounts for approximately 95.5% of the mass in used fuel, can be separated for recycling. The time the fuel burns in the reactor core is constrained by fission-product buildup, which affects the control of neutrons in the fission chain reaction of the fissile uranium–235 isotope. To insure control of the neutron activity, although post-irradiated fuel assemblies contain only a small amount of high-level waste, entire

assemblies are classified as spent fuel, unsuitable for continued use in the reactor core. If the used fuel is reprocessed, the bulk of the mass could be separated, and the volume of remaining used-fuel materials classified as HLW destined for disposal would be significantly reduced.

Pyroprocessing and aqueous processing are the two main routes for treatment of used fuel. Pyroprocessing is the more attractive technology for reprocessing HLW for many reasons. Pyroprocessing employs molten salts, which are highly resistant to radiation damage. Hot fuel can be readily accepted for processing. There is no cooling period required, as is necessary with aqueous reprocessing; therefore, used fuel with high radiation fields can be removed directly from the reactor for processing. Solvent and diluents used in aqueous processing become degraded from high radiation densities, which reduce separation efficiency and form highly reactive products, some of which are salts that are very explosive.[27] No high-level waste liquids in the waste streams generated by pyroprocessing because the molten-salt electrolyte used in the process is solid (M.P. of LiCl = 605°C, and LiCl/KCl eutectic =352°C) when not at the processing temperature. The waste volume is compact in comparison to that produced by aqueous processing, in which large volumes of liquid waste result. The molten-salt medium used for uranium extraction is not subject to radiolytic decomposition and, from a chemical standpoint, is inexpensive when compared to the organic solvents used in aqueous processing.

Pyroprocessing of used fuel requires heavy shielding to protect workers from the intense radiation fields involved. It becomes a high-profile, capital- and technology-intensive process. From the standpoint of proliferation safeguards, this becomes a control parameter, as few countries are equipped with world-class hot-cell facilities with remote capabilities to process "hot" spent fuel.

There are two paths possible for spent oxide fuel. One option is disposal of spent fuel as high-level waste, and the other is reprocessing spent fuel to separate the fissile and fertile isotopes. In addition to separating the fissile and fertile isotopes, there is also the option of processing the remaining long-lived actinides and fission products for transmutation into manageable and less radiotoxic isotopes. Oxide reduction is an important part of reprocessing

and has a key role to convert used oxide fuel to metal suitable for treatment in an electrorefiner. The constituents which are separated from the used fuel in the oxide-reduction process would otherwise need to be disposed of and managed as HLW. These constituents include uranium, plutonium, transuranics, and lanthanide fission products. Because nearly all nuclear-fuel waste generated in the U.S. is from light-water reactor (LWR) fuel from 100 reactors currently in operation, oxide reduction becomes an important technological approach for separating uranium from the highly radioactive LWR fuel waste stream. In the oxide-reduction process uranium oxide is reduced to uranium metal under a low-moisture argon atmosphere in an electrochemical cell containing electrolyte comprising molten LiCl with dissolved Li_2O. Fuel elements are sized by chopping, and then loaded into a cathode basket. An electrical potential is applied between the cathode and anode targeted to reduce the UO_2 to metal, both chemically and electrochemically. The oxide fuel that is converted to metal in the cathode basket after reduction is in suitable compositional form to receive into the electrorefiner for uranium separation and recovery. Volatiles and group I and II fission products are decontaminated from the final, reduced metal product.

An additional motivation for reprocessing spent nuclear fuel stems from the need for making nuclear energy more sustainable and to provide improved nuclear-waste management options. The concept of reprocessing has gained motivation to ensure a sustainable uranium supply in countries with import dependencies as well as countries obtaining domestic uranium supplies in an economy in which uranium demand will assuredly increase in the near future. For example, China, India, and other highly populated countries are planning to expand nuclear capabilities for their continuously growing electricity demands. Many of these countries do not have domestic uranium resources.

Another motivation is based on environmental and economic concerns. The extraction of uranium from mined ore involves complex processing, which results in degradation of the environment. Although there currently are stockpiles of uranium suitable for making nuclear fuel, those stockpiles will soon spend down, and the uranium mining industries will be required to meet a growing demand. When stockpiles of uranium are exhausted the demand for uranium will drive the cost of uranium to rise significantly. New mining areas will need to be established and could take years to be productive. Untapped reserves of uranium are

limited to a handful of countries, and the environmental impact of mining uranium is irreparable and is a significant concern. Analyses of the cost involved in reprocessing spent fuel often conclude that the cost to produce fresh fuel is less than the cost of reprocessing. The management and disposal cost of spent fuel in these comparisons are not included in these analyses and are subject to considerable uncertainty. Undoubtedly, these requirements add significant cost to the open-ended fuel cycle, costs which are not accounted for in the comparison. Through reprocessing, the uncertainty of future risks will be reduced. The majority of uranium in spent fuel is mostly fertile U–238, with approximately 1% fissile U–235 content. Freshly mined natural uranium contains only 0.711% U–235 at best. It takes 4000 times the weight in mined rock mass to obtain an enriched fuel suitable for reactor use. Thus, for the current annual consumption of 65,000 tons-per-year demand, it would be necessary to mine 260 million tons of uranium ore. World mining production in the last year was 78% of world demand.[28]

Reprocessing HLW can improve nuclear-waste-management options. Based on an engineering-controls standpoint, HLW should be reprocessed and burned in fast reactors with pyroprocessing and then transmuted to produce a waste product that is less radiotoxic and manageable within a time frame on the order of hundreds of years (as opposed to on the order of tens of thousands of years). There is uncertainty about the integrity of storage containers over 10,000 years for encapsulation of disposed HLW. Leaving a legacy of high-level waste for future generations to manage is an unacceptable waste-management option. Although a pyroprocessing and transmutation program would require a large capital investment, ensuring the manageability of HLW for future generations would be worth the effort. No matter what the route, dealing with HLW in a satisfactory way will require significant investment.

In order to achieve efficiency in advanced fuel-cycle strategy, careful attention must be paid to the unit operations from a processing standpoint. If these processes are optimized, the advanced nuclear-fuel cycle, including the implementation of pyroprocessing technologies, can help alleviate the need for additional HLW storage space and significantly reduce the radiotoxicity and heat load of SNF from commercial light-water reactors.[5] The oxide-reduction process is the core front-end pyroprocess and involves electrochemically reducing the spent oxide fuel, i.e., uranium oxide (UO_2) and actinide oxides in the LWR fuel,

to metal at the cathode at 650°C in a bath of molten $LiCl-Li_2O$ electrolyte. In the oxide-reduction process, the oxide fuel is converted to metal through electrolytic decomposition. During the 'oxide to metal conversion' of the SNF, uranium metal is separated from the high-heat-load fission products and recovered as an impure metal. Herrmann and Li[3] have reported 99.7% uranium-oxide conversion to metal in this process. Following the oxide-reduction process, the impure metal is transferred to an electrorefiner[3] wherein the material is employed as an anode for the electrorefining process, which yields a high-purity uranium product. The uranium-metal product can be stored in retrievable form in interim storage facilities for recycling to fast reactors[6] and, with slight enrichment, to LWRs.

The high-heat-generating fission products, such as cesium, strontium, and barium, are soluble in the $LiCl-Li_2O$ melt used for the oxide reduction process and, therefore, can be separated from the remainder of the fuel constituents in electrochemical-reduction operations.[5] The reduction potentials which would be necessary for the recovery of these high-heat-load fission products in the spent fuel cannot be achieved, and reduction to metal will not be obtained in the $LiCl-Li_2O$-based melts. During the oxide-reduction process, lithium metal is produced electrochemically at the cathode from the Li_2O dissolved in the LiCl molten salt, and oxygen gas is produced at the anode. The lithium metal chemically reacts with, and reduces the uranium in the UO_2 fuel to uranium metal. Uranium oxide is also reduced electrochemically during the oxide-reduction process because the decomposition potential of UO_2 and Li_2O are very similar. The spent-fuel metal cathode produced is then prepared for subsequent electrorefining. In the next step, the metal recovered during the oxide-reduction process is transferred into a bath of molten $LiCl-KCl-UCl_3$ eutectic at 500°C and electrorefined to yield a high-purity metal product. Uranium metal is electrochemically separated from remaining fission products, transuranics, and minor actinides and the metal recovered during the oxide-reduction process is transferred into an electrorefiner wherein a refined uranium metal is obtained to a purity of >99.99% to be stored for future use in fabricating new fuel.[3, 8]

Although high levels of conversion can be achieved, efficiency can be improved significantly by addressing interference from moisture and contaminants in the salt. Moisture cannot be entirely eliminated because many of the fuels contain moisture to some extent due to their

storage in cooling ponds. Understanding the impact of process conditions—such as the importance of purity of the atmosphere under which this process is conducted—on the efficiency of the recovery of metallic uranium in the oxide-reduction process is critically important. Moisture contamination in the $LiCl-Li_2O$ may be a contributor to parasitic reactions in the molten-salt system and, in this sense, could significantly reduce the efficiency of uranium recovery. Therefore, the focus of this research is aimed toward understanding of the role of moisture in the $LiCl-Li_2O$ molten-salt system.

The results of the research presented here will provide a fundamental understanding of the impact of moisture, the need to purify the molten salt in order to achieve higher throughput, and the method by which this is to be achieved. In addition, this information will help to improve the fundamental understanding of the electrochemistry of $LiCl-Li_2O$ molten-salt systems when the oxide-reduction process is implemented as the primary means of reprocessing LWR spent nuclear fuel in an advanced fuel cycle.

1.2   Literature Review

This literature review provides background on the sources of lithium chemicals. A basic knowledge is helpful for understanding the purity and methods for production from an electrochemical standpoint. Also, the applications of lithium chemicals are summarized and put into perspective the reasons for hygroscopic nature of many lithium-based chemicals.

1.2.1   Sources and Applications of Lithium-Based Chemicals

There are approximately 150 catalogued lithium-containing minerals.[29] Earth's upper crust, approximately 16 km in depth, contains 20–70 ppm lithium by weight.[30] At present, the primary mineral used as a raw material for the production of lithium and its compounds is spodumene, $LiAl(SiO_3)$,[29] a double-lithium aluminum silicate. Petalite, $LiAl(Si_4O_{10})$, is another lithium-containing silicate mineral used commercially. Other important lithium-containing minerals include amblygonite, $(Li,Na)Al(PO_4)(F,OH)$, and lepidolite, $K(Li,Al)_3(Si,Al)_4O_{10}(F,OH)_2$. Regardless of the lithium source, lithium carbonate becomes the most important lithium compound produced.

Two main lithium-extraction processes include concentration of lithium salts in brines by solar evaporation or by mining and concentration of lithium-containing minerals. Lithium metal is prepared by electrolysis in LiCl-KCl eutectic molten salt. Methods and techniques used to win lithium values from pegmatites, natural brines, and clays have been explained.[31,30] Lithium minerals are typically reduced to metal by conversion from carbonate form, which involves alkaline fusion and carbonation or acid roasting, calcination, and carbonation.[32]

Chile and Australia are the largest sources of lithium carbonate and lithium concentrates respectively. There are two main sources of lithium: (1) lithium brines and salt pans, and (2) lithium aluminum silicates. Chile, through the Sociedad Química y Minera (SQM), has been the largest producer of lithium carbonate from brine from locations within the Salar de Atacama, located in the Andes Mountains. Chilean production surpassed that of the U.S. in 1997[33] and Chile currently holds a 30% share in the global lithium supply. The Chilean location has been termed the "Saudi Arabia of Lithium."[34] Australian company Talison Lithium is the largest producer of lithium aluminum silicate spodumene ($LiAl(SiO_3)_2$), producing 200,000 metric tons in 2008, about 69% of the world's supply of lithium minerals in 2008.[33,35] The company reported the discovery of the largest deposit of spodumene in the world, located in Greenbushes, Western Australia.

1.2.2   Production of Lithium

Lithium is produced from brines such as $KLiSO_4$[36] through a process by which it is converted to lithium-carbonate form.[37,38,39] It is important to note that lithium carbonate extracted from brine sources and subsequently converted to LiCl can include boron impurities which can lead to severe process inefficiencies during the high-temperature electrochemical production of Li.[40] The optimal brine at the end of the process is concentrated to nearly 40 wt% lithium.

Lithium can also be produced from minerals such as spodumene ($LiAlSi_2O_6$) through a process which includes froth flotation, acid digestion, filtration, and precipitation. The final product, contains 90 wt% lithium carbonate.[29,41,39]

Lithium carbonate and lithium hydroxide feedstock are the sources for nearly all manufactured lithium chemicals.[31] For example, lithium chloride is manufactured most

commonly by reaction of lithium carbonate (Equation 1) or lithium hydroxide (Equation 2) with hydrochloric acid. The hydrated LiCl, heated in the presence of chlorine gas, will produce anhydrous lithium chloride (Equation 3).

$$Li_2CO_3 + 2HCl \rightarrow 2LiCl + CO_2 + H_2O \qquad (1)$$

$$LiOH \cdot H_2O + HCl \rightarrow LiCl + 2H_2O \qquad (2)$$

$$LiCl \cdot H_2O + Cl_2 \rightarrow LiCl + 2HCl + \tfrac{1}{2}O_2 \qquad (3)$$
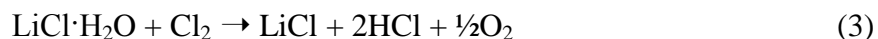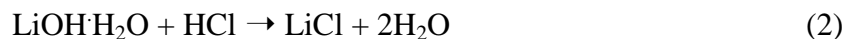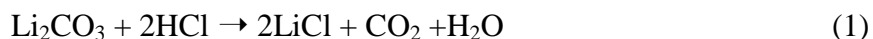
Lithium oxide is produced from lithium hydroxide by heating under vacuum at 800°C (Equation 4), or by reacting metallic lithium with oxygen (Equation 5). Thermal decomposition of lithium peroxide at 450°C will also render lithium oxide (Equation 6).

$$2LiOH \xrightarrow{800°C} Li_2O + H_2O \qquad (4)$$

$$2Li + \tfrac{1}{2}O_2 \rightarrow Li_2O \qquad (5)$$

$$Li_2O_2 \xrightarrow{450°C} Li_2O + \tfrac{1}{2}O_2 \qquad (6)$$

Lithium metal is produced from the electrolysis of LiCl in LiCl-KCl molten salt. Potassium chloride is added to reduce the melting point of the salt by forming a eutectic with LiCl and is also used to improve the conductivity of the melt. Once molten, LiCl becomes ionic (Equation 7). As current is passed between the cathode and anode, the LiCl is electrolyzed. Metallic lithium in the liquid phase is produced at the cathode (Equation 8) and chlorine gas is evolved at the anode (Equation 9). The overall electrochemical reaction is shown in (Equation 10).

$$LiCl \leftrightarrow Li^+ + Cl \qquad (7)$$

$$Li^+ + e^- \rightarrow Li \qquad (8)$$

$$Cl^- \rightarrow \tfrac{1}{2}Cl_2 + e \qquad (9)$$

$$LiCl \rightarrow Li + \tfrac{1}{2}Cl_{2(g)} \qquad (10)$$

The electrolysis process is generally operated most efficiently at 450°C. Additional LiCl is charged into the cell as it is consumed during electrolysis in order to maintain the eutectic composition for process efficiency. The LiCl must not exceed 65 mol % if the melting point is to stay near 450°C.[42] During electrolysis, the reaction products must be separated to prevent

recombination of lithium and chlorine which can lead to process inefficiency as well. Figure 1 illustrates a typical configuration of electrolytic cell for lithium production.[43] It is also important to use high-purity lithium-chloride feedstock; otherwise, impurities in the chemicals can co-deposit, rendering a low-quality product.
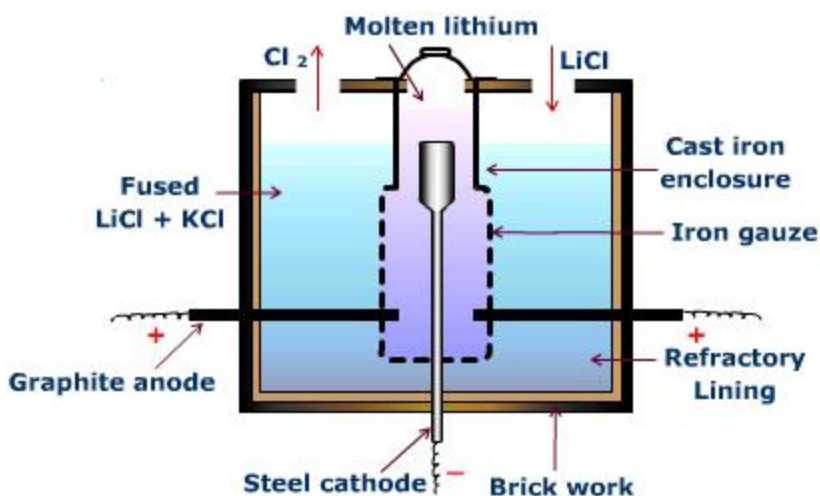
Figure 1. Schematic representation of typical lithium production cell for the electrolysis of LiCl.

1.3   Basic Properties of Lithium and Lithium-Based Compounds

1.3.1   Properties of Lithium Metal

Lithium is the first and lightest metallic element on the periodic table. There are two stable, naturally occurring isotopes of lithium, an element with a relative atomic mass of 6.94 g/mol. The first is lithium-7, with a crustal abundance of 92.58% and atomic mass of 7.016 g/mol, and the second is lithium-6, with a crustal abundance of 7.42% and atomic mass of 6.015 g/mol. In all, lithium is found in concentrations ranging from 20–70 ppm, and lithium ranks as the 30th most abundant element, placing it below nickel, copper, and tungsten and above cerium and tin. The density of solid lithium under ambient conditions is 0.53 g/cm^3, decreasing slightly to 0.516 g/cm^3 upon melting.

Table 2 lists some selected properties of lithium metal.[44] Lithium possesses properties homologous to the alkali elements. The similar properties are appearance, Mohs hardness, low density, high reactivity with halogens to form salt and with water to form hydroxides, formation of single-charged positive cations, low electronegativity, single oxidation state, etc.

Table 3 gives a comparison of selected properties of lithium chemicals with other alkali group elements.

Table 2. Chemical and thermodynamic properties of lithium metal.

Oxidation potential (Standard electrode potential; Li→ Li$^+$)	-3.045 V (3.038); 0.259 g/amp-hr
Specific heat	0.8 cal/g/°C
Vapor pressures (°C, mm Hg):	702, 0.49; 802, 2.82; 902, 12.1; 1002, 41.0; 1052, 70.5; 1077, 91.0
Electron Shells:	$1s^2 2s^1$
Atomic radius	1.52 or (1.55) Å
Radius:	Ionic 0.68 Å; Hydrated 3.40 Å; Covalent 1.23 Å
Atomic volume	13.10 cm^3/mol

Table 3. Selected properties of alkali metals.

Alkali Metal	Standard atomic weight (u)	M.P./B.P. (K)	Density (g·cm^{-3})	Electro-neg ativity (Paulings)	Crystal Structure	Thermal Conductivity (W·cm^{-1}·K^{-}) @ 300 K	Linear Expansion (μm·m^{-1}·K^{-1})	Heat of Fusion/ Vaporization (kJ/mol)
^{3}Li	6.941	453/1615	0.534	0.98	BCC	0.847	46	3/145.92
^{11}Na	22.99	370/1156	0.968	0.93	BCC	1.41	71	2.598/96.96
^{19}K	39.098	336/1032	0.89	0.82	BCC	1.024	83.3	2.334/79.87
^{37}Rb	85.468	312/961	1.532	0.82	BCC	0.582	--	2.192/72.216
^{55}Cs	132.905	301/944	1.93	0.79	BCC	0.359	97	2.092/67.74
^{87}Fr	223	295/950	1.87	0.7	BCC	0.15	--	~2/~65

Because of the high reactivity of lithium, it is never found naturally in elemental form. In metallurgy, lithium can be considered a scavenging element and is a powerful degasifier, deoxidizer, desulfurizer, and dehumidifier. It is used as a purifying agent in various metallurgical and chemical operations. It is of particular interest for industrial applications because of its efficiency and usefulness as a refining agent. Table 4 lists lithium with respect to exothermic energy it releases, its oxygen-scavenging ability compared with other elements, and its purifying power.[45]

Table 4. Comparison of lithium and other elements when reacting with oxygen.

Element	Grams of oxygen which combine with one gram of element	Kcal set free when one gram of element combines with oxygen
Li	1.152	10.33
Na	0.348	2.18
K	0.204	1.11
Rb	0.094	0.46
Cs	0.060	0.31
Be	1.774	15.23
Mg	0.658	6.00
Ca	0.399	3.72
Sr	0.182	1.61
Ba	0.116	0.97
Al	0.890	7.05
Zn	0.245	1.27
Mn	0.292	1.707
Si	1.140	6.80
Ti	0.668	4.56
P	1.289	5.78
Zr	0.350	2.90

The heat capacity of lithium is the highest of all solid elements on the periodic table, and it remains liquid over a large temperature range, making it perfect for applications as a coolant.

Lithium reacts vigorously with water to produce hydrogen and lithium hydroxide. When finely devided lithium powder is introduced with water it ignites. Among alkali-group elements, however, lithium is the least reactive. In air, lithium tarnishes readily, reacting with nitrogen, oxygen, carbon dioxide, and humidity. The tarnish appears opaque and is composed of LiN, $LiCO_3$, LiOH and LiOH hydrate.

1.3.2   Properties of Lithium Oxide

Lithium oxide, also called dilithium monoxide or lithia, with the chemical formula Li_2O, is a strongly alkaline white crystalline compound which readily absorbs carbon dioxide and water to produce lithium carbonate and lithium hydroxide, respectively. It has a molecular weight of 29.88 g/mol, a density of 2.012 g/cm^3, and a melting point of 1570°C.

1.3.3   Properties of Lithium Chloride

Metal oxides are highly soluble in LiCl molten salt, so it is the electrolyte of choice for the treatment of nuclear waste based on uranium-oxide nuclear fuel.[46]

Lithium chloride (LiCl) is an odorless, colorless, hygroscopic, and deliquescent chemical compound with a molecular weight of 42.4 g/mol, melting point of 610°C, boiling point of 1360°C, and density of 2.1 g/cm^3 at room temperature. The liquid density of LiCl for temperatures between 610°C and 781°C can be calculated by (Equation 11):[47]

$$\rho(t) = \rho_m - k(t - t_m) \tag{11}$$

where ρ_m the density at the melting point (1.502 g/cm^3), t_m is the melting point (610°C), and k is an empirical constant (0.000432 g/cm^3). Janz[48] has also published a similar equation (Equation 12) for calculating the density of LiCl as a function of temperature:

$$\rho(t) = A + B (C + t) \tag{12}$$

where ρ is the density in g/cm^3, t is the temperature in Celsius, and A, B and C are constants used to determine the density of LiCl as a function of temperature. The density of LiCl at 650°C, according to both Equations 13 and 14, is 1.485 g/cm^3. According to both equations, the density of LiCl as a function of temperature is as listed in Table 5.

Table 5. Molten salt density for pure LiCl as a function of temperature.

Temperature (°C)	Density, g/cm^3	
	Jantz[48] $\rho(t) = A + B\,(C + t)$	CRC[47] $\rho(t) = \rho_m - k(t - t_m)$
610	1.501973	1.50200
625	1.495481	1.49552
650	1.484661	1.48472
675	1.473841	1.47392
700	1.463021	1.46312
725	1.452201	1.45232
750	1.441381	1.44152
775	1.430561	1.43072
780	1.428397	1.42856

The solubility of lithium chloride in water is approximately 83g/100 ml at 20°C. Table 6 gives values for solubility of LiCl in terms of molality at ambient temperatures between 10°C and 40°C.

Table 6. Aqueous solubility given in molality*(M)*.

Salt	10°C	15°C	20°C	25°C
LiCl[49]	19.296	19.456	19.670	19.935
NaCl[50]	6.110	6.121	6.136	6.153

Aqueous solubility of LiCl at ambient temperatures is more than three times that of NaCl. Because the lithium ion (Li^+) is the smallest of the alkali metals, its solubility is very large in polar solvents, by comparison.

Lithium chloride is unique in forming solid hydrates under ordinary conditions in comparison with other alkali chlorides. Besides anhydrous LiCl , the monohydrate form is the most common; however, under certain conditions, mono-, bi-, tri-, and pentahydrates are known.[51,39,31] The phase diagram in Figure 2 shows LiCl solubility in pure water.[52] The lithium number (Li 1-5) refers to number of hydrated water molecules. The structure of solid LiCl is octahedral.
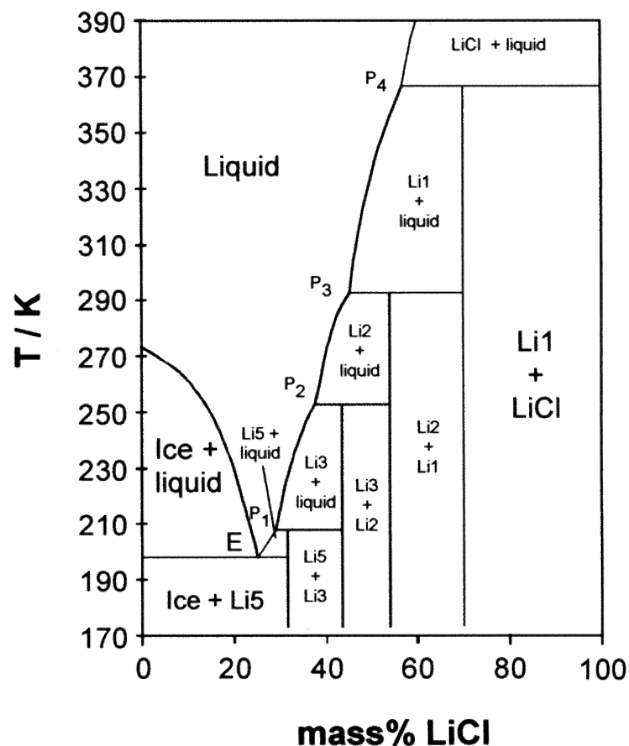
Figure 2. Phase diagram of the H$_2$O-LiCl system.

When molten, LiCl possesses an expansive electrochemical window and high thermodynamic stability as compared to aqueous solutions. For example, aqueous solutions are limited to the decomposition of the water to form O$_2$ and H$_2$. This property makes lithium chloride a good candidate for electrochemical separation of nuclear materials, which have decomposition potentials far exceeding that of water in aqueous-based system. Lithium chloride is a commonly used solvent for molten-salt experiments and is useful in electrometallurgical operations (i.e., pyroprocessing) for the nuclear fuel cycle. Pyroprocessing operations using LiCl molten-salt systems have many inherent advantages which will be further discussed below.

Lithium chloride has a lattice constant of 5.14 Å at 25°C and an interionic distance of 2.57 Å. At room temperature, the molar volume, V$_M$, of LiCl is 20.442 cm^3/mol. The molecular volume of LiCl is 33.945 Å^3/molecule. Lithium chloride possesses a NaCl-type crystal structure. The structure of lithium chloride in solid and molten phases was investigated by McGreevy and Howe,[53] who reported that LiCl upon melting retains an octahedral-like structural symmetry of its face-centered cubic (FCC) rock-salt crystal structure.

Liquid lithium can be explosive on contact with water, interacts actively with air, carbon dioxide, and nitrogen at high temperatures,[54] and can interact with concrete and ceramic materials.[55] Upon melting, its electrical conductivity rises drastically, and lithium has a volume expansion of nearly 20% due to the number of vacant sites (15%) which represent the difference between the crystal and liquid states.[54,7]

The cell potential of LiCl is temperature-dependent.[10] Figure 3 shows the temperature dependence of the cell potentials for LiCl based on calculated thermodynamic data. The cathodic limit is given by the reduction potential of the least stable cation, and the oxidation limit gives the anodic potential of the anion. Of all alkaline-halide salts, LiCl has the least stable cation (i.e., Rb>Cs>K>Li) but one of the most stable halide anions (i.e., F>Cl>Br>I).
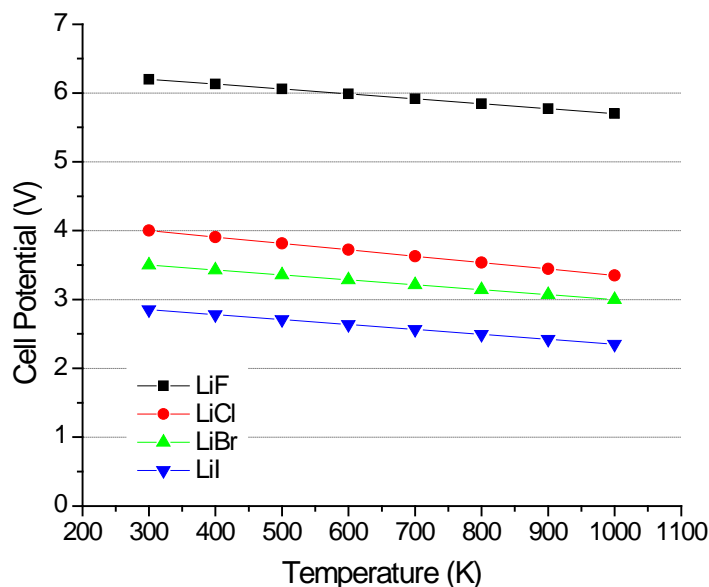
Figure 3. Cell potential as a function of temperature for, LiF, LiCl, LiBr, and LiI.

For the purpose of the pyroprocessing of nuclear fuel, lithium-based electrolytes do not have a voltage range sufficiently wide to be used for recovery of specific fission products, such as cesium, barium, strontium and rubidium, due to their thermodynamic stability in the molten salt. Many fission products are soluble in lithium-based electrolyte; however, they are stable as a chloride beyond the stability range of the lithium salt. Because of this thermodynamic boundary, these fission products cannot be electrochemically separated. Table 7 lists noble

metals in spent metallic fuel which are likely resist reaction with the salt during the electrorefining process. Uranium, which is electrorefined, is more noble than many other transuranics and fission products that dissolve into the salt and form stable chlorides; however, under certain operating conditions, these can be electrochemically recovered. The fission products that remain in the salt are those which are more stable in the dissolved form than lithium. That is, before electrochemical recovery of these metals, lithium is recovered. By exploiting the thermodynamic tendency of the molten salt system, the preference of certain fission-product metals more stable as a chloride than uranium, spent fuel can effectively be decontaminated from the fission products and transuranics, and a high-purity uranium metal can be recovered.

Table 7. Gibbs free energy of formation for elements contained in spent metallic fuel.

Overall	ΔG formation, 500°C (kcal)	Moles Cl	ΔG (kcal)/mol Cl	Category
$Tc + 1.5Cl_2(g) = TcCl_3$	-31.841	3	-10.614	Noble Metals Remain in metal form. Will not react with salt.
$Fe + 1.5Cl_2(g) = FeCl_3$	-60.066	3	-20.022	
$Mo + 1.5Cl_2(g) = MoCl_3$	-64.875	3	-21.625	
$Zr + 2Cl_2(g) = ZrCl_4$	-179.523	4	-44.881	
$U + 1.5Cl_2(g) = UCl_3$	-165.822	3	-55.274	Uranium Cathode
$Np + 1.5Cl_2(g) = NpCl_3$	-173.324	3	-57.775	Active Metals Dissolve into salt and form stable chlorides.
$Cm + 1.5Cl_2(g) = CmCl_3$	-183.324	3	-61.108	
$Pu + 1.5Cl_2(g) = PuCl_3$	-188.261	3	-62.754	
$Am + 1.5Cl_2(g) = AmCl_3$	-190.077	3	-63.359	
$Nd + 1.5Cl_2(g) = NdCl_3$	-203.799	3	-67.933	
$Ce + 1.5Cl_2(g) = CeCl_3$	-206.378	3	-68.793	
$Pr + 1.5Cl_2(g) = PrCl_3$	-206.984	3	-68.995	

Overall	ΔG formation, 500°C (kcal)	Moles Cl	ΔG (kcal)/mol Cl	Category
La + 1.5Cl$_2$(g) = LaCl$_3$	-210.531	3	-70.177	
2Na + Cl$_2$(g) = 2NaCl	-162.219	2	-81.110	
2Li + Cl$_2$(g) = 2LiCl	-164.839	2	-82.420	
Sr + Cl$_2$(g) = SrCl$_2$	-170.133	2	-85.067	Active Metals
2Rb + Cl$_2$(g) = 2RbCl	-172.755	2	-86.378	Dissolve into salt and form stable chlorides which cannot be removed electrochemically
2K + Cl$_2$(g) = 2KCl	-173.354	2	-86.677	
Ba + Cl$_2$(g) = BaCl$_2$	-175.235	2	-87.618	
2Cs + Cl$_2$(g) = 2CsCl	-175.244	2	-87.622	

Lithium-based electrolytes exhibit the highest ionic conductivities due to the high mobility of the lithium cation, as compared to other alkali-based electrolytes.[7] Therefore, the higher the atomic fraction of lithium, the higher the ionic conductivity of the electrolyte, giving LiCl one of the highest conductivities of alkali-chloride molten salts.

Alkali halides are particularly sensitive to moisture, and the hygroscopicity of the alkali metals decreases in sensitivity from Li>Na>K. The halide reactivity to moisture decreases from I>Br>Cl>Fl. Lithium chloride, as well as other lithium salts, will form hydrates in the form of LiX·nH$_2$O, where X = Cl, F, Br, or I, and n is the number of hydrates depending on the anion.[7] LiCl crystallizes water to form LiCl·H$_2$O and LiCl·1/2 H$_2$O, the first of which has been reported to thermally decompose at 98–110°C and the latter at 152–162°C. The hydrates exhibit incongruent[11] melting behavior. Hydrates of LiCl are taken as crystalline form, and their thermal stability depends upon hydrate number, the properties of the anion, and H$_2$O partial pressure.[7] Figure 4 shows the differential-scanning calorimetry (DSC)/thermogravametric analysis (TGA) results of LiCl·H$_2$O decomposition.[7] Under an inert helium atmosphere, the temperature of the hydrated LiCl salt was scanned at a rate of 1°C/min. The first major weight loss occurs at approximately 100°C at which temperature an

endothermic reaction of dehydration for LiCl·H$_2$O takes place and decomposes to LiCl·1/2H$_2$O. The thermal stability of the LiCl·1/2H$_2$O is higher, and a sharp endothermic spike is seen at 160°C, at which temperature the hydrate experiences a weight loss of approximately 27%.
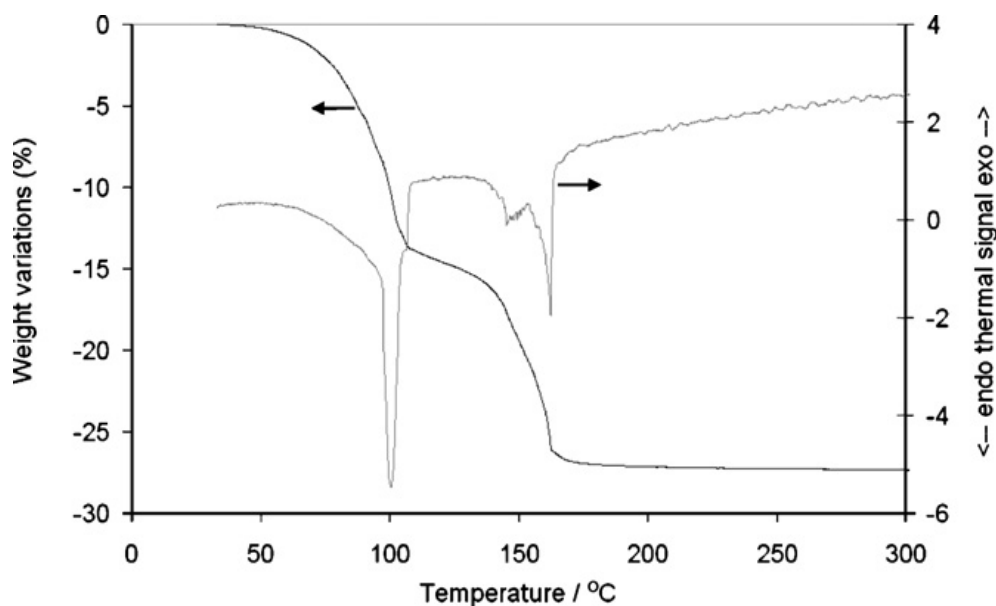
Figure 4. DSC/TGA of LiCl·H$_2$O sample.

1.3.4   Applications of Major Lithium Compounds

Unique properties of lithium and its chemicals make it important in the development of diverse industrial, chemical, and pharmacological applications. Lithium is well known for the ability to function as a mood stabilizer and has been the standard pharmacological treatment for bipolar disorder for over 60 years[56,57] because of its effectiveness in counteracting both mania and depression. Lithium carbonate is one of many examples of mood-stabilizing agents. The lithium ion in various salts affects the central nervous system by increasing levels of serotonin and serotonin metabolite in the brain, which stabilizes mood.

Lithium is also used to make advanced anode materials for energy-storage devices, such as lithium-ion batteries.[58] Lithium is often used as a coolant because of its high specific-heat capacity. Due to its low atomic number, it has long been considered for application in the Tokamak fusion reactor as a plasma-facing material.[59]

Lithium materials are the main source of tritium via neutron capture reactions. Tritium can be produced through neutron capture reactions of ^{6}Li and ^{7}Li[60] (Equation 13 and Equation 14). For fusion driven hybrid reactors, lithium based materials are used in order to supply tritium self-sufficiency.[60] Examples of lithium based materials for solid tritium breeding materials are: Li_2O, Li_2TiO_3, and Li_8ZrO_6.

$$^6Li + n \rightarrow {}^4He + {}^3H + 4.784 \text{ MeV} \tag{13}$$
$$^7Li + n \rightarrow {}^4He + {}^3H + n \tag{14}$$

The ^{6}Li isotope has a larger neutron-capture cross section for low-energy neutrons, and the ^{7}Li isotope has a larger neutron-capture cross section for neutron energies greater than 1 MeV. As mentioned previously, natural lithium contains 92.5% ^{7}Li and 7.5 % ^{6}Li.

Lithium molten salts, such as Flibe (Li_2BeF_4) and Flinabe (Na LiF BeF_4), are efficient coolant and heat-transfer media used as nuclear-reactor coolants. Lithium metal has a wide temperature window as a liquid: the melting temperature is 180°C, and the natural boiling point is 1343°C.

Rechargeable lithium-ion cells are key components of the portable entertainment, computing, and telecommunication equipment.[61,62] Between 2003 and 2007, the battery industry doubled its consumption of lithium carbonate, the most common ingredient used in lithium-based products.[34] Advantages of lithium-battery technology are its higher voltage potential (3 volts for Li batteries and 2.1 volts for Pb/Zn batteries) and low atomic mass, which allows for a higher power-to-weight ratio.

Lithium-chloride-based molten salts are used in pyroprocessing of spent nuclear fuel for their many inherent advantages over aqueous-processing operations. For example, cooling storage time, essential and significant in aqueous processing, is not necessary. LiCl-based salts have a high heat-load capacity and radiation-field tolerance. Also, significant waste-volume reduction (of up to a factor of 100) can be achieved due to the capacity to separate transuranic elements, as well as cesium and strontium from uranium, plutonium, and minor actinides, allowing for their use as fuel in fast reactors.

Lithium oxide is used as a neutron target for tritium reaction.[63] Lithium oxide has high melting point (1,427 °C), and the purity of lithium oxide is critical to tritium reactions. Lithium carbonate and other impurity concentrations can reduce the melting point causing adverse effects.

Lithium oxide may also be used in the electrolytic-reduction process to expand the electrometallurgical treatment to include oxide fuels.[15] The electrochemical reduction of lithium in the fused lithium-chloride/lithium-oxide system has a more narrow range of voltage, very close to the electrochemical reduction of uranium, making possible simultaneous chemical- and electrochemical-reduction processes. Because most commercial nuclear fuel is in the form of oxides, the development of such technology is being pursued in the United States and Republic of Korea, among others. Table 8 summarizes major applications of lithium and lithium compounds.

Table 8. Applications of lithium and lithium compounds.

Application Category	Chemical Form	Applications
Chemical Uses	LiCl, LiBr	Desiccants
Nuclear Applications	$^6Li^2H$, LiF-BeF$_2$, finely divided LiF powder, Li$_2$O, LiTiO$_3$, LiZrO$_6$	Atomic bomb or nuclear weapons, liquid fluoride nuclear reactors. Thermoluminescent radiation dosimeters (TLDs), Tritium production for fusion power
Rocketry	Li, Li(AlH$_4$) Li$_2$O$_2$, LiNO$_3$, LiClO$_4$, LiClO$_4$	Propellant additives Oxidizers
Electronic/ Electrical	Li-MnO$_2$ LiPF$_6$, LiAsF6, LiClO$_4$, LiBF$_4$, LiCF$_3$SO$_3$	Disposable batteries Lithium-ion batteries (non-aqueous electrolytes)
General Engineering	LiC$_{18}$H$_{35}$O$_2$ LiCl	Lubricant Aluminum brazing flux
Aluminum Alloys	Alloy 8090 (Li-2.45, Zr-0.12, Cu-1.3, Mg-0.95) Alloy 2091 (Cu-2.1, Li-2.0, Zr-0.10) Alloy 2090 (Cu-2.7, Li-2.2, Ag-0.4, Zr-0.12) Weldalite 049 (Cu-5.4, Li-1.3, Ag-0.4, Mg-0.4, Zr-0.14)	Aerospace, cryogenic, welding
Other uses	Li$_2$CO$_3$, LiOH, Li$_2$O$_2$ Li$_2$NO$_3$, Li, LiCl-KCl, LiCl-Li$_2$O	Soap, lubricants, air purification, pyrotechnic colorant (red), torpedo steam generation Production of metal through pyrometallurgy

Chapter 2: Review of Molten Salt Electrochemistry

Molten salts, also known as fused salts or ionic liquids, were actually the first electrolytes used in experiments by Sir Humphry Davy in 1802.[9] Molten salts are favored in cases where aqueous solutions cannot be used because the decomposition voltage of water is lower than that of the salt in question.[8] Molten salts have good thermal stability, very high electrochemical stability, high electrical conductivity, and low vapor pressures. They do not suffer radiolysis and are good solvents for many inorganic compounds. Another advantage of molten salts is the observed high reaction kinetics (either chemical or electrochemical).[7] The main disadvantages of many single-component molten salts are their high melting temperatures and the corrosive tendency to materials of construction, especially when atmospheric moisture is present. With careful selection of materials and the use of dry inert-atmosphere gloveboxes, the disadvantages associated with molten salts become irrelevant. The molten-salt systems used in this work are (i) completely ionized ionic melts. Other classifications of molten salts include (ii) molecular melts which have no ionization, (iii) partially ionic melts, (iv) polyionic melts, and (v) hydrate melts. For this reason, the term ionic melt cannot be universally applied to molten salts.[9] Table 9 lists the different classifications for molten salt systems.

Table 9. Molten-salt classifications.

Molten salt classification	Examples
(i) Ionic (full ionization)	LiCl, KCl, NaBr
(ii) Partially ionized glass melts	K_3PO_4
(iii) Molecular (no ionization)	$AlCl_3$
(iv) Polynionic	$NaNO_3$, K_2SO_4
(v) Hydrate melts	$Ca(NO_3)_2 \cdot 4H_2O$

In electrolytic conduction, positive and negative ions are transported toward electrodes. Electrolytic conduction is different from electronic conduction in that it involves a mass transport of ions from one part of the electrolyte to another. Current flow is due to oxidation and reduction reactions at the electrode/electrolyte interface. Classification of chemical changes that may occur at the anode and cathode[64] are listed in Table 10. Both electronic and electrolytic-type conductors allow the flow of current; however, in electronic conductors,

there is no chemical change in the form of the conductor. In electrolytic conductors, the flow of current is due to the movement of ions to the oppositely charged electrodes. Electrolytic conduction increases with a rise in temperature due to an increase in the mobility of the ions and an increase in the degree of ionization in the electrolytes. Electronic conduction decreases with a rise in temperature.[64]

Table 10. Classification of cathodic and anodic reactions.

Cathodic Reactions	Example	Anodic Reactions	Example
Metal deposition or reduction	$M^{n+} + ne^- \rightarrow M$ $Li^+ + e^- \rightarrow Li$	Metal dissolution or oxidation	$M \rightarrow M^{n+} + n\,e$ $Li \rightarrow Li^+ + e^-$
Gas evolution	$2\,H^+ + 2\,e^- \rightarrow H_2$	Gas evolution	$4\,(OH)^- \rightarrow 2H_2O + O_2 + 4e^-$
Gas absorption	$O_2 + 2\,H_2O + 4\,e^- \rightarrow 4\,(OH)^-$	Gas desorption	$H_2 \rightarrow 2H^+ + 2e^-$
Reduction of an ion from a higher to lower valency	$M^{n+} + x\,e^- \rightarrow M^{(n-x)}$ $U^{4+} + e^- \rightarrow U^{3+}$	Oxidation of an ion from a lower to higher valency	$M^{(n-x)} \rightarrow M^{n+} + x\,e^-$ $Fe^{2+} \rightarrow Fe^{3+} + e^-$

The choice of electrolyte is important in electrometallurgical processes because it may affect the efficiency of the process and the quality of the product. In addition to providing a wide voltage range, halide molten salts such as LiCl exhibit low vapor pressures at molten temperatures, good electrolytic conductivity, and high solubility with other metal salts. This can be particularly beneficial when lower operational temperatures are sought. Chlorides and fluoride salts can sometimes be partially covalent and partially ionic. The covalent compounds typically have low boiling/sublimation temperatures and, for that reason, have low retention in the electrolytes at operating temperatures. Better retention of halide compounds of a covalent nature can be achieved by altering the oxidation state and by complexing.

2.1   Pyroprocessing of Nuclear Fuels

Pyroprocessing refers to the complete set of unit operations required to recover fissile elements from spent fuel and retain them in the fuel cycle for use in the manufacture of new fuel.[65] A simplified flowsheet for pyroprocessing is shown in Figure 5. Spent oxide fuel is removed in a fuel-element-dismantling step, where the fuel undergoes a voloxidation process[66] to remove fission-product gases and to prepare the fuel for the oxide-reduction process, in which the fuel is reduced to a metal form. In addition to reduction of uranium oxide to uranium metal, transuranics and rare-earth fission products are also reduced to metals. The LiCl-Li$_2$O salt from the oxide-reduction process is then distilled off of the reduced metal prior to introduction into the electrorefing step, which is done to decontaminate the uranium metal from the transuranics and rare-earth fission products. Once the pure uranium metal is recovered, it can be mixed to enrich or downblend its isotopic makeup, prepared as an oxide, and cast into fuel pins that can be recycled into a nuclear reactor.
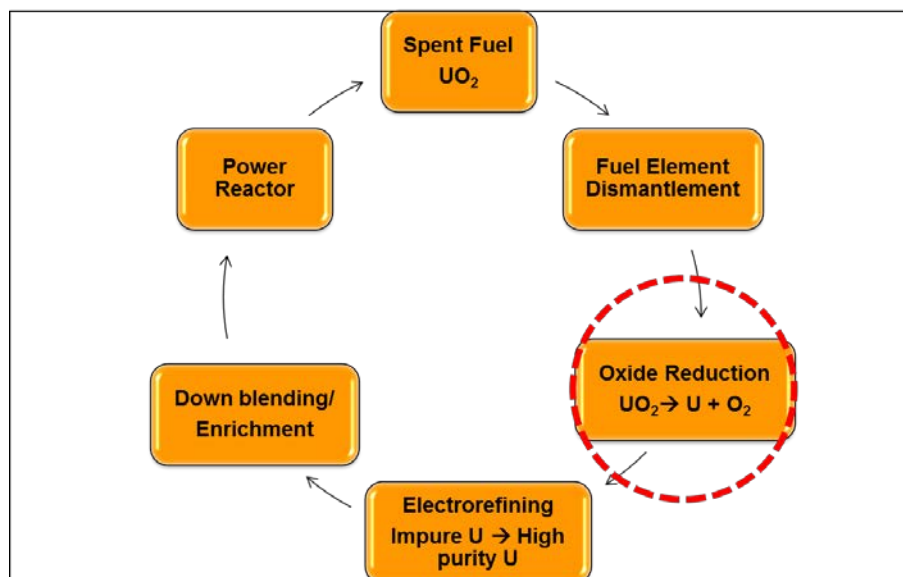
Figure 5. Pyroprocessing fuel cycle flowsheet.

Pyrochemical methods were developed during the Manhattan Project to reduce and purify uranium and plutonium.[67] Pyroprocessing is the optimal means of treating spent metal fuels from metal fast fuel reactors and can be effectively extended to treat oxide fuels by applying an electrochemical reduction.[68] Therefore, the fuels which are treated using pyroprocessing methods can be of oxide ceramic or metallic configurations. A more general definition of pyroprocessing, also known as pyrochemical reprocessing, is as follows:[69]

> Pyrochemical reprocessing methods uses high temperature oxidation-reduction reactions in a non-aqueous media to separate the actinides, U and Pu from the fission products. These methods exploit the differences in the volatilities or thermodynamic stabilities of the compounds of actinides and fission products to achieve the separation. Pyrochemical separations can be achieved by using electrochemical methods instead of chemical equilibrations.

There are more than 430 commercial nuclear thermal reactors using UO_2 fuel, 100 of which are power reactors operating in the U.S. The operation of this current fleet of nuclear power plants produces 10,000 metric tons of spent fuel per year. If all accumulated spent fuel were to be reprocessed, some 1,700 metric tons of plutonium and 190,000 metric tons of natural

uranium equivalents would be made available for fuelling nuclear power plants. By 2015, it is predicted that nearly 87,000 metric tons of spent fuel will be generated in the U.S. alone.[65]

When irradiated fuel is removed from the nuclear reactor, approximately one-twentieth of the potentially fissionable atoms in it have been burned, so "spent fuel" still contains about 95% of unreacted uranium.

Though several methods of pyroprocessing are known, only two methods based on electrochemical separations have been investigated extensively and developed to plant scale. One is the electrorefining method for metallic fuels developed by Argonne National Laboratory (ANL) for the Integral Fast Reactor concept[70] and the other is the pyroelectrochemical method for oxide fuels developed by Russian Institute for Atomic Reactors (RIAR), Russia. Both ANL and RIAR have pioneered the development of pyrochemical reprocessing routs.[71,72,73]

Pyroprocessing offers several advantages over aqueous reprocessing methods; these far outweigh the methods challenges make the techniques increasingly popular. Some advantages of pyroprocessing are:[74]

1. The ability to accommodate short-cooled high-burnup fuel due to the higher radiation stabilities of non-aqueous reagents.
2. Low process volumes and compact equipment due to the higher solubility of the actinides in molten salt than in aqueous solutions. It is said that the total volume of a pyrochemical reprocessing plant for a 1000 MW reactor would be forty times smaller than a plant operating on the aqueous route of an equivalent capacity. Furthermore, several process steps can be performed in a single vessel.
3. A wide temperature range to amplify the differences in the thermodynamic stabilities that control the separation factors.
4. Very small volume of waste in solid form (molten salts and metals are solid at room temperature), making waste treatment much easier.
5. Lower criticality problems due to the absence of moderating solution (aqueous).

The plutonium uranium extraction (PUREX) process,[75] by comparison, separates pure uranium and pure plutonium but leaves the other transuranics, or minor actinides, in the stream with fission products, primarily lanthanides. Additional aqueous-separation processes are required for the extraction of neptunium, americium and curium. Costly synthetic organic solvents are required, and increased waste stream volume is associated.

During pyroprocessing, electrolytic decomposition of a compound is dissolved into a molten salt. The compound undergoing electrolytic decomposition is derived from various forms of spent fuel.[76]. This process is used to recover fissionable actinides and to separate and drop out the radioactive transuranic fission products. Pyroprocessing techniques used for reprocessing spent nuclear fuels have been discussed in detail in references 1 and 2. Hur et al[6] have explained that the enhanced rate of reduction of UO_2 for the production of U-metal by *in-situ* produced lithium from lithium oxide is due to the fast kinetics of lithium reduction from Li_2O (as compared with the oxygen ion diffusion from the uranium oxides matrix of the conventional direct metal oxide reduction method). The oxide reduction process enhances the direct electrolytic reduction of uranium oxides due to the fact that either the direct electrolytic reduction of uranium oxides or the chemical reduction of uranium oxides. Indeed, both will occur in this process, thereby enhancing the overall production of U from uranium oxides.

2.1.1   Oxide Reduction

Pyroprocessing of spent oxide nuclear fuel can significantly reduce nuclear waste volume. Development of spent-oxide-fuel treatment facilities is essential because the majority of commercial reactors operate on oxide fuels and onsite capacity of spent-fuel storage has exceeded limits. Licensing extensions on spent fuel is needed from the Nuclear Regulatory Commission (NRC) to continue storage regimes.[77] Further, spent nuclear fuel contains considerable amounts of fissile U–235 in addition to other valuable actinides with fertile and fissile materials that contain usable energy.

The *in-situ* production of metallic lithium in liquid phase for the reduction of used uranium-oxide-based nuclear fuels can be employed to recover useable values from spent nuclear fuels. The fuel cycle can be designed such that no fissile material leaves the processing site, greatly decreasing its possible use in weapons.[78]

One issue in oxide reduction is low current efficiencies in the Li_2O-reduction process. This low current efficiency is attributed to the recombination of lithium with oxygen in the cell[17] and a decrease in oxide-ion concentration from Li_2O degradation in the bulk molten salt. These are concerns that may need to be addressed if efficiency becomes a concern when pyroprocessing is scaled to larger, industrial reprocessing facilities for SNF.

2.1.2 Solubility of Li and Li_2O in LiCl and LiCl-KCl Molten Salts

Lithium is slightly soluble in LiCl, at approximately 0.08 wt% at 650°C and 0.164 wt% at 750°C.[79,16] However, the solubility of lithium oxide in LiCl is reported in the range of 8.7–12 wt% at 650°C.[18,80] Lithium solubility in LiCl-KCl eutectic was found to be 0.087 wt% at 750°C, which is only about half of the solubility of lithium in LiCl. The solubility of Li_2O in molten LiCl-KCl systems was also determined in the temperature range of 400–650°C. The melt with a higher content of LiCl in molten LiCl-KCl systems has a higher solubility of Li_2O.

The solubility of Li_2O is much lower than lithium in LiCl-KCl eutectic salt.[17] The solubility of Li_2O in LiCl-KCl is less than 1 wt%.[7] It was reported by Karell et al[14] that, at low oxide-ion concentrations (less than 0.5 wt% Li_2O in LiCl), the platinum anode will begin to degrade, and cell efficiency drastically decreases. However, there was no anode degradation in LiCl-Li_2O when the Li_2O concentrations were maintained at ~3.5 wt%. Also, low solubility of metal oxides, in general, proves the requirement for LiCl instead of LiCl-KCl for metal-oxide-reduction processes. Y. J. Shin et al[19] reported a simulated molten-salt mixture used for treating spent oxide fuel contained 19.7 wt% Li_2O at discharge post oxide reduction of a simulated spent LWR fuel. T. Usami et al[20] and calculated that solubility of Li_2O at 650°C to be 8.8 wt% and B. H. Park et al[21] reported the concentration of Li_2O to be 8.4 wt% in Li_2O at 650°C. Sakumara[22] determined the concentration of Li_2O at 600 and 650°C to be 7 wt% and 8–8.3 wt% respectively. It has been determined that, with higher concentrations of Li_2O in the LiCl, the reaction rate can decrease. If spent fuel is to be reduced, a concentration of 5.1% Li_2O will prevent americium dioxide from reducing to metallic form.[20]

2.1.3 Effect of Moisture in LiCl Molten Salts

Due to the hygroscopic nature of LiCl- and LiCl-Li$_2$O-based salts, water will react with the lithium product that is formed during electrolysis to form unwanted Li$_2$O (Equation 15) and LiOH (Equation 16), respectively. If the goal is to produce lithium, this can be a serious consequence.

$$\text{Li} + \tfrac{1}{2}\text{H}_2\text{O}_{(g)} = \tfrac{1}{2}\text{Li}_2\text{O} + \tfrac{1}{2}\text{H}_{2(g)} \quad \Delta G_{650°C} = -33.317 \text{ kcal/mol} \tag{15}$$

$$\text{Li}_2\text{O} + \text{H}_2\text{O}_{(g)} = 2\text{LiOH}_{(l)} \quad \Delta G_{650°C} = -16.89 \text{ kcal/mol} \tag{16}$$

The solubility of moisture in LiCl- and LiCl-KCl-based melts has been observed by many authors following many different moisture-removal treatments.[12] In addition, the solubility of LiOH in Li$_2$O has also been studied by Tetenbaum et al.[13] These are important observations to note because moisture tends to reside in the LiCl-Li$_2$O-based molten salts in this form. Research regarding this subject proved that the residual concentration of LiOH is likely in the temperature range of 627–1027°C.

2.1.4 Motivation and Objectives

The interaction of LiCl and Li$_2$O of technical grade will inevitably cause the formation of LiOH if either of these chemicals contains moisture impurities. If Li$_2$O is charged into the LiCl subsequent to its melting, the formation of LiOH will not occur, according to the results suggested in these studies. For the simultaneous chemical and electrochemical reduction of spent oxide fuel, direct implications may be associated with lithium production that are necessary for the success of the process. Lithium and Li$_2$O are added to the electrochemical cell together prior to melting.[92] Lithium oxide generally will contain significant LiOH concentrations and, if the case, hydrogen will be produced at the cathode in place of lithium. This effect increases the precurrent, which is cathodic current observed prior to the standard reduction potential of lithium in the LiCl-Li$_2$O-based molten-salt system, quite drastically. Cathodic precurrent of between 1 and 2 A were observed in some cases,[81] which may indicate LiOH contamination.

The mode of interaction that Li_2O encounters in a moisture-containing $LiCl$-Li_2O molten-salt system must be understood. This goal of this research is, therefore, to elucidate the behavior of lithium in the presence of moisture and to understand the mechanism of hydrolysis of the $LiCl$-Li_2O systems.

Chapter 3: Experimental

3.1 General

The electrochemistry of the molten-salt systems was studied in the range of 620–750°C. All experiments were carried out in an ultra-high-purity argon atmosphere. Anhydrous lithium chloride (99.7%), as well as ACS-grade LiCl (99+%, ACRŌS Organics) was used. The Li_2O (99.5%), and LiOH (prepared from LiOH monohydrate) were purchased from Alfa Aesar. Ultra-high-purity LiCl (Alfa Aesar, 99.995%) was used as a control for the lower-grade LiCl. The working electrode was made of 1-mm-diameter nickel or molybdenum (Puratronic 99.9945%). The counter-electrode was made of 3-mm-diameter high-purity graphite rod or 6-mm-diameter glassy-carbon rod. A 0.5-mm-diameter molybdenum wire was used as a quasi-reference electrode (QRE) due to its consistent stability in the molten-salt systems studied. In addition, molybdenum does not adsorb or form alloys with lithium; this is why it was chosen over platinum, which is known to react with lithium.[82]

For these experiments, a three-electrode electrochemical-cell arrangement was used. A schematic of the electrochemical cell is shown as Figure 6.
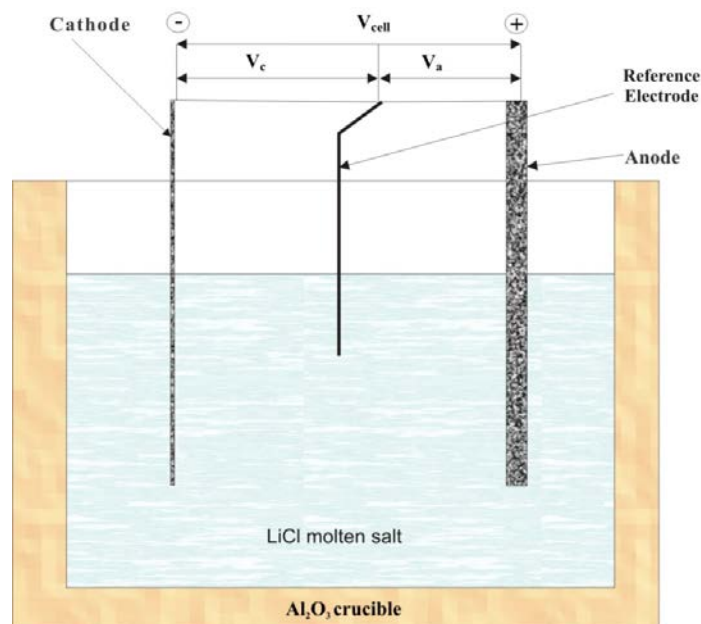
Figure 6. Schematic diagram of the electrochemical cell.

The electrochemistry of the LiCl-Li$_2$O molten-salt systems was studied in a temperature range between 650 and 750°C. The experimental setup included a furnace with a graphite jacket to support a 20 ml crucible and a Watlow temperature controller combined with a k-type thermocouple inserted into the inner wall of the graphite insulator jacket. The equipment maintained the melt temperature within ±5°C of the programmed temperature set point. The working electrode (WE) was suspended from above the melt with a micropositioner arm to control the immersion depth and surface area. To further control the surface area of the WE, the immersion area of the electrode was measured with high-precision digital calipers, subsequent to running experiments. A Biologic USA VSP potentiostat controlled by EC Lab v9.95–v9.98 software was used to perform all electrochemical experiments and data acquisition.

In order to isolate moisture and oxygen-sensitive materials from the ambient atmosphere and other sources of environmental contamination, electrochemical experiments, storage, and handling of all chemicals were carried out in a Labconco glovebox, model 50700. Oxygen content in the glovebox atmosphere was monitored with an Alph Omega 3000 trace-oxygen analyzer, and levels inside the glovebox were maintained below 20 ppm. The glovebox atmosphere was purged with ultra-high-purity-grade argon from Oxarc (CAS number 7440-37-2), containing less than 3 ppm O$_2$. Figure 7 shows the full experimental setup.
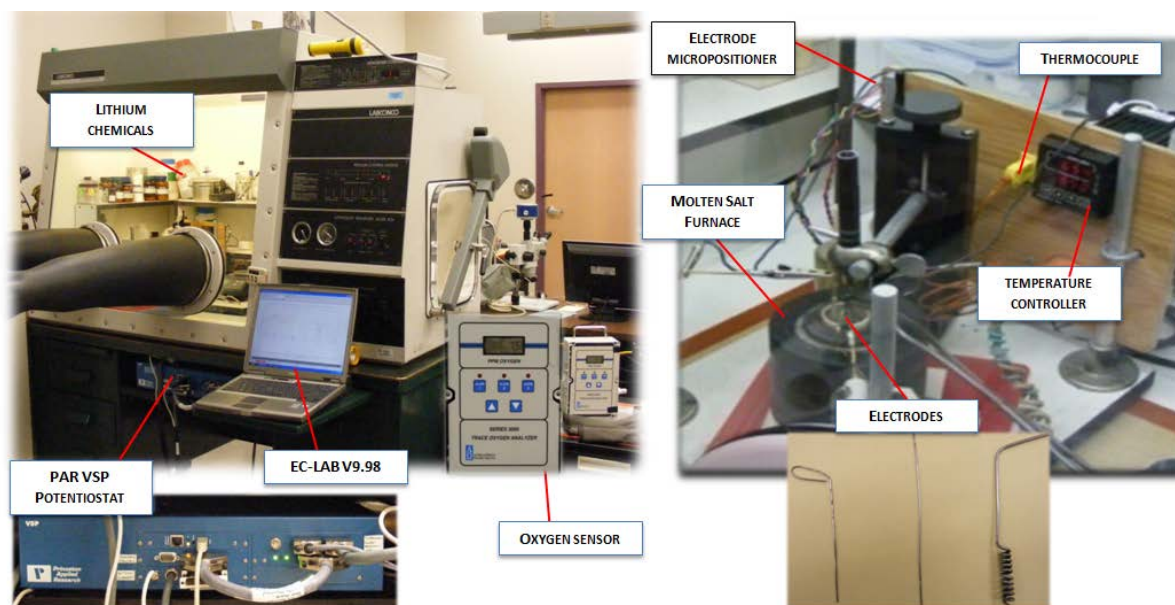
Figure 7. Experimental setup: Labconco glovebox, molten-salt furnace, electrodes, and potentiostat.

The electrolyte chemicals, lithium chloride anhydrous 99.7%, Li_2O 99.5% metals basis and LiOH prepared from LiOH monohydrate were all procured through Alfa Aesar. Alumina (Al_2O_3) 20 ml flat-based crucibles from Alfa Aesar were used for melting the LiCl salts. The electrode materials were also purchased from Alfa Aesar and were of purity greater than 99.99%. The working electrode was made of 1 mm diameter Ni, Mo or SS 304. The counter-electrode was composed of 3 mm high-purity graphite or 1.5 mm Mo coil. Molybdenum wire (0.5 mm) was employed as a quasi-reference electrode (QRE). Molybdenum was determined suitable as a QRE because it could establish reasonable equilibrium potentials with minimal potential drift and it generated reproducible results for the duration of all experiments run and in all of the molten-salt systems investigated throughout this work. Figure 8 shows the electrochemical cell in its normal operating configuration.
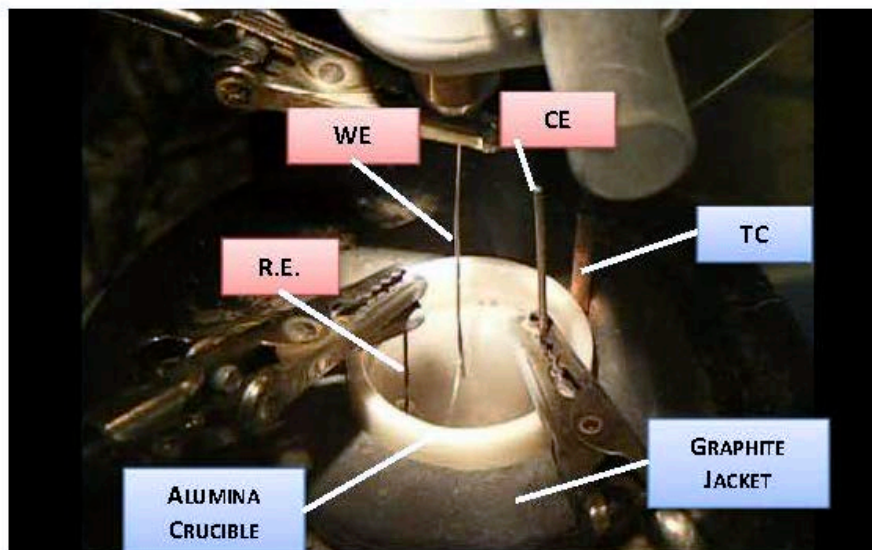
Figure 8. Electrochemical cell and electrodes immersed in LiCl-Li$_2$O molten salt at 650°C.

In preparation for experimental runs, the electrodes were placed in an ultrasonic cleaner containing methanol to remove salt and impurities from previous uses. Once sonicated in an ultrasonic cleaner for 90 seconds, the electrode surfaces were rinsed thoroughly with DI water, lightly sanded with 300- and 600-grit sandpaper, rinsed again with DI water between changes in abrasive levels of sandpaper. After sanding, the electrodes were placed in the ultrasonic cleaner containing methanol once again, for 90 seconds, dried momentarily with a hot air gun to drive off any residual moisture, inserted into an airtight argon capsule, and transferred into the inert-atmosphere glovebox.

To prepare the lithium chemicals for the molten-salt experiments, the hygroscopic nature of each chemical and potential moisture contamination were considered. Guidelines for dehydration of LiCl, Li$_2$O, and LiOH, chemicals have been listed in Table 11. The dehydration of Li$_2$O is the same as the dissociation of LiOH due to the fact that when Li$_2$O reacts with moisture, and as a result, LiOH impurity forms. When heat treating or dehydrating Li$_2$O, it was apparent that there was, in fact, moisture contained in the form of LiOH because the Li$_2$O would agglomerate due to the low melting point of LiOH impurities. To sufficiently remove any LiOH, 5 g of Li$_2$O were spread uniformly in the bottom of an alumina crucible and placed in a furnace and treated at 800°C for 5 hours.

Table 11. Guidelines for moisture removal from lithium chemicals.

Chemical	Reaction		Temperature (°C)	ρ(g/cm^3)
LiCl	Dehydration	LiCl H$_2$O → LiCl$_{(s)}$ + H$_2$O$_{(g)}$	94	2.068 (25°C)
	Melting	LiCl$_{(s)}$ →LiCl$_{(l)}$	610	1.464 (650°C)*
LiOH	Dehydration	LiOH H$_2$O → LiOH$_{(s)}$ + H$_2$O$_{(g)}$	127	1.46 (25°C)
	Melting	LiOH$_{(s)}$ → LiOH$_{(l)}$	471	
	Dissociation	LiOH$_{(l)}$ → ½Li$_2$O$_{(s)}$ + ½H$_2$O$_{(l)}$	600	
Li$_2$O	Dehydration	See LiOH dissociation, above.	600	2.013 (25°C)

* ρ(t) = ρ_m –k(t–t$_m$); where ρ_m = 1.503 g/cm^3, k (cm^3 °C^{-1}) = 0.00432, t$_m$ is the melting point.
For LiCl: ρ(t, C°) = 1.503 – 0.000432(t–610).

Anhydrous LiOH (99.7%) was heat treated to remove any possible moisture impurities.
Lithium hydroxide monohydrate is decomposed to LiOH near 100°C, melts near 480°C, and
can be converted into Li$_2$O above 700°C. Therefore, the LiOH was prepared by heating to
molten phase between 380–500°C. The dehydration temperature of the LiOH was specifically
targeted to fall between the dehydration point of LiOH and below the dissociation of LiOH
into Li$_2$O and H$_2$O. The process of dehydration of LiOH·H$_2$O has been documented
elsewhere.[83,84]

Each molten salt batch was prepared by loading 20 g of LiCl in an alumina (Al_2O_3) crucible and heating to 750°C for several hours to bake off any slag. The temperature of the salt was then reduced to 650°C. Prior to use, each alumina crucible was wiped with methanol, and then baked-out at 850°C for at least 2 hours prior to use. Following the bake-out, the crucibles were immediately stored under vacuum (approximately 20 mm Hg) in the glovebox transfer chamber after evacuating with argon. The furnace temperature controller was set to 700–720°C in order to achieve 650–665°C in the salt. After inserting the electrodes in the molten salt, the open circuit potential (OCP) was monitored for 30 minutes or until a reasonable equilibration was reached (indication that solutes such as Li_2O, LiOH had dissolved or fully dissociated). The working electrode (WE) was removed and re-immersed into the melt to free up any slag into melt as well as any slag collected due to the cold finger effect around the top of the electrode. The other electrodes were tapped to dislodge any adsorbed gas bubbles and traces of debris and then repositioned following the °CP monitoring before running electrochemical experiments.

3.1.1 Crucible Cleaning

Most of the alumina crucibles used for containment of the molten salts were new, in which case they were baked out prior to use by heating in an air-atmosphere furnace at 900°C for 2 hours. If the alumina crucibles were used in prior experiments, then they were soaked in in tap water overnight, rinsed with reverse-osmosis water, boiled in DI water for 2 hours, then rinsed with DI water and boiled in 1% HCl-DI for 2 hours. The crucible was then heated in an air-atmosphere furnace to a set point of 900°C for 2 hours and cooled down in furnace prior to use.

3.2 Salt Preparation

3.2.1 Lithium Chloride

Although LiCl was purchased in anhydrous form, it was heat treated in the glovebox to ensure that there remained no water that might have been absorbed from the atmosphere during storage. The heat treatment temperatures were based on the dehydration of LiCl explained by Masset[85] and others based on the dehydration of LiCl above 160°C in conjunction with experimental data of this work, as depicted in Figure 23(a)(b).

To prepare the LiCl for experiments, it was heat treated in the glovebox by holding it at a temperature of 585°C, or just below its melting point of 605°C for 5 hours. The reason for holding below the melting point was due to the finding that suggests that, at extreme temperatures, hydrolysis can occur.[101] It was then cooled inside the inert atmosphere glovebox to ambient temperature and stored in an air-tight amber bottle under ultra-high-purity argon.

To prepare experiments with LiCl molten salt, 20 g of the heat-treated anhydrous LiCl was loaded into a clean alumina crucible and heated to 750°C. Experiments were run as explained in Section 3.1 above.

3.2.2   Lithium Chloride with Li$_2$O

To prepare LiCl molten salts with Li$_2$O, in addition to the LiCl preparations listed in Section 3.2.1, the lithium oxide required heat treatment prior to charging into the molten LiCl. In this process, 5 gram batches of Li$_2$O were placed into a cleaned alumina crucible and calcined in an air-atmosphere furnace at 850°C for 5 hours to ensure that any potential moisture impurities would be driven off. After heat treatment, the lithium oxide was charged into the LiCl molten salt. The flow diagram in Figure 9 shows the steps for preparing the molten salt for electrochemical experiments.

Heat treat LiCl·H$_2$O

↓

Return to R.T.

↓

Add Li$_2$O

↓

Melt LiCl mixture

↓
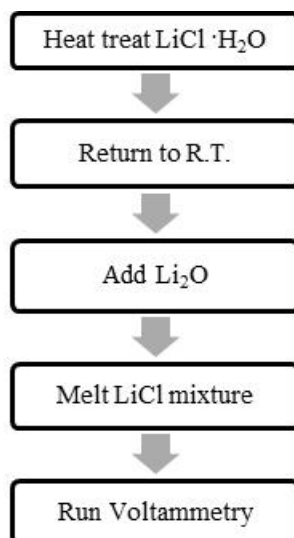
Run Voltammetry

Figure 9. Preparation of LiCl-Li$_2$O molten salts.

The purity of the heat-treated LiCl (99.6%) was tested by comparing it with cyclic-voltammetry (CV) experiments run with 99.995% ultra-dry LiCl. The ampoule of 99.995% ultra-dry LiCl was not opened until immediately before the experimental run.

3.2.3   Lithium Chloride Solution with LiOH

To prepare anhydrous LiOH, LiOH·H_2O was heat-treated at 380°C to remove the physically absorbed water. In order to confirm that LiOH was pure, a melting-point test was run. This confirmed that, at 470°C (the melting point for LiOH), the LiOH melted. To prepare the LiCl-LiOH solution, the specified amount of LiOH was added to 20 g of LiCl and homogenized by grinding prior to melting.

3.3   Experimental Techniques

Cyclic voltammetry (CV), chronopotentiometry (CP), and chronoamperometry (CA) were carried out in an electrochemical cell with a three-electrode setup. A Princeton Applied Research (PAR) VSP potentiostat was used with exclusive EC-Lab V9.98 electrochemical software.

During CV runs, the potential is varied linearly as a function of time, with scan rate v and, typically, the current is recorded as a function of potential. This method is informative as to the qualitative aspects of an electrode process. Cyclic voltammetry is the most widely employed technique in the field of voltammetry to study electrode kinetics. Figure 10 shows a generalized schematic of the potential scan applied to a working electrode during a CV run.[86] For the case of a reversible electrode process, the peak current in a cyclic voltammogram is given by the Randles- Sevčik equation,[87] which will be described in more detail in Section 4.4.2.1.
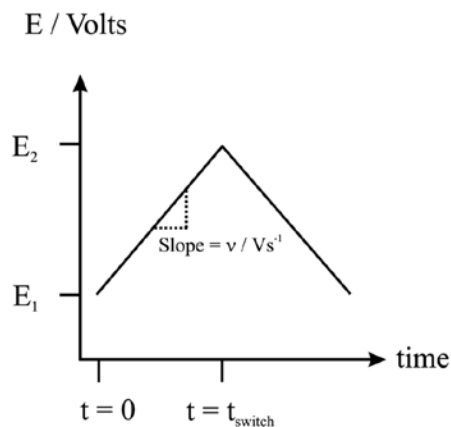
Figure 10. Potential waveform of applied to the working electrode during a cyclic voltammetry run.

Chronopotentiometry is a controlled-current technique wherein a constant current is applied at the working electrode, and the variation of potential with time is recorded on the working electrode. The Sand equation, which will be described in more detail in Section 4.6, gives the transition time, τ, as shown in Figure 11,[87] and the diffusion coefficient for the diffusing species can be determined.
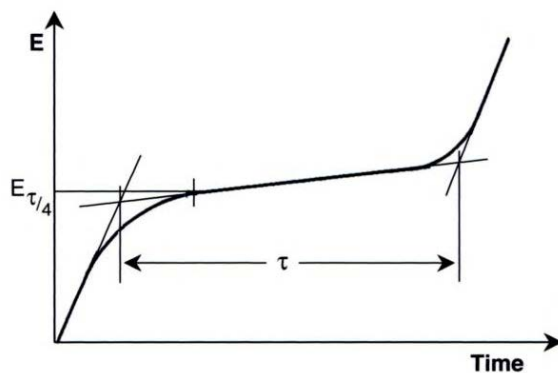
Figure 11. CP schematic for a reversible electrode process indicating τ.

Chronoamperometry is a controlled-potential technique and is another technique which can be used to determine the diffusion coefficient of diffusing species in the analyte. During a chronoamperometry experiment, a constant voltage is applied, and the current is measured as a function of time. Chronoamperometry is a useful technique in those cases in which CV does not succeed in identifying the electrode mechanisms underlying certain redox changes.[88] The governing equation for CA is the Cottrell equation, which indicates that, for a diffusion

controlled process, the concentration of electroactive species present in the bulk of the solution decays following a function which is inversely proportional to the square root of time.[88] The Cottrell equation will be described in further detail in Section 4.5. A schematic of a typical wave form of the applied potential and the current response is shown in Figure 12, where the diffusion controlled current is governed by the Cottrell equation.[89]
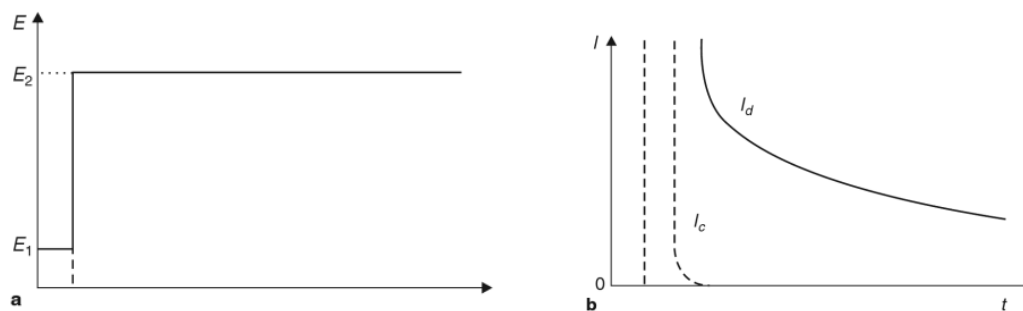
Figure 12. CA schematic potential step (a) and resultant current flow (b) for capacitive current, I_c, and diffusion controlled current I_d.

Chapter 4: Results

The electrochemical behavior of Li_2O in LiCl molten salt and the effect of moisture interaction in this molten salt system were studied. The salt systems and techniques used for this study have been outlined in Figure 13.
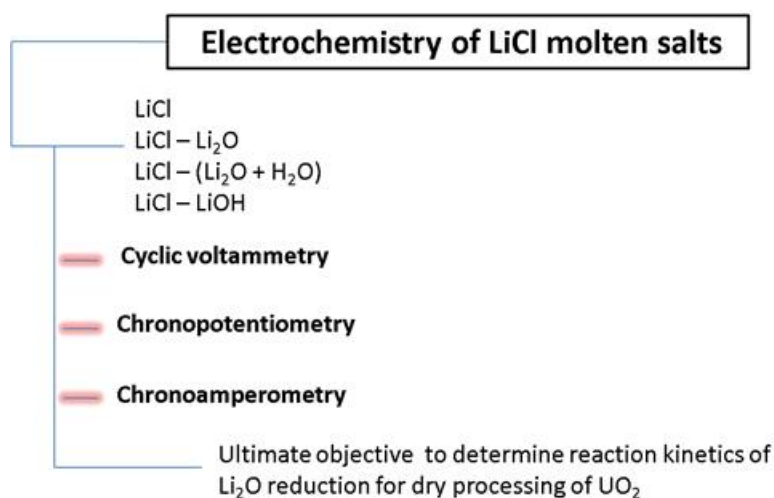
Figure 13. Outline of the salt systems and electrochemical techniques.

4.1   Overview

The results from CV studies for each salt composition will be discussed first. The effect of moisture in 1) LiCl, (2) LiCl-Li_2O, (3) LiCl-(Li_2O + H_2O) and (4) LiCl-LiOH molten-salt compositions will be addressed. Chronopotentiometry and chronoamperometry were ancillary techniques used to confirm result from CV experiments.

According to the results of the CV, the presence of 1 wt% Li_2O in LiCl will cause a positive shift in the reduction potential of lithium by 0.8 V. The shift of reduction potential in LiCl-Li_2O was also confirmed by CP. Because of the highly hygroscopic nature of LiCl and reactivity of Li_2O with water, it was decided to examine the effect of moisture with the cyclic voltammetry technique. For that purpose, aliquot amounts of water were pipetted to LiCl salts, and the effect monitored was the development of a precurrent, which is defined as current prior to the onset of the lithium-ion-reduction current. It should be noted that, in the experimental conditions, precurrents were noticeable even with ultra-dry LiCl salts of 99.995% purity.

Hur et al.[6] found that the decomposition voltage of Li_2O is based on an activity coefficient of 8.4 for Li_2O in LiCl and on the measured solubility of 11.9 mol% (8.7 wt%) at 650°C. The reduction of lithium from $LiCl-Li_2O$ (Equation 17) can be expressed by the Nernst relationship (Equation 18) where $E°$ is the standard potential of an electrode, R is the gas constants, T is the temperature and F is the Faraday constant. The activity of metallic lithium (Li°) and lithium ions (Li^+) are given as $a_{Li°}$ and a_{Li+}, respectively.

$$Li^+ + e = Li° \tag{17}$$
$$E = E° + RT/nF*ln(a_{Li+}/a_{Li°}) \tag{18}$$

When more than a monolayer of lithium is deposited on a solid electrode at any given time, the activity for lithium, $a_{Li°}$, can be assumed to be equal to 1 and, consequently, $E = E°$. However, when there is less than a monolayer of lithium deposited on the surface of the electrode, the activity of lithium is not equal to 1, $a_{Li°} \neq 1$. For the latter case, lithium deposition will begin at underpotential, which is deposition at a potential more positive than values where deposition of lithium occurs on pre-deposited lithium.[6] Therefore, when lithium is reduced and then dissolved into the melt, the electrode surface is continuously in the $a_{Li°} \neq 1$ state, and lithium underpotential deposition (UPD) will occur.

4.2   Electrode Materials Observations

Finding materials that are stable in the molten-salt systems can be a challenge. In early experiments, a Ag/AgCl-based reference electrode with mullite sheathing was used as a reference electrode, and molybdenum was used as a counter-electrode, then tungsten was attempted but, after the experimenter observed significant reactivity during lithium production runs, the use of these electrodes was discontinued. Scanning electron microcopy (SEM) and energy-dispersive spectroscopy (EDS) analysis of post-test mullite with black deposit is provided in Appendix A-1, and for molybdenum and black deposit of tungsten or a tungsten compound, in Appendix A-2 and Appendix A-3, respectively.

Platinum was another material used as an electrode during electrochemistry experimentation in $LiCl-Li_2O$ molten salts; however, reactivity with lithium caused spalling and cracking. SEM analysis of the electrode tip confirmed these results, as shown in Figure 14.
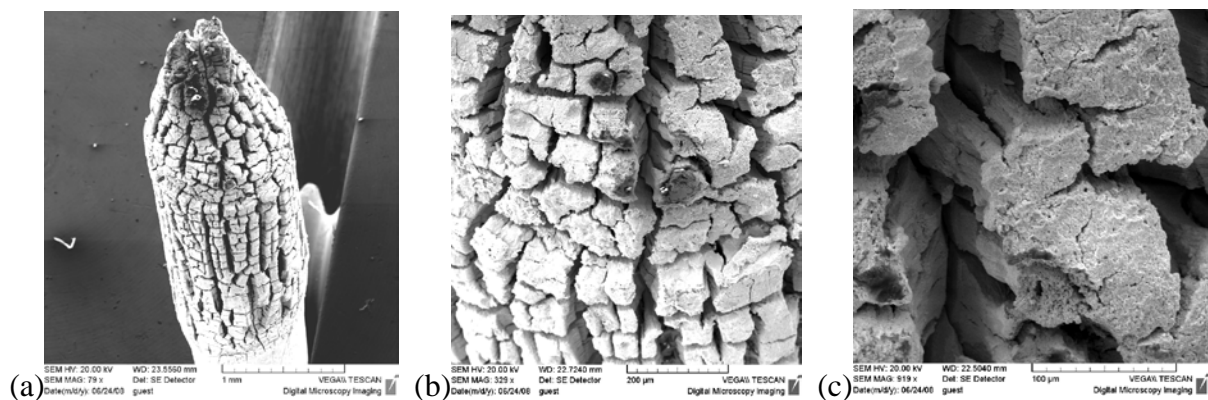
Figure 14. SEM images of platinum wire used for a cathode material at (a) 79×, (b) 329×, and (c) 919×.

Another material used as an electrode was stainless steel (SS) 304. Corroded SS 304, used as a working electrode for some of the electrochemistry runs in LiCl-Li$_2$O-based molten salts, is shown in Figure 15. Early on, studies using SS 304 as electrode materials were performed. However, reactivity with lithium was observed during cyclic voltammetry runs (Appendix D). EDS analysis indicated oxygen in the corrosion-scale region on the SS 304 post-test electrode. Nickel and iron were also present, but uniformly across the whole specimen, and not segregated like oxygen.
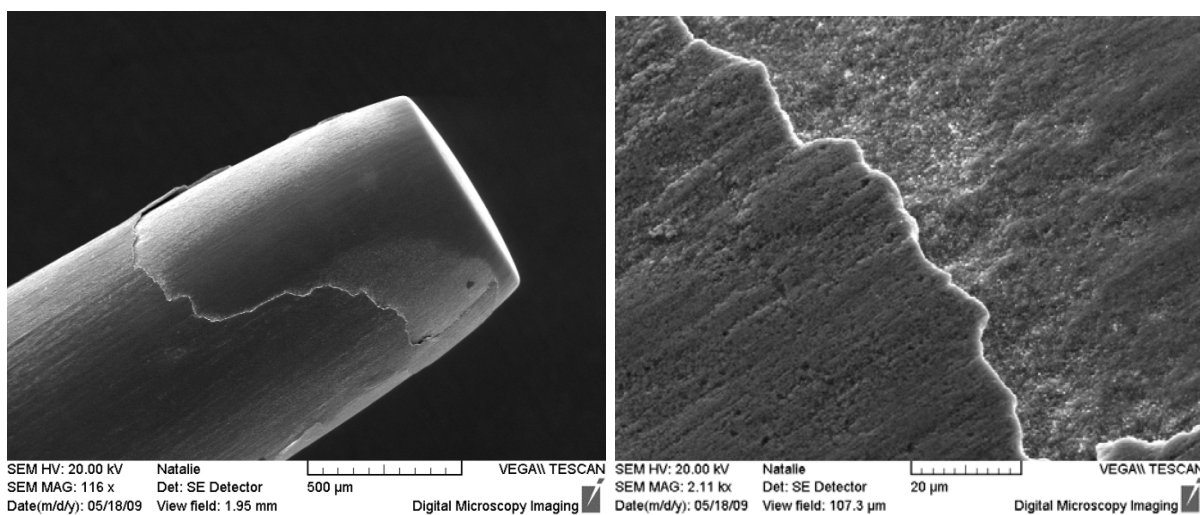
Figure 15. SEM SE images of corrosion scale on SS 304 corroded in LiCl-1 wt% Li2O, 4 hours, taken at 116× (left) and 2.11k× (right).

Corrosion of tungsten used as a counter-electrode can be observed in Figure 16. SEM SE images show pits in the metal that formed after being exposed to LiCl-Li$_2$O-based molten salt for approximately 4 hours while being used as a counter-electrode during various electrochemical runs.
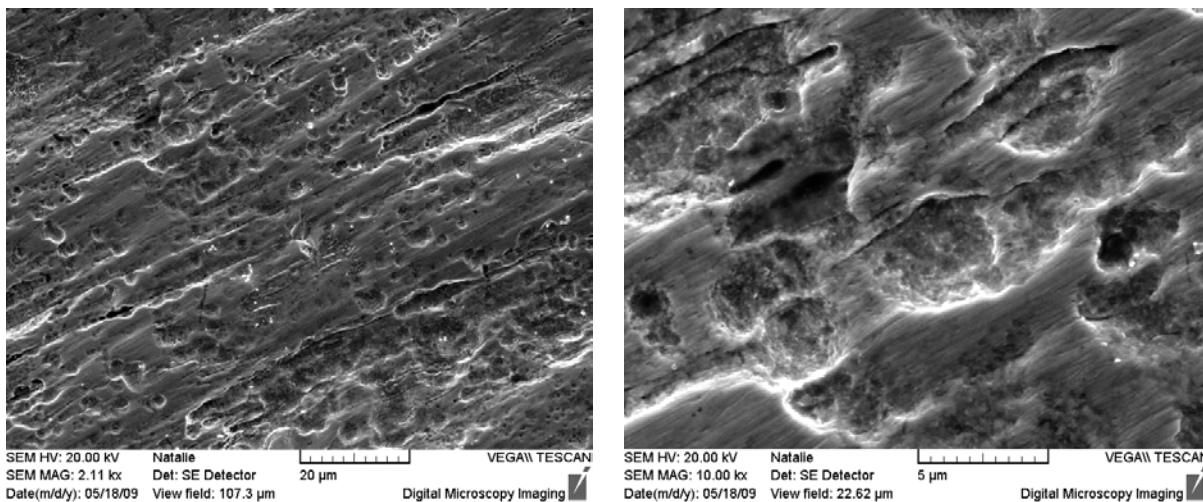
Figure 16. SEM SE images of W corroded in LiCl-1 wt% Li$_2$O, 4 hours, 2.11 k× (left), 10,000 k× (right).

The electrode materials which performed well as working electrodes were nickel and molybdenum. For the counter-electrode, glassy carbon, or high-purity graphite, was used, and molybdenum was used as a quasi-reference electrode, but not as a counter-electrode due to observed degradation indicated in the SEM results included in Appendix A-2. Although the carbon based counter-electrodes did undergo some degradation, the formation of CO$_2$ was expected and to evolve out of the system. However, in the case of tungsten, and molybdenum, blue discoloration in the salt indicating the formation of tungsten and molybdenum oxides were not favorable reactions for this study because the deposition of these compounds, soluble in the molten salt, were a possibility. A tungsten-based dendritic deposit formed on a nickel working electrode due to tungsten degradation during electrochemistry experimentation in the LiCl-Li$_2$O-based molten-salt system can be seen in the SEM SE image in Figure 17.

SEM HV: 20.00 kV   Natalie   [scale bar]   VEGA\\ TESCAN
SEM MAG: 19.91 kx   Det: SE Detector   2 μm
Date(m/d/y): 06/17/09   View field: 11.36 μm   Digital Microscopy Imaging
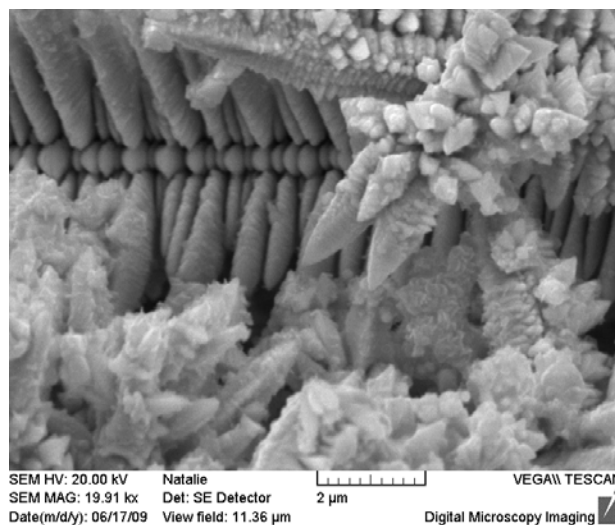
Figure 17. Black-tungsten-based deposit found on nickel working electrode.

Thermodynamics suggest that WO2 (ΔGf = -100.248 kcal/mol) and MoO2 (ΔGf = -113.703 kcal/mol) will have a tendency to form and comprise the violet or purple color that has been observed in the molten salt following electrochemical runs when these materials were employed as counter-electrodes. The cell potential for both the reduction at 650°C of WO2 (-2.18 V) and MoO2 (-2.17 V) is slightly less that the cell potential for Li2O (-2.46 V) which means that these species are likely going to deposit if present in the molten salt.

Information on a lithium-intercalated graphite counter-electrode is discussed in Appendix B. An unsuccessful attempt was made using this kind of electrode to aid the kinetics of lithium reduction.

Anodic polarization and corrosion studies in LiCl, LiCl-Li2O and LiCl-LiOH systems can be reviewed in Appendix C and Appendix E.

4.3   Moisture Removal Attempted by Chronoamperometry Method

Early experiments conducted in the LiCl-Li$_2$O-based molten-salt system attempted to remove moisture content from the salt by applying a constant potential of -0.7 V until the current decayed toward zero, indicating that moisture was removed. However, after 2 hours, and passing 1203 coulombs charge, the cathodic current remained steady. This indicated that more than a trace amount of moisture had contaminated the salt. The charge passed corresponded to 0.012 mole electrons. For a two electron charge transfer process this corresponds to 6.291x10^{-3} moles of an unknown species. For the reduction of water, this corresponds to 6.291 $\times$ 10^{-3} g H$_{2(g)}$ produced.
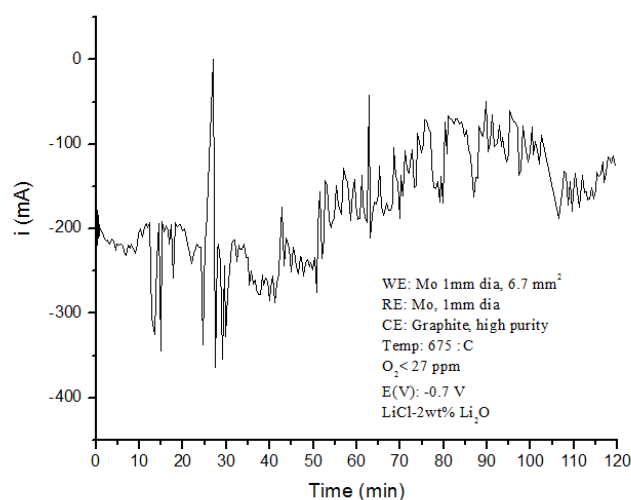
Figure 18. Electrolysis of LiCl-Li$_2$O in attempt to remove moisture contamination for 2 hour at -0.7 V, Mo WE, Mo RE and graphite CE.

As the electrolysis proceeded, the salt went from being clear and translucent in appearance to a deep, metallic greyish black and opaque. This observation will be discussed in subsequent sections as black metal fog and is shown in Figure 19. It appears that lithium reduction was occurring in a region prior to the standard potential for the onset of lithium reduction simultaneously with hydrogen's being generated at the cathode. This is indicated by the black buildup of insoluble metallic lithium.

Figure 19. Electrolysis of LiCl-Li₂O in attempt to remove moisture contamination for 2 hour at -0.7 V, Mo WE, Mo RE and graphite CE.

Because of the metallic lithium and build up and black discoloration during this attempt to remove moisture contamination, the heat-treatment method for removing moisture from LiCl was applied to all salts for preparation.

4.3.1 Removal of H₂ from the LiCl-LiOH System

In attempt to determine whether it would be possible to electrochemically purify moisture-containing molten salt from the reaction of Li_2O with H_2O to form LiOH, a controlled salt composition, LiCl-0.5wt% LiOH, was used to demonstrate the feasibility of electrochemical purification of the salt. To this end, the application of constant potential at a selected voltage in the pre-lithium-reduction range was applied; however, it was calculated that the amount of charge necessary for the removal of H_2 from the system was nearly four times more than the coulombs charge that was passed during these constant-potential runs (Equation 19).

$$\frac{96480 \text{ C}}{\text{mol·eq}} * (0.020886 \text{mole } H_2)(\text{eq}) = 2015 \text{ C} \tag{19}$$

A control experiment was run in the blank LiCl system by applying a constant potential of -1.0 V as indicated on the CV in Figure 19(a). The resulting current for the control is shown in Figure 19(b). Potentials selected from CVs run in the LiCl-0.5 wt% LiOH system, with a graphite counter-electrode and a shrouded graphite counter-electrode, were selected at -1.2 V and -1.0 V respectively. These voltages were selected at the maximum-cathodic-peak current, as indicated in Figure 19(a).
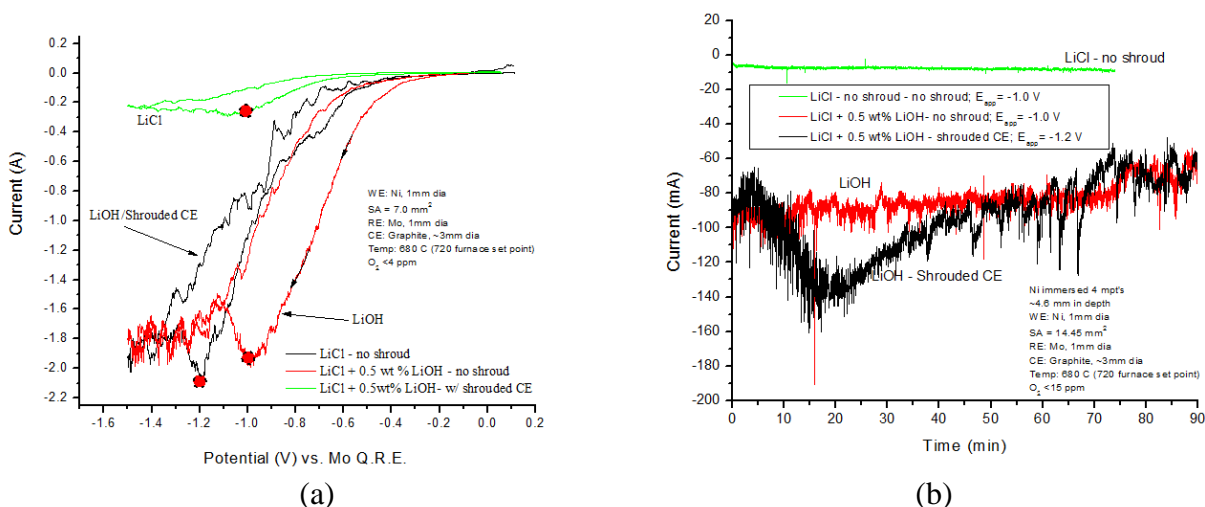
Figure 20. CV of (a)LiCl, LiCl-LiOH, and LiCl-LiOH with shrouded electrode and (b) constant potential runs in attempt to exhaust hydrogen from the system.

A summary of conditions for these experiments is listed in Table 12. A second run with a shrouded counter-electrode was performed to determine the effect of removal of H_2 from the LiCl molten salt. However, the use of the shroud caused a negative shift for the onset of the reduction current, and it was concluded that the shroud caused increased cell resistance due to the tortuous path necessary for the diffusing anions through a porous alumina shroud. Gas bubbling up through the shroud also caused salt to solidify at the top opening of the shroud and eventually, sealed off the top opening and precluded gaseous reaction product, O_2, from escaping through the shroud. Small oxygen bubbles then coalesced to form a large oxygen bubble, which finally ruptured and escaped through the salt under the shroud. Because the shroud was not effective for this type of experiment, it was not used in future experiments.

Table 12. Parameters for constant potential runs to remove moisture.

Salt Composition	Applied Potential (V)	Time (min)	Shrouded CE ?	Actual Charge Passed (C)	H_2 (moles)	Total Theoretical Charge needed for removal of H_2 Assuming 100% current efficiency (C)
LiCl (for background/control)	-1.0	70	No	33.695	--	--
LiCl + 0.5wt% LiOH	-1.0	90	No	450.423	0.020886	2015.19
LiCl + 0.5wt% LiOH w/shrouded CE	-1.2	90	Yes	509.055	0.020886	2015.19
[†] Note: moles of reduced reactant were calculated by subtracting the background current from the LiCl control						

After these experiments were run, it was determined that electrochemical removal of moisture from the salt was not the most effective approach. Heat-treating LiCl and then electrochemical removal of residual trace quantities of moisture would be a more efficient approach.

4.4   Cyclic Voltammetry

Cyclic voltammetry was carried out in a three-electrode electrochemical cell and was studied in three different molten-salt systems: (1) LiCl (2) LiCl-Li$_2$O and (3) LiCl-LiOH. Figure 21 shows the thermodynamic effect on the cyclic voltammetry for Li$_2$O addition to LiCl molten salt. Cyclic voltammetry of LiCl and LiCl-Li$_2$O molten-salt systems shown in Figure 21 were run at 650°C at a scan rate of 20 mV/s. Lithium-oxide concentration of 1 wt% was added to molten lithium chloride.
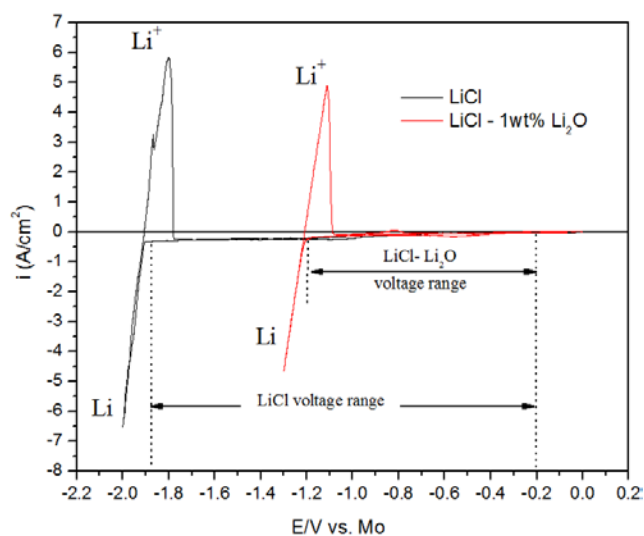
Figure 21. Lithium reduction from LiCl and LiCl-Li$_2$O molten salts at 650°C, characterized by CV at 20 mV/s scan rate (left), and by CP at -100 mA imposed current (right). Conditions: WE(Ni), QRE(Mo), CE(glassy carbon).

The reduction potential of Li from Li$_2$O in molten LiCl should be shifted by 1 V; i.e., the electrochemical window for the reduction of lithium is reduced by 1 V. Calculations, based on Gibbs free energy of formation, have been provided in Table 13. Calculations for uranium and moisture have also been included for comparison and to show reduction of both lithium and uranium will be preceded by the reduction of hydrogen when moisture is present in the LiCl-Li$_2$O-based molten salt.

Table 13. Thermodynamic values for electrochemical redox at 650°C.

Overall	ΔG (kcal/mol)	Half-cell reactions	Standard Potential E(V) vs. SHE
$LiCl = Li° + \frac{1}{2}Cl_{2(g)}$	79.76	Cathode: $Li^+ + e = Li°$ Anode: $Cl^- = \frac{1}{2}Cl_2 + e$	-3.46
$Li_2O_{(LiCl)} = 2Li° + \frac{1}{2}O_{2(g)}$	113.70	Cathode: $2Li^+ + 2e = Li°$ Anode: $O^{2-} = \frac{1}{2}O_2 + 2e$	-2.46
$UO_2 = U° + O_2(g)$	79.76	Cathode: $U^{4+} + 4e = U$ Anode: $2O^{2-} = O_2 + 4e$	-2.40
$H_2O = H_2(g) + \frac{1}{2}O_2(g)$	36.57	Cathode: $2OH^- + 2e = H_2 + 2O^{2-}$ Anode: $O^{2-} = \frac{1}{2}O + 2e$	-1.59

The standard reduction potentials for lithium reduction with and without the addition of Li_2O are listed in Table 13. In theory, the addition on Li_2O will make lithium reduction more thermodynamically favorable, thus shifting the reduction potential of lithium by nearly 1 V.

Control experiments using a molybdenum (Mo) working electrode were carried out in the molten LiCl and showed no significant peaks within the electrochemical window from −2.0 V (Li^+ reduction) to 0 V vs. a Mo quasi-reference electrode.

The dehydration of lithium-chloride salt is important. When lithium oxide is added, LiOH can form if the LiCl is not anhydrous. Because LiCl is very hygroscopic, trace amount of moisture are easily reacted with the lithium oxide to produce lithium hydroxide. Purity of LiCl was a concern, so aside from the typical anhydrous LiCl (99.995%) used, an ultra-dry grade was used as a control to ensure that the purification for the lower-purity anhydrous LiCl (99.6%) was sufficient, as shown in Figure 22.
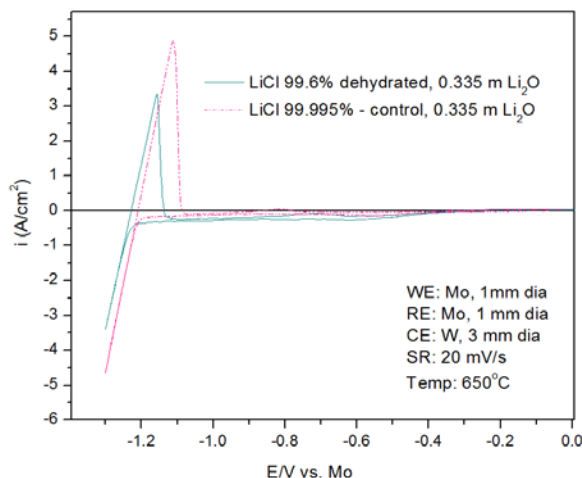
Figure 22. Cyclic voltammograms of LiCl-Li$_2$O molten salts.

CV experiments were run to compare the lower-grade lithium chloride to that of the ultra-dry, high-purity grade. The lower grade showed reasonable purity, as can be seen by the extent of the cathodic precurrent prior to the reduction of lithium at about -2.25 V. The CV runs shown in Figure 22 indicate by the low-current values prior to the onset of lithium reduction (-1.25 V) that the 99.6%-purity heat-treated LiCl had slightly higher precurrent values between the 0 and -1.2 V prior to lithium reduction, which occurs at approximately -1.25 V versus a molybdenum quasi-reference electrode. Because the same dehydrate Li$_2$O was used for both runs, additional moisture of hydroxide must be present in the lower-purity salt.

4.4.1   Salt Heat-Treatment Tests

To further address the effectiveness of the heat-treatment method employed for the purification of LiCl salts, the experimental procedure outlined in Figure 9 was employed to run a set of CV experiments as a function of heat-treatment temperature with LiCl salt containing 0.5 wt% H$_2$O. After the heat treatment of the LiCl-0.5wt% H$_2$O, a 2 wt% amount of Li$_2$O was added to the salt at molten temperatures. These results indicate that heat treatment for a very short time duration (1 hour) effectively removes moisture from the LiCl sufficiently above treatment temperatures of 400°C. The heat treatment should be performed on all lower-grade LiCl salt prior to mixing with Li$_2$O in order to preclude hydroxide formation.
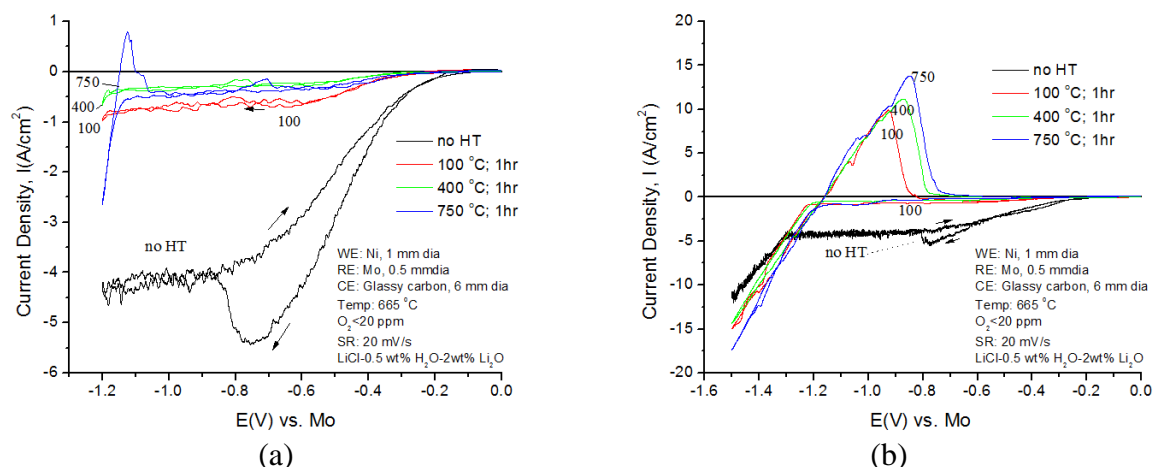
Figure 23. Effect of heat-treatment temperature on moisture removal from of LiCl as a function of CV vertex potential of (a) -1.2 V and (b) -1.5 V.

Because there was residual unreacted Li_2O in the non-heat-treated salt, there was likely simultaneously reduction of lithium and hydrogen. This is indicated by the onset of lithium reduction at approximately -1.4 V. However, in the presence of hydrogen reduction, the lithium was either reacted or scavenged away from the electrode, restricting availability for oxidation, which is indicated by the absence of the anodic peak in the CV of the non-heat-treated salt, shown in Figure 23(b). The anodic-peak current also increases with increasing heat-treatment temperature. At 750°C, a maximum anodic peak current was obtained.

4.4.2   Cyclic Voltammetry in the LiCl System

In the LiCl molten-salt system, moisture content does not play a significant role in the electrochemistry of lithium. Lithium chloride containing moisture by itself will not show retention of moisture. The reason for this is that hydrated lithium chloride will release moisture if heat treated above 94°C. The LiCl system was used as a control to compare with the $LiCl-Li_2O$, and LiCl-LiOH systems. Various concentrations of moisture were added to LiCl salt prior to melting. Cyclic voltammograms were recorded for 0.25, 0.5, 1, and 2 wt% H_2O. There was no variation in the CV characteristics for scan rates run at 20 and 500 mV/s.

4.4.2.1   Effect of Scan Rate

To study the LiCl system the effect of scan rate was varied between 2.5 and 50 V/s for several different temperatures. It appears that a reaction occurs at approximately -1.2 V, as seen in Figure 24. For high and low scan rates, the system showed reversible behavior according to Randles-Ševčík equation (Equation 15), where n is the number of electron transferred, v is the scan rate (V/s), F is Faraday's constant, 96,485 coulombs/(mole e), A is the electrode surface area (cm^2), R is the gas constant 8.314 J/(mole K), T is the temperature (K), and D is the diffusion coefficient of the electroactive specie (cm^2/s). If the Randles-Ševčík equation is linearized, then there is reversible electron transfer, and the peak height versus the square root of the scan rate produces a linear plot; thus, the diffusion coefficient can be determined.

$$i_p = 0.4463 \text{ n F A C} \left(\frac{n F v D}{R T}\right)^{\frac{1}{2}} \tag{20}$$

For the LiCl system, when the scanning rate exceeds 50 V/s, the reaction begins to be challenged; however, for this molten-salt system, there was no Randles-Ševčík relationship found. As the lithium ion was abundant near the cathode, there was no polarization of the concentration of Li^+ around the cathode and no limiting current was observed. In the range between open-circuit voltage and greater than -1.8 V cathode potential, cyclic voltammograms of LiCl were performed between 20 and 1000 mV/s, as shown in Figure 24(a). Low cathodic precurrents were observed, indicating no effect of scan rate for CV scans within the pre-lithium-reduction voltage window scanned. There were no reactions of interest observed. In the voltage range between -2.2 V and open-circuit potential (0.150 V), CVs of LiCl were performed between 1 and 200 V/s, as shown in Figure 24(b).
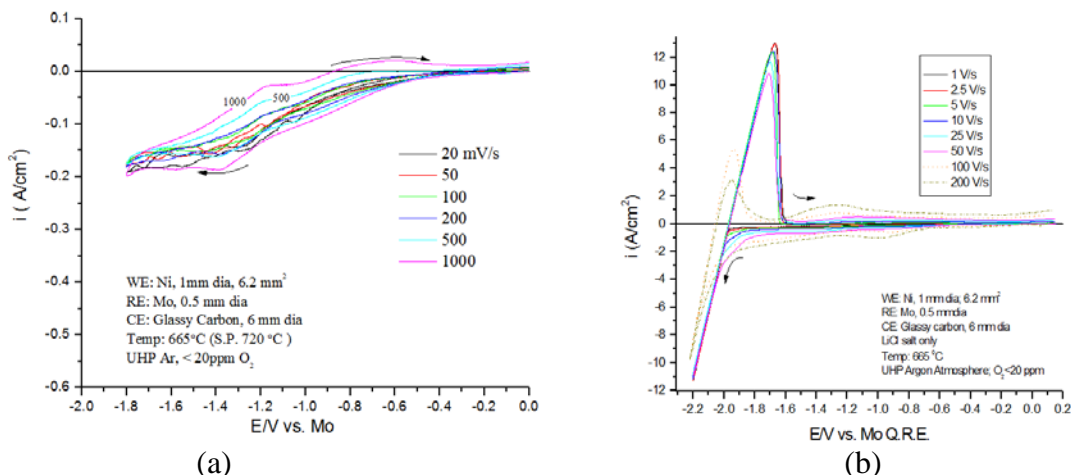
Figure 24. Cyclic voltammograms of Li reduction from LiCl molten salts as a function of scan rate on Mo WE at 720°C with Mo counter-electrode and Mo reference electrode in blank LiCl molten salt. Scan rates: (a) 20, 50, 100, 200, 500, and 1000 mV/s and (b) 1, 2.5, 5, 10, 25, 50, 100, and 200 V/s.

For CVs of the reduction in LiCl molten salt, scan rates (a) 20, 50, 100, 200, 500, and 1000 mV/s showed a minimal dependence on the increase of scan rate. However, when the scan rates were increased to 1, 2.5, 5, 10, 25, 50, 100, and 200 V/s, the reaction was challenged when the scan rate exceeded 50 V/s.

At the slow scan rates, low cathodic precurrents prior to lithium reduction occurring at potentials more anodic than -2.0 V were observed, and no effect of scan rate corresponding to the Randles-Ševčík relationship for a diffusion-controlled process was observed for CV scans of the LiCl molten-salt system, as shown in Figure 24(a). The electrode reactions in the LiCl molten-salt systems were found to be exceptionally fast.

Fast-scan cyclic voltammetry was run in the LiCl-based system at 670, 700, 720, and 750°C, as shown in Figure 25(a-d).
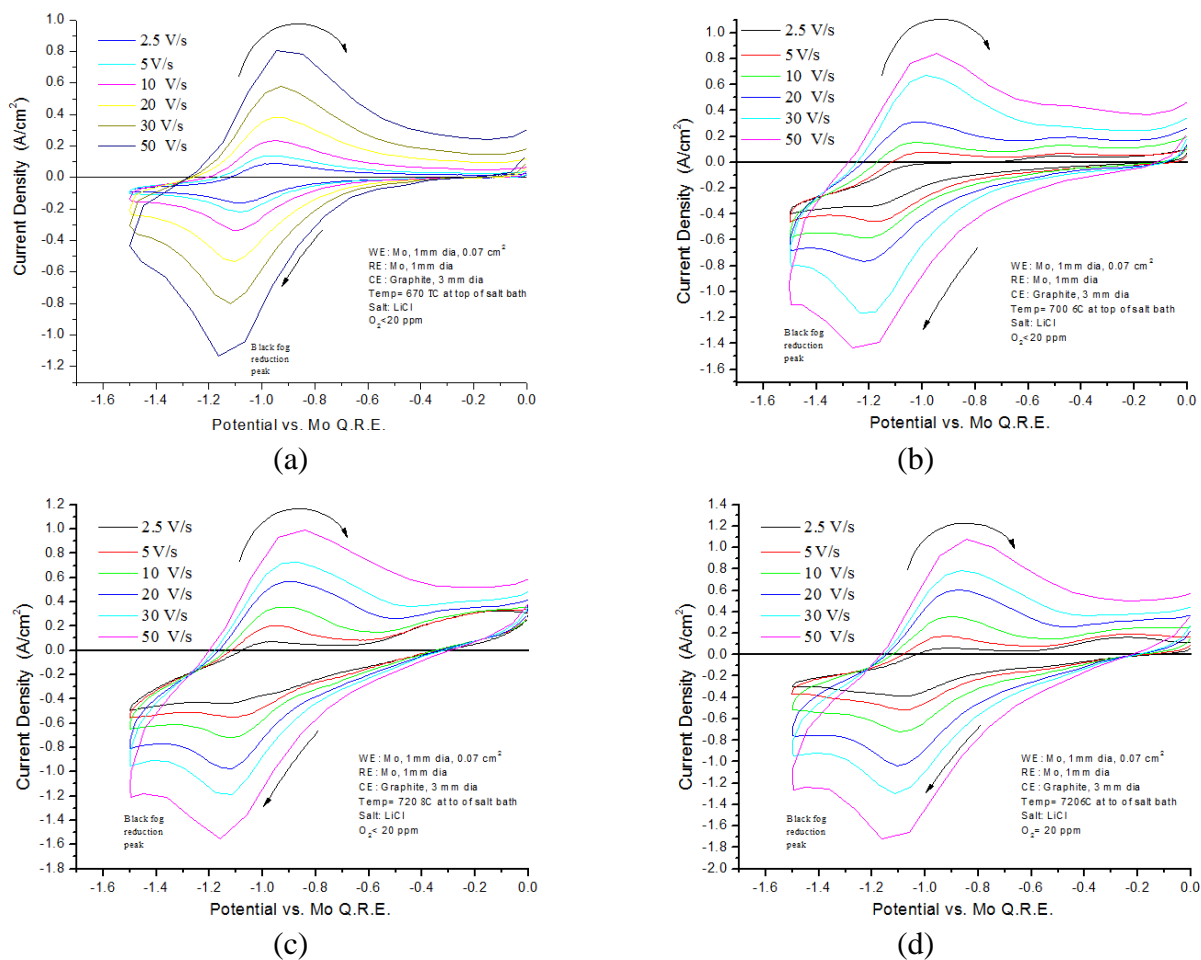
Figure 25. Fast scan cyclic voltammetry as a function of temperature for (a) 670°C, (b) 700°C, (c) 720°C, (d) 750°C.

For each temperature, the cathodic peak current versus the square root of the scan rate was plotted to determine the scan rate dependence, as shown in Figure 26.
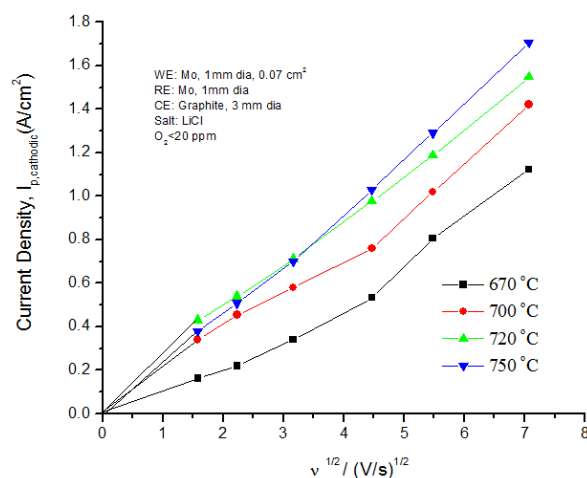
Figure 26. Randles-Ševčík plot as a function of temperature.

4.4.2.2 Effect of Scan Range

The effect of scan range was studied to pinpoint the onset of various reactions in the precurrent ranges, as shown in Figure 27, on both molybdenum and nickel working-electrode materials. Black metal fog[90, 91] was observed at the working electrode in CV experiments runs during the forward scan in the cathodic direction. Black fog was visible in the full precurrent range and beyond. The precurrent range is defined by current generated prior to the onset of reduction of lithium at -1.8 V. This black fog may be attributed to the underpotential deposition (UPD) of lithium.

(a)	(b)
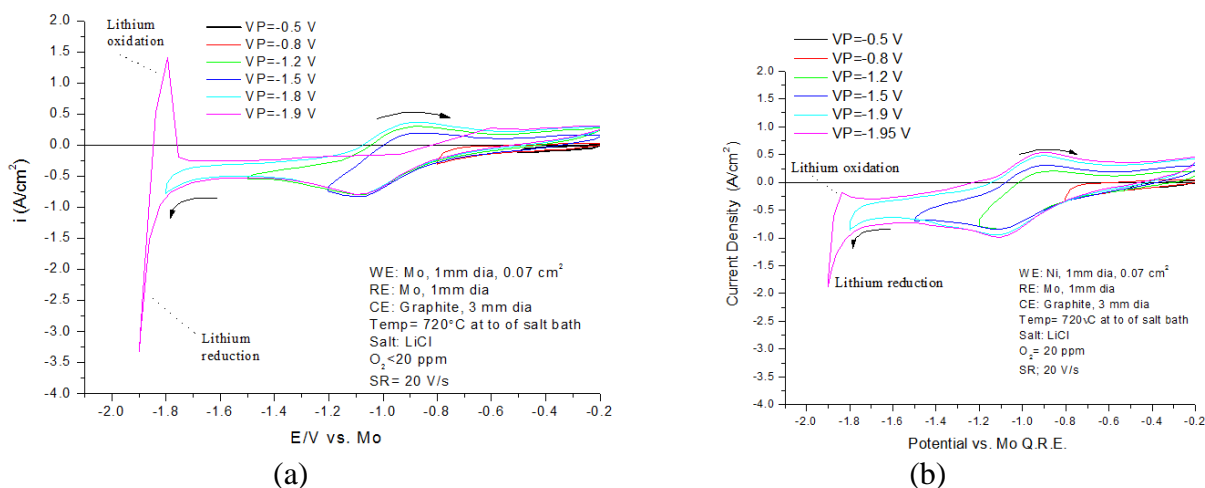
Figure 27. Effect of scan range on CV of LiCl molten salt at 20 V/s for a series of vertex potentials that were run in order from OCP and then scanned to specified vertex potential in the negative sweep direction then back to OCP.

It is the UPD of lithium that is likely responsible for this kind of cathodic precurrent. When the activity of lithium is less than 1, the redox potential is shifted positively, as was explained in Section 4.1. To reiterate, according to the Nernst equation, when the value for activity is less than 1, the values for the reduction potential become more positive (less cathodic). For lithium reduction in Equation 21, the reduction potential is -3.048 V (SHE).

$$LiCl \leftrightarrow Li_{(l)} + \frac{1}{2} Cl_{2(g)} \tag{21}$$

Therefore, when the Nernst equation is applied (Equation 19), it may be presented as:

$$E_{Li} = E°_{Li} - \frac{2.3RT}{nF} \log(a_{Li}); a_{Li} < 1 \tag{22}$$

This behavior is common for reduction of metals on foreign-metal substrates. Additionally, atomized metal in molten-salt solutions have been reported, by other authors, to appear black, which may explain the visible black fog produced in the underpotential region during voltammetric experiments run in the present LiCl molten-salt system. The so-called metal fog was observed in the molten salt near the cathode and has been explained as the deposition of liquid metal from molten salt. This formation is due to the low solubility of the metal in molten salt and is an indication of a supersaturated solution, as well as poor wetting properties of the cathode material.[91]

4.4.3 LiCl-Li$_2$O System

The CV of the LiCl-Li$_2$O system was studied to determine the behavior of lithium reduction and to investigate the effect of moisture interaction within this molten-salt system. CV runs were performed on the LiCl electrolyte after each lithium-oxide addition. A total of 2.2 g of Li$_2$O (99.7%, heat-treated) was added to molten LiCl in increments to produce concentrations of 0.5, 2.0, 4.0, and 11.0 wt%. Figure 28 shows the effect on CV of Li$_2$O concentration in LiCl molten salt. As the concentration is increased from 0–11 wt% Li$_2$O, additional cathodic precurrent was observed. This may be caused by increased activity of lithium due to the high concentration of Li$_2$O. A voltage shift of 0.9 V anodic was observed in the presence of 11 wt% Li$_2$O. In all, a series of five electrolytic-reduction experiments were performed with a single salt loading.
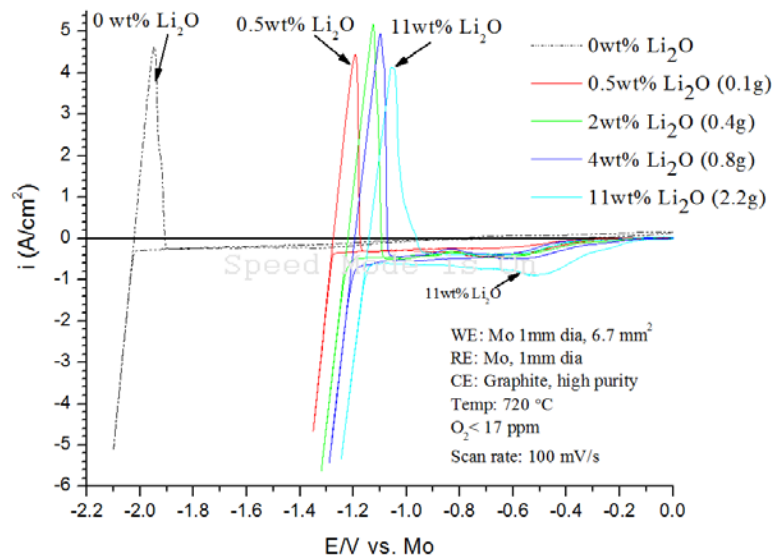
Figure 28. CV of Mo in molten LiCl as a function of Li_2O concentration for 100 mV/s at 720°C.

The resulting potential shift of the $Li^+/Li°$ redox, coupled by approximately 0.9 V is different from the results found in Herrmann, et. Al,[92] who found with the addition of 0.5 wt% Li_2O was a voltage shift of only 0.2 V versus a Ni/NiO reference electrode in a magnesia tube with porous magnesia frit. This is most likely due to the difference in the reference electrodes used. In the present work, molybdenum has been used as a quasi-reference electrode.

4.4.3.1   Effect of Fast Scan Cyclic Voltammetry in LiCl-Li₂O

The effect of scan rate was also studied in the LiCl-Li₂O molten-salt system. At scan rates lower than 1 V/s, there was not a pronounced effect in the scan rate. Once the scan rates exceeded 1 V/s, the precurrent became more pronounced as shown in Figure 29. The cathodic precurrent peaks also drifted to more-cathodic potentials with the increase in scan rates. This is suggestive of a quasi-reversible reaction, most likely due to the kinetic parameters associated with lithium.

There are two reactions which may contribute to the precurrent observed prior to the onset of lithium reduction (1) UPD of lithium and (2) reduction of OH⁻ ions. CVs run at less than 1 V/s were found to be independent of scan rate. Above 1 V/s, the precurrent observed prior to the onset of lithium reduction became more pronounced. The reaction between hydrogen produced at the

working electrode from the reduction of OH⁻ with UPD lithium is fast and cannot be resolved by CVs run at less than 1 V/s. Therefore, scan rates were extended beyond 10 V/s to resolve the scan rate dependencies of these reactions. Figure 29(b) shows the Randles–Sevčik relationship between the peak current values versus the square root of scan rate.

(a)   (b)
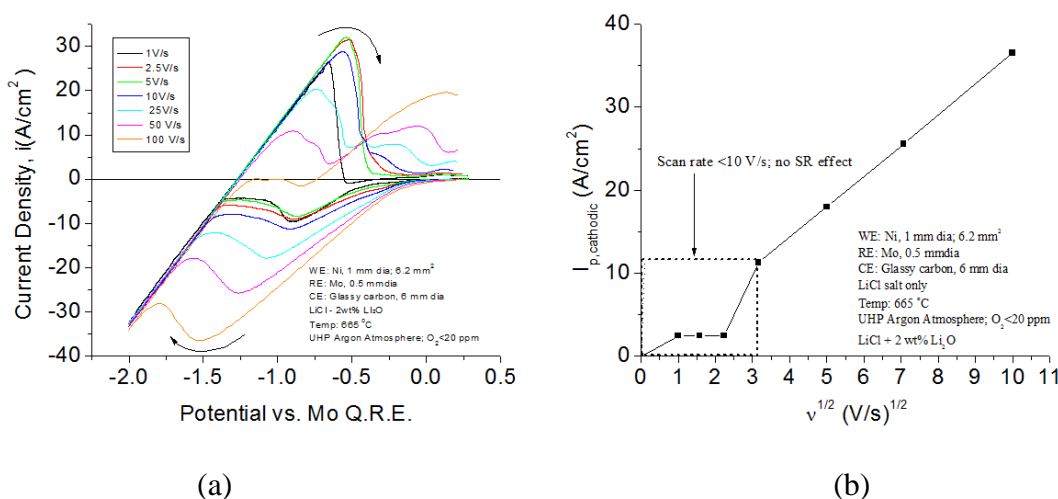
Figure 29. (a) Effect of scan rate on CV of LiCl-2wt% Li$_2$O molten salt at 665°C, and (b) corresponding Randles-Ševčík plot indicating quasi-reversible behavior for scan rates greater than 10 V/s. Conditions: WE(Ni), QRE(Mo), CE(glassy carbon).

There are two scan-rate regions represented in the Randles-Ševčík plot in Figure 29(b): (1) 0–10 V/s and (2) 10–100 V/s. The data for the second region can be extrapolated through the origin. The linear behavior indicates a reversible reaction system, and the diffusion coefficient can be calculated from the Randles-Ševčík relationship if the concentration is known (Equation 22) at 650°C.

$$I_p = -1.53 \times 10^5 \cdot n^{3/2} A \cdot D^{1/2} \cdot C_i \cdot v^{1/2} \tag{23}$$

In this equation, n = the number of electrons, A = the electrode surface area (cm^2), C$_i$ = the concentration of OH⁻ (moles/cm^3), v = scan rate, and D = the diffusion coefficient (cm^2/s). One possibility is that the reactions being observed at scan rates greater than 10 V/s are OH⁻ (LiOH) reduction to produce hydrogen (Equation 23), which then proceeds to form LiH (Equation 24).
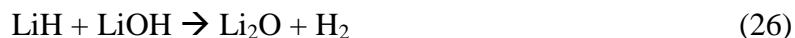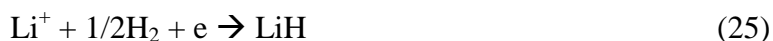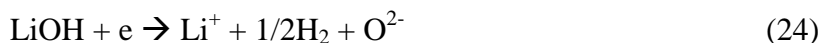
$$LiOH + e \rightarrow Li^+ + 1/2H_2 + O^{2-} \tag{24}$$

$$Li^+ + 1/2H_2 + e \rightarrow LiH \tag{25}$$

$$LiH + LiOH \rightarrow Li_2O + H_2 \tag{26}$$

The LiH is very stable at the temperature used for these experiments, and the currents observed in the pre-lithium-reduction range are likely produced by both the reduction of lithium and H_2-gas evolution.[93] In addition, LiH and LiOH can react to form Li_2O and H_2 gas (Equation 25).

The precurrent reaction could also be due to the underpotential deposition of lithium. For this reason, the scan-range window was restricted to a vertex potential of -0.9 V to isolate the phenomenon. Only at fast scan rates does the scan-rate dependence show linear behavior according to the Randles-Ševčík equation. Fast-scan CV was performed on molybdenum and nickel working electrodes in LiCl-2wt% Li_2O molten salt, as shown in Figure 30 and Figure 31.

(a)   (b)
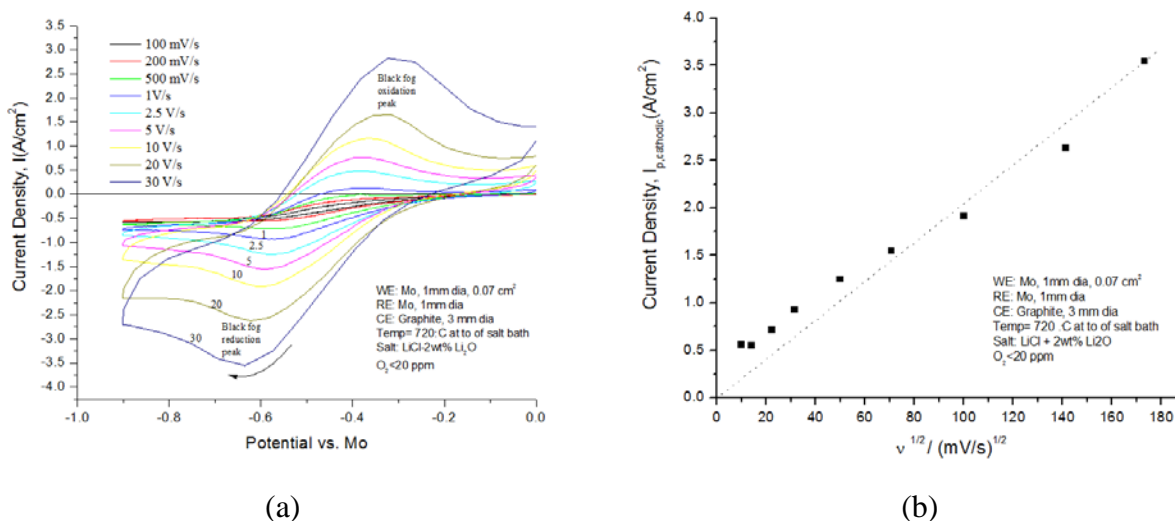
Figure 30. (a) CV-challenging reaction rate with extremely fast scanning rates LiCl + 2wt% Li_2O molten salt at 665°C, and (b) corresponding Randles-Ševčík plot indicating quasi-reversible behavior for scan rates greater than 10 V/s. Conditions: WE(Ni), QRE(Mo), CE(glassy carbon).

The response to the redox system for this black metallic fog redox couple was observed to be more pronounced on the molybdenum than the nickel working electrode. Because the concentration of this species is unknown, the diffusion coefficient could not be determined.

However, the Randles-Ševčík plots for molybdenum and nickel shown in Figure 30 and

Figure 31 are sufficiently linear for the fast-scan rates that were the basis for this experiment.

(a)   (b)
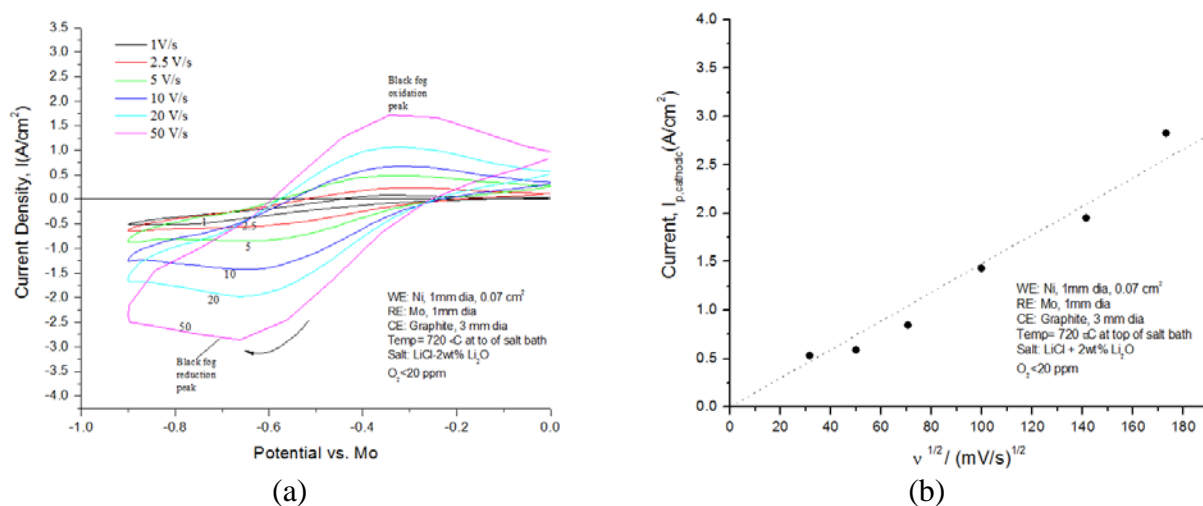
Figure 31. (a) CV-challenging reduction rate with extremely fast scanning rates LiCl + 2wt% Li$_2$O molten salt at 665°C, and (b) corresponding Randles-Ševčík plot indicating quasi-reversible behavior for scan rates greater than 10 V/s. Conditions: WE(Ni), QRE(Mo), CE(glassy carbon).

4.4.4   LiCl-LiOH System

The effect of fast scan rate was evaluated in the LiCl-LiOH system. At scan rates less than

1 V/s, the anodic peak disappeared, as shown in Figure 32(a). This indicates that the reduction

product is gaseous and had time to escape from the electrode vicinity before it could be

oxidized.

(a)   (b)
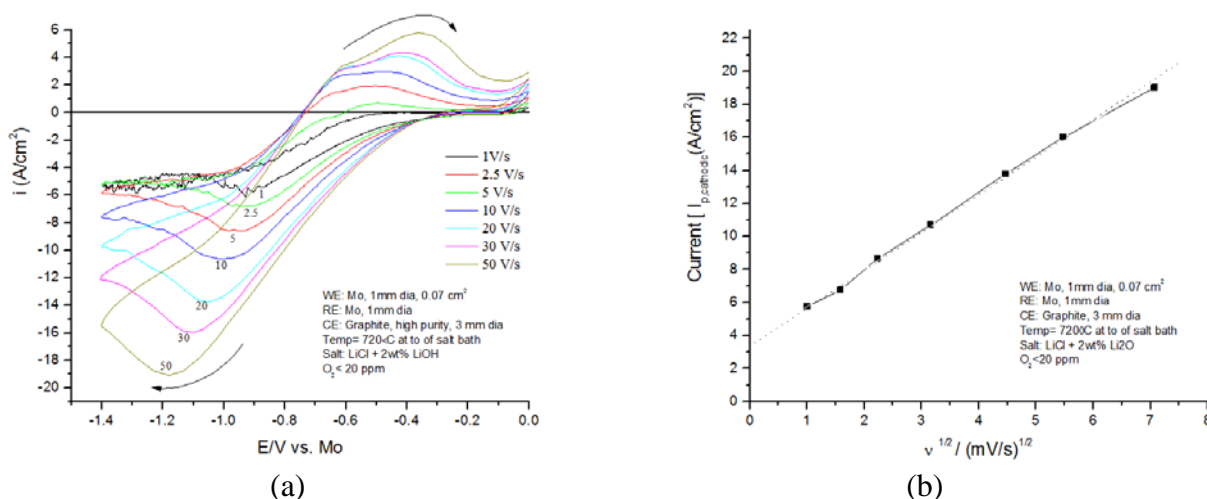
Figure 32. CV as a function of scan rate - LiOH salt system (a). Randles-Ševčík Behavior of Mo in LiCl + 2wt% LiOH at high scan rates (b).

At scan rates greater than 1 V/s, the growth of both the cathodic and anodic peaks was observed, indicating scan-rate dependence of both the reducing and oxidizing species only at the scan rates above 1 V/s. The scan-rate dependence for reduction was linear, but did not go through the origin, as indicated in Fibure 32(b).Figure 32 Therefore, the redox system is not completely reversible. Only at fast scan rates can the species be oxidized. This is consistent for systems where gaseous species are reduced and leave or react with other constituents in the salt.

4.4.4.1   Effect of Scan Range in LiCl-LiOH

The effect of scan range was studied in the LiCl-LiOH system with expansions on the potential range in both the cathodic and anodic direction, as indicted in Figure 33.
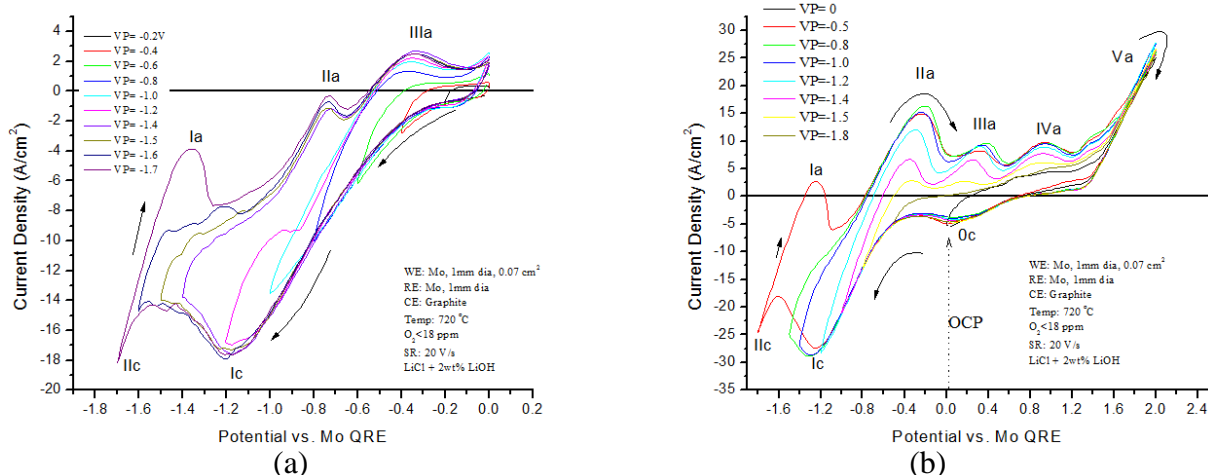
Figure 33. Effect of scan range on CV of molybdenum in LiCl-2wt% LiOH at 20 V/s.

The onset of various reactions can be pinpointed by these CV runs. Cathodic peak Ic, at approximately -1.2 V, contributes to the IIa, IIIa, and IVa oxidation peaks. Cathodic peak IIc is due exclusively to the reduction of lithium from the LiOH in the LiCl, and cathodic peak 0C and Va are due to the oxygen-redox couple.

4.4.5   Effect of Scan Range in the LiCl-Li$_2$O System

The effect of scan range was studied in the LiCl-Li$_2$O molten salt system and is shown in Figure 34. As the voltage range increased cathodically, the precurrent began to increase. As compared to the LiCl system in Figure 27, the precurrents are much higher prior to the onset of lithium reduction.
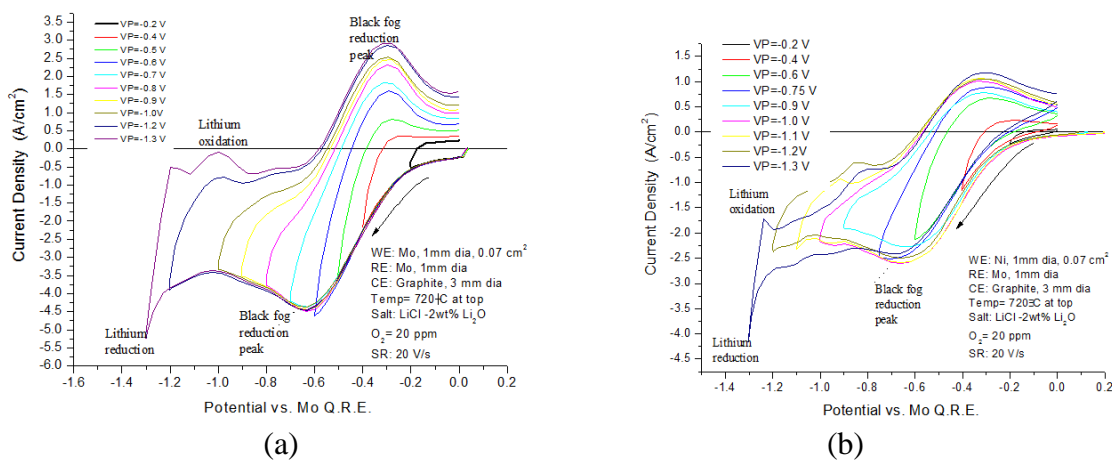
Figure 34. Effect of scan range on CV of (a) molybdenum and (b) nickel in LiCl-2wt% Li$_2$O at 20 V/s.

Additionally, when compared to the LiCl system, the effect of scan range for the LiCl-Li$_2$O system more effectively shows the occurrence of pre-lithium-reduction reactions. The oxidation and reduction peaks at -0.3 V and -0.6 V, respectively, are closer together than those found in the LiCl system alone. This could indicate that these peaks are lithium related because it is also seen that the window for reduction and oxidation is smaller compared to the redox range in blank LiCl.

4.4.6   Role of Moisture

In LiCl-Li$_2$O molten-salt systems, moisture can enter the melt from the atmosphere, Li$_2$O, and from LiCl. The order of addition of Li$_2$O to LiCl molten salt was examined to determine how the moisture can interfere with LiCl-Li$_2$O molten-salt system. In the first approach, to determine the role of moisture in the LiCl-Li$_2$O molten-salt system, a measured amount of dionized (DI) H$_2$O was added to LiCl salt at room temperature and ground together with LiCl using a mortar and pestle. The mixture was then melted to 720°C and 1wt% Li$_2$O was added to the molten LiCl-H$_2$O melt. Figure 35 shows CV as a function of wt% H$_2$O in LiCl-1wt% Li$_2$O melt. In the first approach, Li$_2$O was added to molten LiCl-H$_2$O. In the second approach, instead of adding 0.5 wt% Li$_2$O to the molten LiCl-H$_2$O mixture, it was added in the first stage and mixed with room-temperature LiCl-H$_2$O. When Li$_2$O is mixed with the LiCl-H$_2$O mixture at 20°C, the Li$_2$O and H$_2$O react to form LiOH, as demonstrated in Equation 24.

$$Li_2O_{(s)} + H_2O_{(l)} \text{ (LiCl)} = 2LiOH_{(s)} \text{ (LiCl)}; \Delta G_{20°C} = -19.038 \text{ kcal/mol} \quad (27)$$
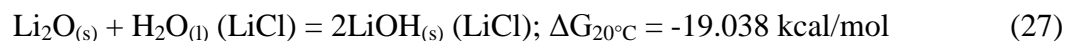
When Li$_2$O is added to the molten LiCl-H$_2$O mixture, the physical water is evaporated at 94°C.[12] Therefore, when the Li$_2$O is added to the molten mixture, there is no water available for interaction with Li$_2$O and thus LiOH cannot form. Even trace amounts of H$_2$O will react with Li$_2$O to form LiOH, especially at molten temperatures for the melt. In Figure 35, the Li$_2$O was added to solid LiCl that contained 1wt% H$_2$O. The Li$_2$O in this case, reacts with the H$_2$O to form LiOH.

After increasing the Li$_2$O concentration 2wt%, it is no longer a limiting reactant as shown for the CV with 1.00 wt% H$_2$O in Figure 39. Water is allowed to fully react with the Li$_2$O and is not limited as before for 1 wt% H$_2$O as shown in Figure 35(a) and (c). In Figure 35(b) and (d)

the current increase with the LiCl-2wt% Li_2O-1wt% H_2O molten mixture. During these reactions, when concentrations on H_2O were increased above 0.5 wt%, bubbling on the cathode was observed as seen in Figure 37.
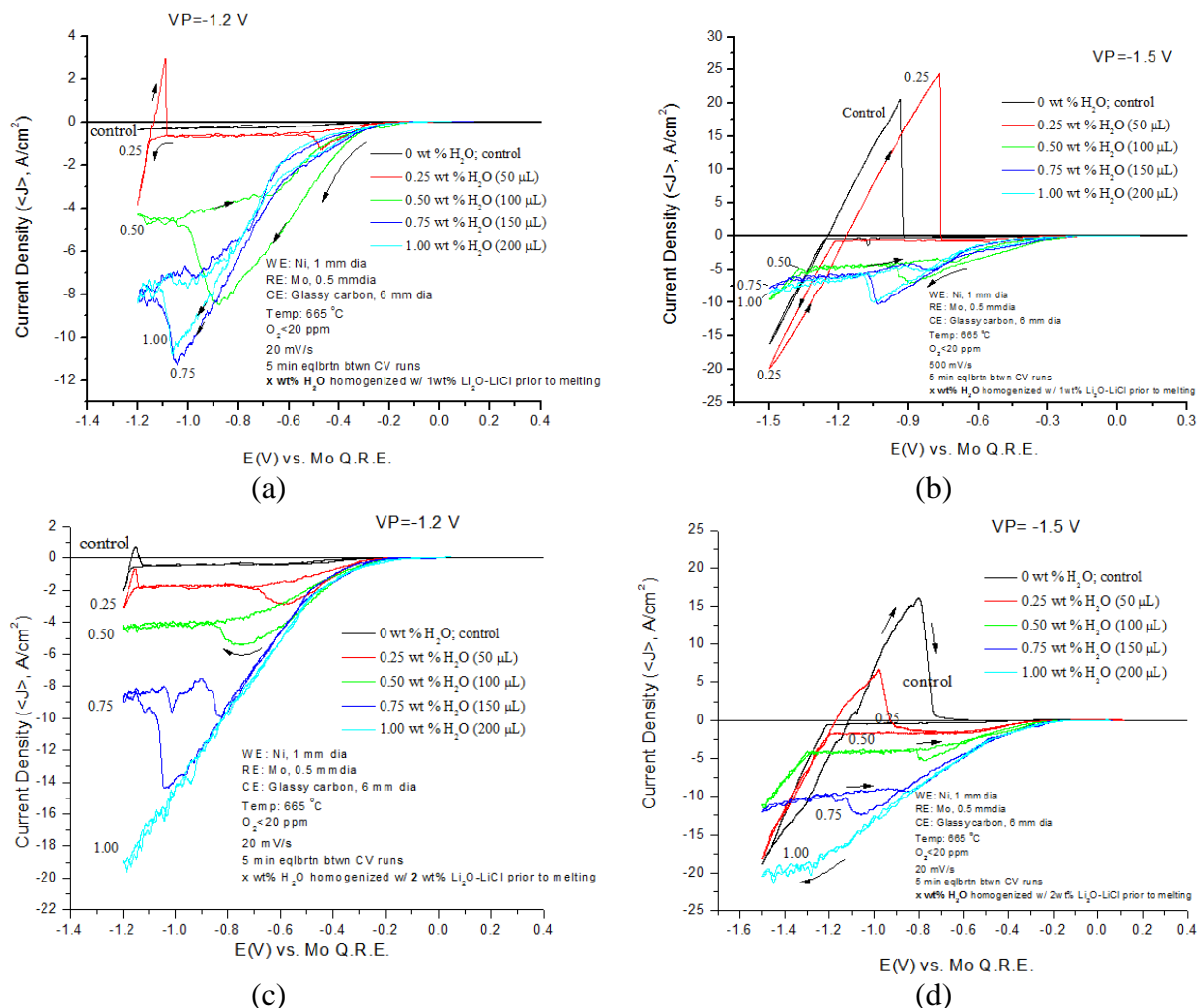
Figure 35. Effect of moisture concentration on CV of Ni in LiCl-1wt%Li_2O-X wt% H_2O molten salt for (a) -1.2 V vertex potential and (b) -1.5 V vertex potential and CV of Ni in LiCl-2wt%Li_2O-X wt% H_2O molten salt for (c) -1.2 V vertex potential and (d) -1.5 V vertex potential.

The peak current versus moisture concentration has been plotted in Figure 36. For the system containing 1 wt% Li_2O, the limiting current, I_L, plateaus above 0.5 wt% H_2O; however, for salt containing 2wt% Li_2O, the limiting current continues to increase.
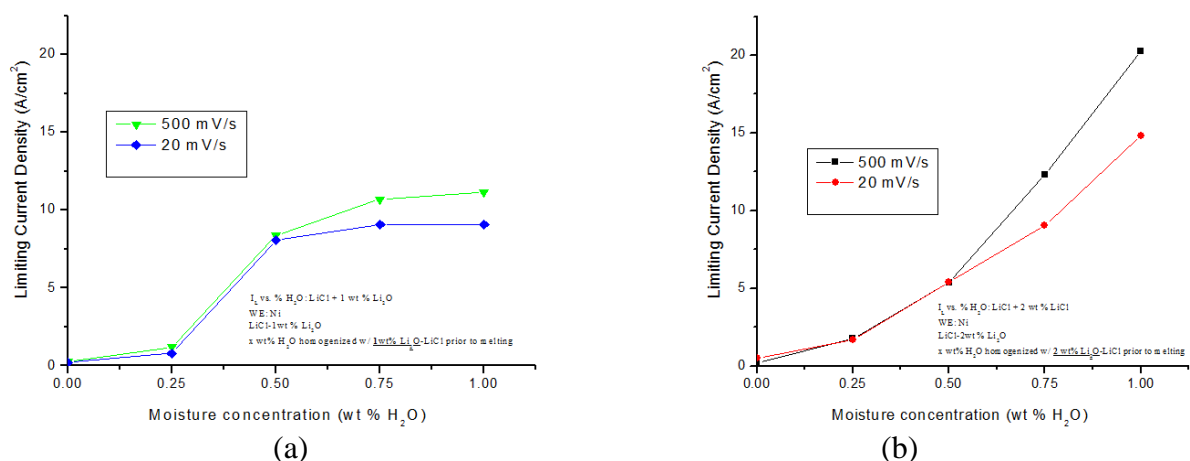
Figure 36. Effect of moisture concentration on CV of Ni in LiCl-Li$_2$O-H$_2$O molten salt for (a) LiCl-1wt% Li$_2$O and (b) LiCl-2wt% Li$_2$O.

Figure 37(a) shows the visible effects of moisture during the CV run, where hydrogen gas was evolving from a molybdenum working electrode. Instead of lithium production at the working electrode shown in Figure 26(b), hydrogen gas is evolved from the working electrode and participates in a parasitic reaction with any lithium metal which is simultaneously reduced.
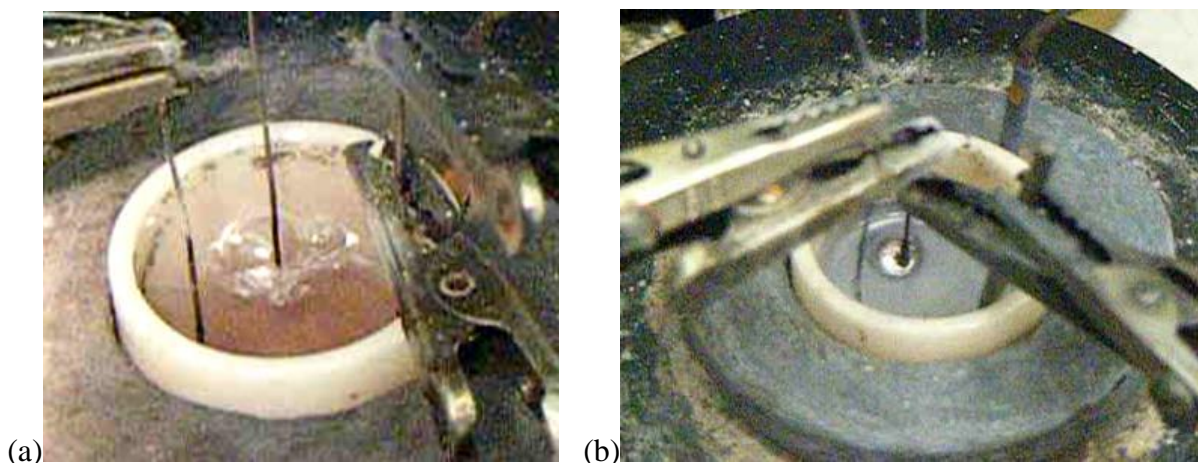
Figure 37. Effect of moisture seen in the electrochemical cell during experimental runs in (a) moisture-containing LiCl-Li$_2$O system and (b) in moisture-free LiCl-Li$_2$O system.

Lithium produced during reduction is reacted with the moisture contained in the salt, which is most likely in the form of OH$^-$ (Equation 28) in a chemical-reaction step after electrochemical lithium reduction. Together these steps comprise an electro-chemical (EC) mechanism and are believed to operate simultaneously.

$$2Li + H_2O_{(g)} = Li_2O + \tfrac{1}{2} H_{2(g)};\ \Delta G_{650°C} = -66.634\ \text{kcal/mol} \qquad (28)$$
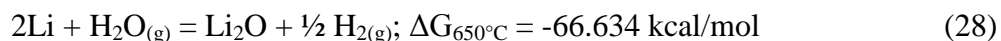
In a LiCl-Li$_2$O system with no moisture contamination, some of the Li$_2$O may recombine with oxygen according to Equation 29.

$$4Li + O_2(g) = 2Li_2O;\ \Delta G_{650°C} = -227.406\ \text{kcal/mol} \qquad (29)$$

In Figure 38, the Gibbs free-energy values were determined for the reaction of atmospheric moisture with LiCl-Li$_2$O molten salt. As the LiCl-Li$_2$O salt is melted, the thermodynamic tendency for Li$_2$O to react with H$_2$O increases significantly at temperatures above the LiCl melting point. This suggests that the salt will react with trace amounts of moisture in the atmosphere.
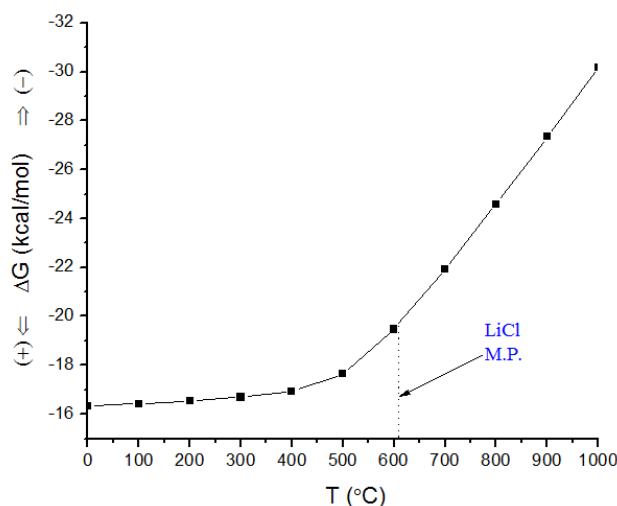
Figure 38. Gibbs free energy of LiCl-Li$_2$O reaction with H$_2$O to form LiOH according to LiCl*H$_2$O + Li$_2$O = 2LiOH + LiCl.

To show that the pre-peak currents are related to the presence of water in the molten salts, known amounts of H$_2$O were added to LiCl-Li$_2$O salt and known amounts of LiOH were added to LiCl salt. Next, electrochemical measurements of each system were made. The formation of LiOH from reaction of Li$_2$O with H$_2$O in LiCl-Li$_2$O molten salt was confirmed by running CVs as a function of H$_2$O concentration shown in Figure 39(a). Controlled amounts of LiOH were added to LiCl to confirm that LiOH forms from interaction of Li$_2$O with hydrated LiCl. CV of LiCl-LiOH molten salt was used to compare to the CVs run in LiCl-Li2O-H$_2$O system as shown in Figure 39(b).

The concentration of LiOH was varied from 0.5–2 wt%. The cathodic current increased with LiOH concentration. Excessive gas production on the working electrode was observed, in addition to simultaneous production of black metal fog. For both the LiCl-Li$_2$O-H$_2$O and LiCl-LiOH systems, bubbling was observed at the counter-electrode; however, it was not observed to the extent that was seen to evolve from the working electrode. The same features were present for both LiCl-Li$_2$O-H$_2$O and LiCl-LiOH systems, thereby demonstrating that the Li$_2$O containing LiCl salt formed LiOH when contaminated with moisture.

Another interesting effect was observed when the addition of moisture to the LiCl-1wt% Li$_2$O system. As the moisture concentration increased, the current also increased until the 0.75 wt% moisture concentration was reached. Beyond 0.75 wt% moisture, there was no further increase in the cathodic-current response. Water reacts with Li$_2$O, however, beyond 0.75 wt% H$_2$O. all 1 wt% Li$_2$O had been reacted to form LiOH and for the 1 wt% H$_2$O, the cathodic current did not increase. This limiting effect of Li$_2$O is seen in Figure 35. This reaction is evidence that LiOH forms according to Equation 27. Additional water, added to the LiCl-Li$_2$O system beyond 0.75 wt% H$_2$O, had nothing with which to react and was free to leave the molten salt because it was not bound to the salt by formation of LiOH. This is the way water leaves the LiCl system.

Because it has been assumed in previous sections that formation of LiOH in LiCl-Li$_2$O molten salts is possible both as a function of moisture in LiCl or from trace amounts of moisture in the atmosphere, controlled amounts of LiOH were added to LiCl molten salt. Cyclic voltammetry of LiCl-LiOH molten-salt solutions was used to compare with the CVs run in LiCl-Li$_2$O-H$_2$O system. The concentration of LiOH was varied from 0.5–2 wt%. As the concentration of LiOH was increased, the cathodic current also increased. Excessive gas production on the cathode was observed. Small, more-adherent bubbling was visible observed to be generated at the anode, however, not to the extent that was observed to evolve from the cathode (Figure 39).

The formation of LiOH from reaction of Li$_2$O with H$_2$O in LiCl-Li$_2$O molten salt was confirmed by running CVs as a function of H$_2$O concentration shown in Figure 39(a). Controlled amounts of LiOH were added to LiCl to confirm that LiOH forms from interaction

of Li_2O with hydrated LiCl. CV of LiCl-LiOH molten salt was used to compare to the CVs run in LiCl-Li_2O-H_2O system as shown in Figure 39(b). The concentration of LiOH was varied from 0.5 wt% to 2 wt%. The cathodic current increased with LiOH concentration. Excessive gas production on the working electrode was observed in addition to simultaneous production of black fog. For both the LiCl-Li_2O-H_2O and LiCl-LiOH systems, bubbling was observed at the counter-electrode, however, not to the extent that was observed to evolve off the working electrode. The same features were present for both LiCl-Li_2O-H_2O and LiCl-LiOH systems, therefore, demonstrating that the Li_2O containing LiCl salt formed LiOH when contaminated with moisture.
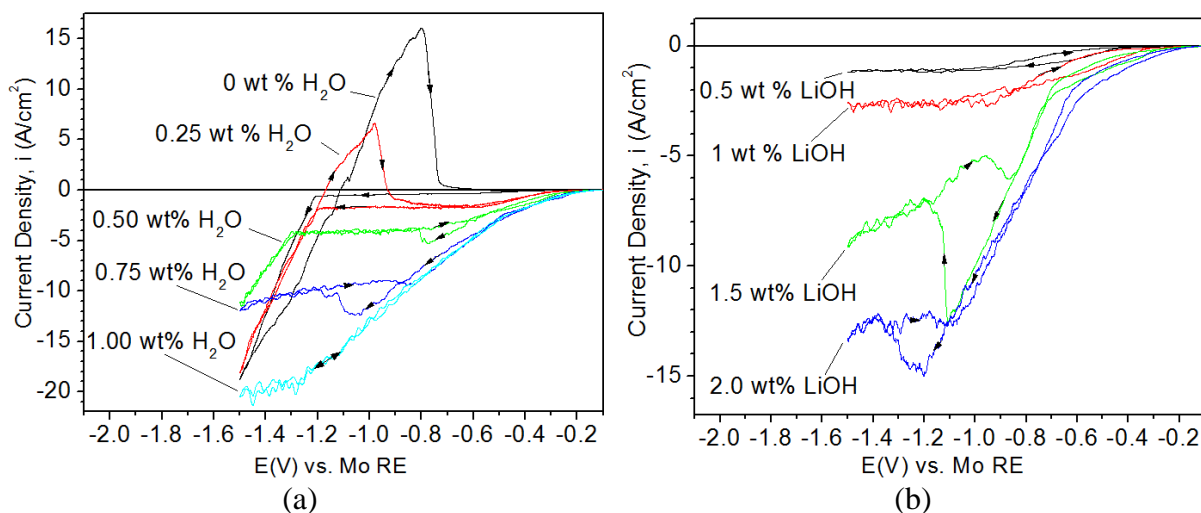
Figure 39. Effect of concentration of (a) H_2O on CV of LiCl-2wt% Li_2O, and (b) concentration of LiOH in LiCl, molten salts at 665°C. Scan rate = 20 mV/s. Conditions: WE(Ni), QRE(Mo), CE(glassy carbon).

In both salt systems, LiCl-Li_2O-H_2O and LiCl-LiOH, the common feature was high bubbling rate of gas produced at the working electrode. The product was hydrogen gas, as confirmed by gas chromatography (GC) in Figure 40(a). The thermal conductivity response (TCD) versus retention time show peaks verified for the helium carrier gas and hydrogen gas found in the sample. The gas sample analyzed was obtained between -1.2 and -1.5 V during a CV run shown in Figure 40(b).
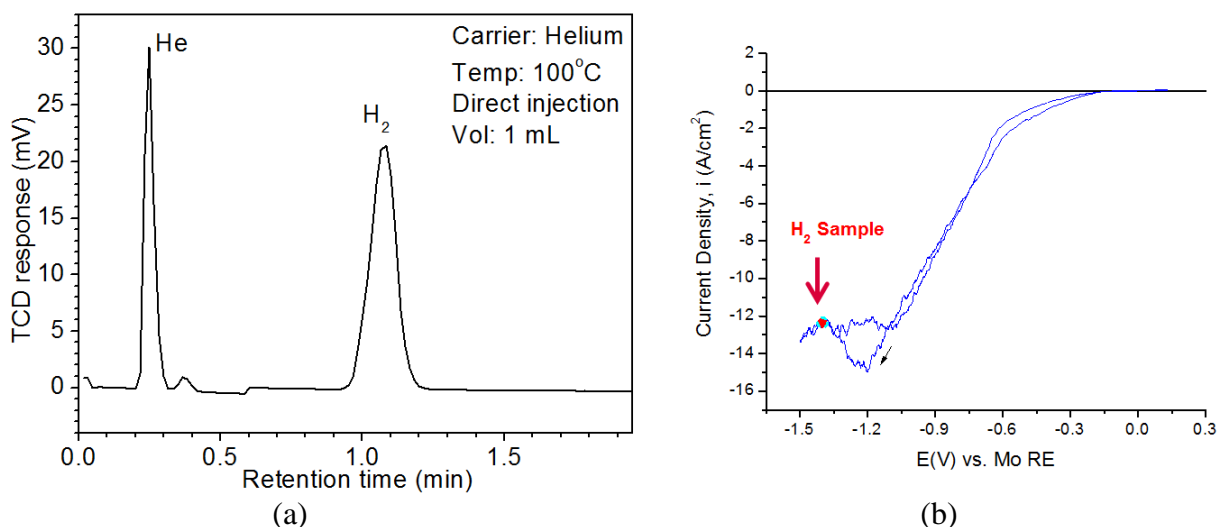
Figure 40. Gas chromatogram (a) of gaseous reaction product collected at the working electrode was obtained during CV of LiCl-2wt% LiOH system at 665°C (b) at 20 mV/s. Conditions: WE(Ni), QRE(Mo), CE(glassy carbon).

Based on the data presented in Figure 39(a) and (b), and the results confirmed by the analyzed gas sample (Figure 40[a]), the following reaction scheme (Equation [30]-[35]), is proposed.

Salt:

$$Li_2O + H_2O \rightarrow 2LiOH \tag{30}$$

$$2LiOH \rightarrow 2Li^+ + 2OH^- \tag{31}$$

Working electrode:

$$2OH^- + 2e \rightarrow H_2 + 2O^{2-} \tag{32}$$

Salt:

$$2Li^+ + 2O^{2-} \rightarrow Li_2O + O^{2-} \tag{33}$$

Counter-electrode:

$$O^{2-} \rightarrow 1/2O_2 + 2e \tag{34}$$

Overall:

$$H_2O \rightarrow H_2 + 1/2O_2 \tag{35}$$

In the salt, Li_2O reacts with H_2O to form LiOH (Equation 30), which dissociates to Li^+ and OH^- (Equation 31). The hydroxide ion reacts at the working electrode to produce hydrogen gas and oxide ion O^{2-} (Equation 32). Lithium ions and oxide ions produced at the working electrode react to regenerate Li_2O (Equation 33). Oxide ions that reach the counter-electrode

are oxidized to form oxygen gas (Equation 34). The overall reaction (Equation 35) is dissociation of water into hydrogen gas and oxygen, without any lithium produced.

Also, lithium metal dispersed in the salt may also react with moisture to produce LiOH and $H_{2(g)}$ according to Equation 36.

$$2Li + 2H_2O = 2LiOH + H_2(g); \Delta G_{650°C} = \text{-92.159 kcal/mol} \tag{36}$$
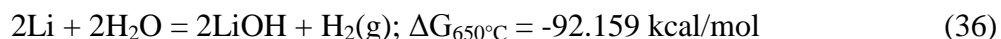
Salt containing less moisture remained more black at the end of the test-matrix cycle than salts within <0.25 wt% moisture. The working electrode turned black in salt containing less moisture. In salt containing less moisture, lithium is produced, and the salt is therefore darker in color, and the electrode turns black. Lithium redox was observed up to 0.5 wt% moisture. For the CVs run at 20 mV/s, there was large cathodic-peak growth and a clear transition at -1.1 V. CVs run for scan rates between 200–1000 mV/s showed a sort of current fusion between these two regions, which is a combination of the sharp jump and the plateau region seen for the 20 mV/s CV.

4.4.7   Molten-Salt Reaction with Atmospheric Moisture

It is possible for moisture from the atmosphere to react with molten $LiCl$-Li_2O salt. To confirm this effect, 15 mL of water was allowed to stand inside the glovebox (425-L-vol. argon atmosphere), and the regeneration system for moisture removal was shut off. Cyclic voltammetry was run as a function of the time that the salt was exposed to the moisture-containing atmosphere, as shown in Figure 41(a). An uptake of moisture in the salt after 8 hours of exposure was equivalent to the results with 0.75 wt% H_2O in the LiCl-2 wt% Li_2O salt at temperature of 665°C, as shown in Figure 41(a). The amount of cathodic current generated corresponds to roughly 7500 ppm H_2O. In addition, CVs were run as a function of the time in LiCl-2wt% Li_2O molten salt at 665°C which was exposed to the standard dry-argon atmosphere in the glovebox as a control (Figure 41[b]), which shows that there was no uptake of moisture in the salt after 8 hours of exposure.
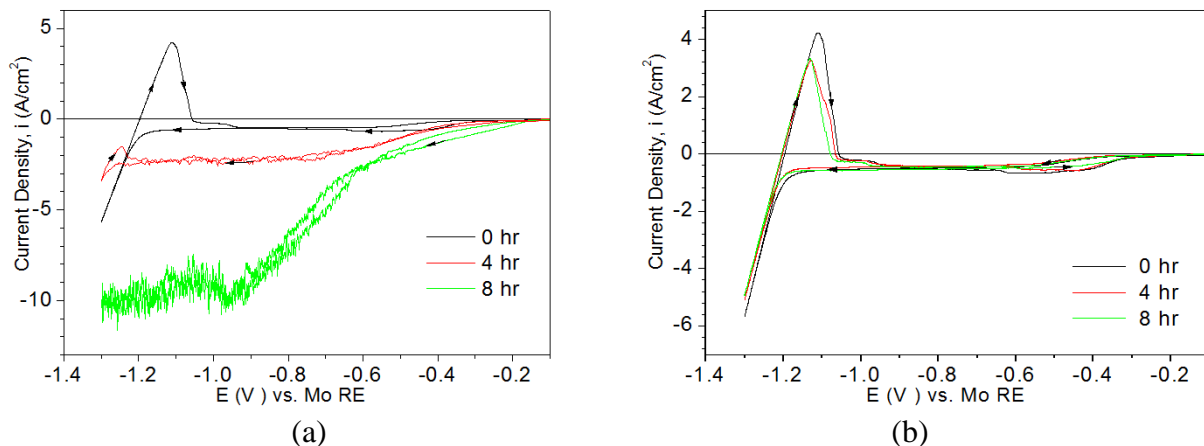
Figure 41. CV of LiCl-2wt% Li$_2$O at 665°C as a function of time (a) exposed to argon-containing-moisture atmosphere and (b) ordinary argon atmosphere. Conditions: Scan rate = 20 mV/s. WE (Mo), QRE(Mo), CE(graphite).

This set of experiments is a sure indicator that atmospheric moisture can easily enter LiCl-Li$_2$O molten salts at molten temperatures. The H$_2$O scavenging effect of the salt will continue until all of the Li$_2$O has reacted to form LiOH.

4.4.8   Effect of Order of Addition of Li$_2$O and Scan Rate

The order of addition of Li$_2$O to LiCl (1) molten or (2) to LiCl solid granules can have an effect on how the lithium oxide interacts with the moisture impurities in the salt. If moisture impurities are present in the salts at room temperature, and lithium oxide is added to the salt while the LiCl is still solid, LiOH will form. Cyclic voltammetry was run as a function of the order in which Li$_2$O was added to hydrated LiCl salt to determine how moisture can enter and interfere with the LiCl-Li$_2$O salt system. In the first approach, water and LiCl salt were mixed at room temperature and subsequently heated to 665°C to melt the salt, upon which 1 wt% Li$_2$O was added to the melt. In the second approach, water, LiCl, and Li$_2$O were mixed at room temperature and subsequently heated to 665°C to melt the salt.
Figure 42 (a) shows the effect of the order of addition of Li$_2$O.
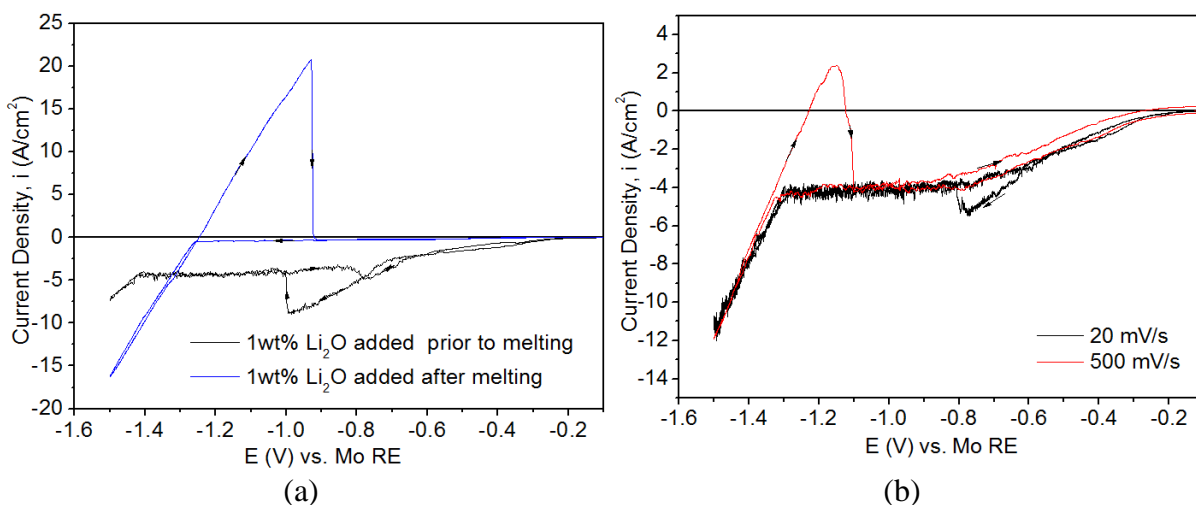
Figure 42. CV of LiCl-2wt% Li_2O as a function of order of addition of Li_2O to LiCl-0.5wt% H_2O salt at 665°C. (a) Addition of 2wt% Li_2O to LiCl-0.5wt% H_2O before (solid line), and after salt melting (dashed line). Scan rate = 20mV/s. (b) Effect of scan rate on CV when equivalent 2wt% Li_2O was added prior to melting of LiCl. Conditions: WE(Mo), QRE(Mo), CE (graphite).

According to Figure 42(a), in the first approach, when Li_2O is charged into the LiCl subsequent to its melting, the formation of LiOH will not occur, resulting in a typical lithium-reduction cyclic voltammogram. LiOH is not able to form because all of the added water evaporates during heating and melting of hydrated LiCl salt.[12] However, in the second approach, when Li_2O was added to LiCl-hydrate at room temperature prior to melting, Li_2O reacts readily with the water to produce LiOH. As a consequence, its formation is responsible for significant precurrents, Figure 42 (a). Similar cathodic precurrent has also been observed in other studies, indicating LiOH participation.[82] On the scan reversal for the CV run at 20 mV/s, the peak for lithium is absent due to the consumption of lithium in a chemical reaction with hydrogen, which is produced simultaneously on the working electrode. At the faster scan rate run at 500 mV/s, a lithium peak is observed because the reaction between lithium and hydrogen cannot occur fast enough to mask the presence of lithium on the electrode. The large current due to hydrogen reduction is still present. The effect of scan rate is shown in Figure 42 (b).

4.4.9   Effect of Electrode Material

The performance of nickel and molybdenum working-electrode materials was investigated in LiCl and LiCl-Li$_2$O melts. There was no effect on CV behavior in LiCl molten salt. Both working-electrode materials behaved reproducibly (Figure 43[a]).
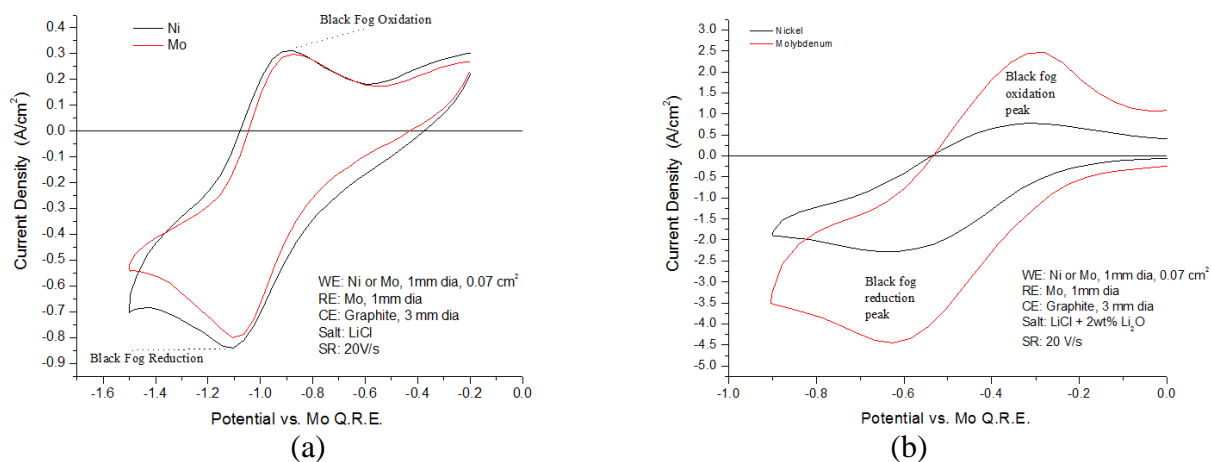
Figure 43. Cyclic voltammetry scanned at 20 V/s on (a) nickel and (b) molybdenum working electrodes in LiCl molten salt system at 650°C.

Cyclic voltammetry of nickel and molybdenum working electrodes was also compared in LiCl-2wt% Li$_2$O (Figure 43[b]). The compared CVs on nickel and molybdenum indicate that interaction with nickel is may occur, and that it is an alloying electrode. The CVs compared also indicate that molybdenum is less likely to alloy with lithium. The lower current and the irreversible nature of the CV of nickel, compared to that of molybdenum, supports this claim. If these redox couples are due to the underpotential deposition of lithium, it makes sense that the less-reactive electrode material would have more reversible behavior. On the nickel working electrode, the lithium produced reacts with nickel to form an intermetallic. The anodic-peak current is less because some of the lithium reacted with nickel and is thus not readily available for oxidation.

4.5   Chronoamperometry

Chronoamperometry was used as a complimentary technique to CV. The parameters studied were applied voltage to show the current response at a particular voltage step to determine the reaction. In the cases in which voltage was applied near the lithium reduction potentials, the currents were large, and the currents were expected to plateau at a larger value and drop off

with time much faster. In an attempt to determine the diffusion coefficient for lithium in the LiCl and LiCl-Li$_2$O systems, the Cottrell equation (Equation 37) was used.

$$|I| = n \, F \, A \, D^{1/2} \frac{c^{\infty}}{t^{1/2} \pi^{1/2}} \tag{37}$$

Where n is the number of electrons transferred, F is Faraday's constant, D is the diffusion coefficient (m^2/s), c is the concentration in bulk solution (mM), and t is the time (s). Therefore, a plot of I versus $t^{-1/2}$ should be linear and pass through the origin for a diffusion-controlled process. The diffusion coefficient of species of the reducing species can be found from the slope of the straight line of this plot.[98]

When a constant voltage is applied, the current drops off with time according to the Cottrell equation because species must diffuse to the electrode surface. Thus, for the data taken between $0.001 \, s < t < 10 \, s$, the plot I versus the square root of time in seconds should be linear. The slope of this line can be determined, and the diffusion coefficients can be calculated.

Stepped cathodic voltages were applied in LiCl. The current responses were very small for the LiCl systems for voltages applied in the pre-lithium-reduction range as would be expected (Figure 44).

(a)   (b)
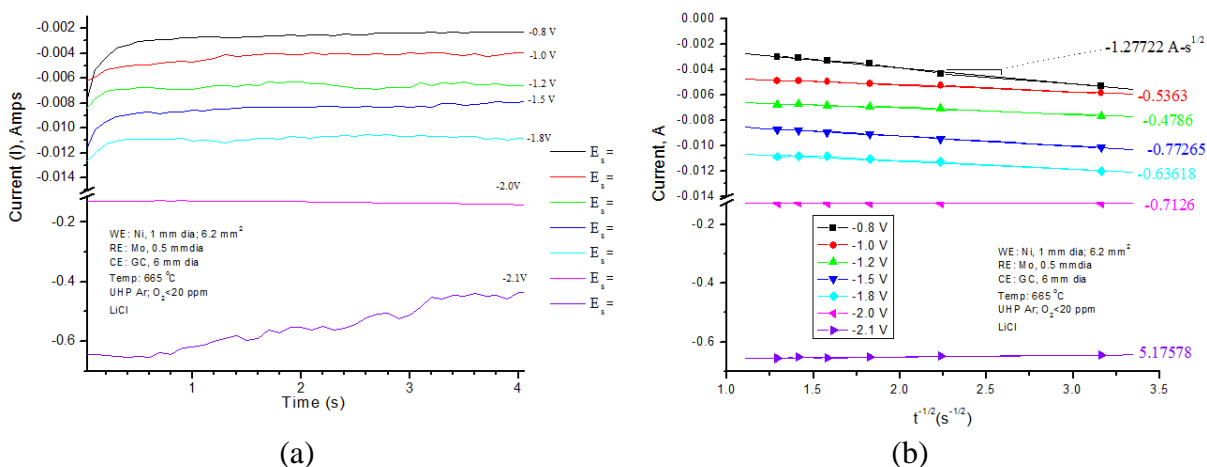
Figure 44. Effect of applied cathodic potential (a) and (b) data linearized for application to the Cottrell equation to determine the diffusion coefficients for Li in LiCl.

For the cathodic potentials applied in the LiCl system, prior to a cathodic potential at which lithium would be reduced, only very small currents were observed. The linearity of these values was in good agreement, but the line did not go through the origin. This indicates that the diffusing species in the cathodic-potential range prior to the reduction of lithium are not diffusion-controlled. This further confirms that the underpotential deposition of lithium is likely occurring and that the lithium formed does not reside long enough at the electrode. The next set of chronoamperometric experiments were in the LiCl-Li$_2$O molten-salt system (Figure 45).
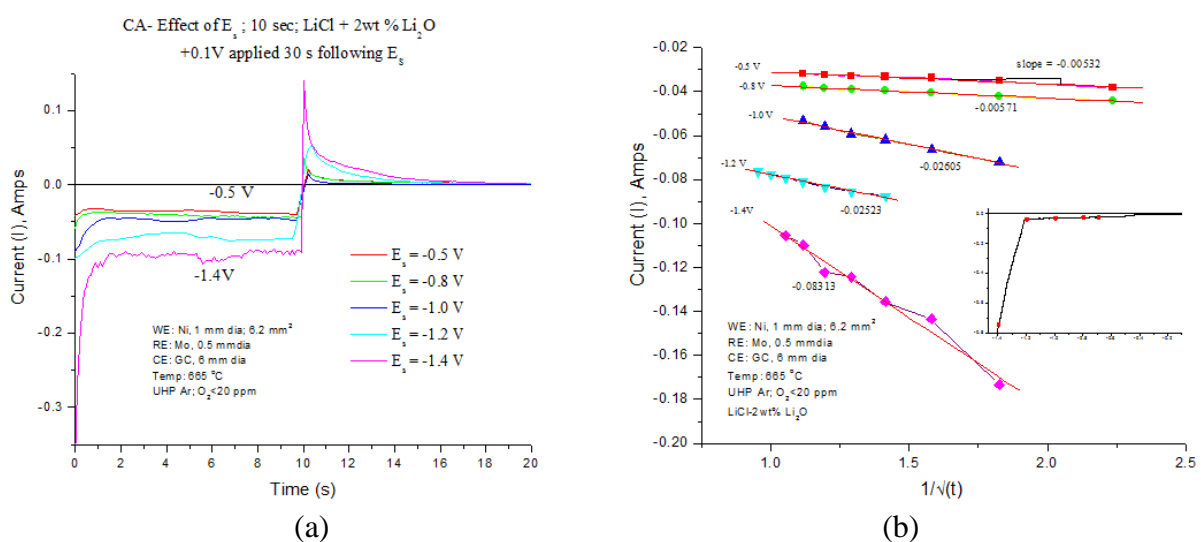
Figure 45. Effect of applied cathodic potential with reverse pulse for electrode cleaning in LiCl-Li$_2$O molten salts (a) and data linearized for application to the Cottrell equation to determine the diffusion coefficients for Li in LiCl-Li$_2$O.

Chronoamperometry run in the LiCl-Li$_2$O-H$_2$O system if shown in Figure 46. Approximately -0.3 A current was generated for moisture in the -0.8 to -1.2 V range. At -1.4 V, the current response indicates a diffusion-controlled reaction due to the reduction of Li$_2$O.

(a)   (b)
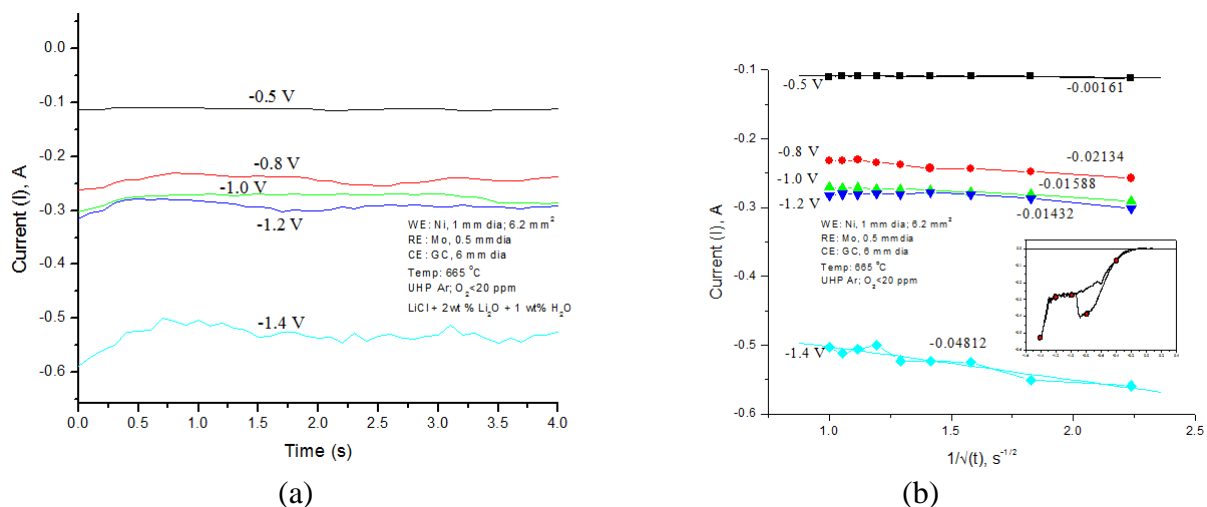
Figure 46. Effect of applied cathodic potential with reverse pulse for electrode cleaning in LiCl-Li$_2$O molten salts (a) and data linearized for application to the Cottrell equation to determine the diffusion coefficients for Li in LiCl-Li$_2$O.

A comparison of the current response for each of the systems under an applied potential of -1.2 V is provided in Figure 47(a) and Cottrell plots in Figure 47(b). The Cottrell plots indicate that the LiCl-Li$_2$O system is diffusion-controlled. But the LiCL system is not diffusion-controlled. Additionally, the LiCl-Li$_2$O-H$_2$O system is diffusion-controlled, but with several diffusion-limiting species.

(a)   (b)
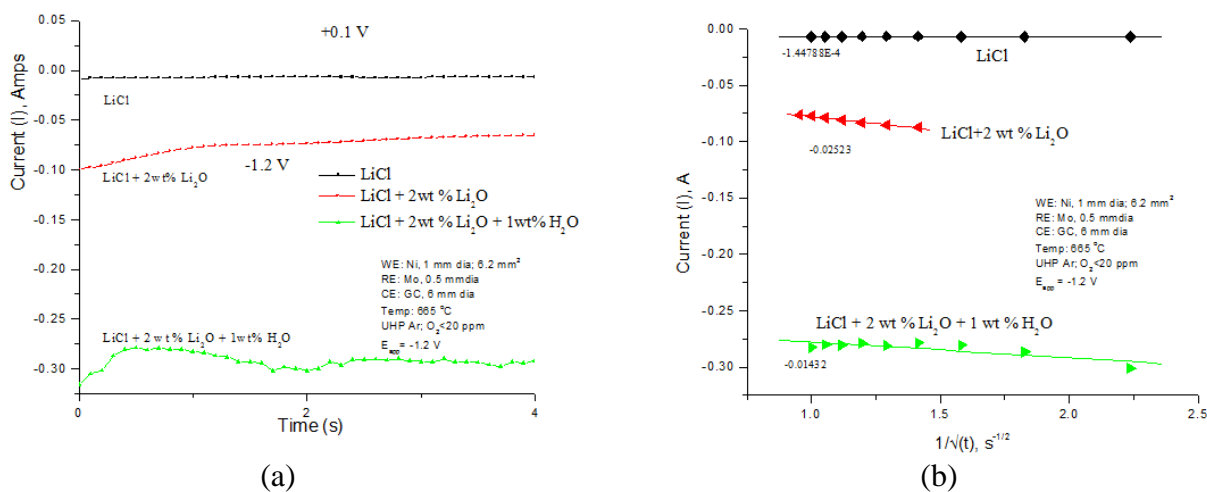
Figure 47. Effect of applied cathodic potential with reverse pulse for electrode cleaning in LiCl-Li$_2$O molten salts (a) and data linearized for application to the Cottrell equation to determine the diffusion coefficients for Li in LiCl-Li$_2$O.

4.5.1 Differential Pulse Chronoamperometry

Differential-pulse voltammetry experiments were run in LiCl and LiCl-Li$_2$O systems. The potential-time profile as well as the resulting current with time is shown in Figure 48. As the cathodic potential was increased, the anodic-current response for the anodic pulse of 0.2 V increased until -1.2 V for LiCl. For LiCl-LiOH molten-salt system, there was no increase in anodic current after the cathodic pulse of -0.8 V as shown in Figure 48.
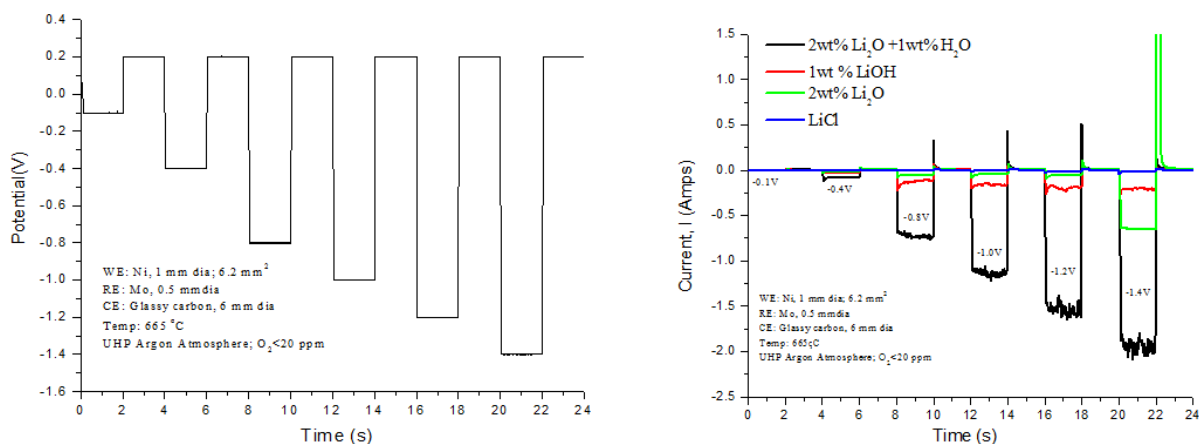
Figure 48. Chronoamperometry potential-wave form applied in LiCl systems (left) and current-time response (right) for cathodically staircase pulse potential, followed by anodic pulse at 0.2 V. Pulse width: 2 seconds (for all).

For the H$_2$O system, 0.52 g of LiOH (~2.5 wt%) should have been made due to the reaction of Li$_2$O with H$_2$O. In addition to 0.52 g LiOH, there is 0.068 g of residual Li$_2$O. The combined effects of LiOH and Li$_2$O create much larger currents than for the current produced in the 1 wt% LiOH + LiCl salt.

The current response for the LiCl system shown in Figure 48(a) increases steadily and plateaus at approximately -15 mA at potentials more cathodic than -1.2 V. All of the potentials applied in this series were selected in the regime prior to the onset of lithium reduction. The increasingly cathodic response shows that in the LiCl system, there is a possible current contribution from the underpotential deposition of lithium. In the pure LiCl system, there are no other electroactive species known. In the LiCl-LiOH system, large cathodic current was observed for applied potentials beyond -0.4 V. The current-contribution form possible under potential deposition of lithium is negligible, and the large majority of cathodic current is from reduction moisture in the LiCl-LiOH system.

4.5.2 Double Pulse Chronoamperometry as a Function of Rest Time

Another pulsing technique was used to investigate the cathodic-current response for potentials in the pre-lithium-reduction range. For a potential of -1.3 V applied in the LiCl system, the current response was measured for 10 seconds, then the potential was stopped for 0.05, 0.5, 10 and 30 seconds (Figure 49[a-d]).

(a)

(b)

(c)

(d)
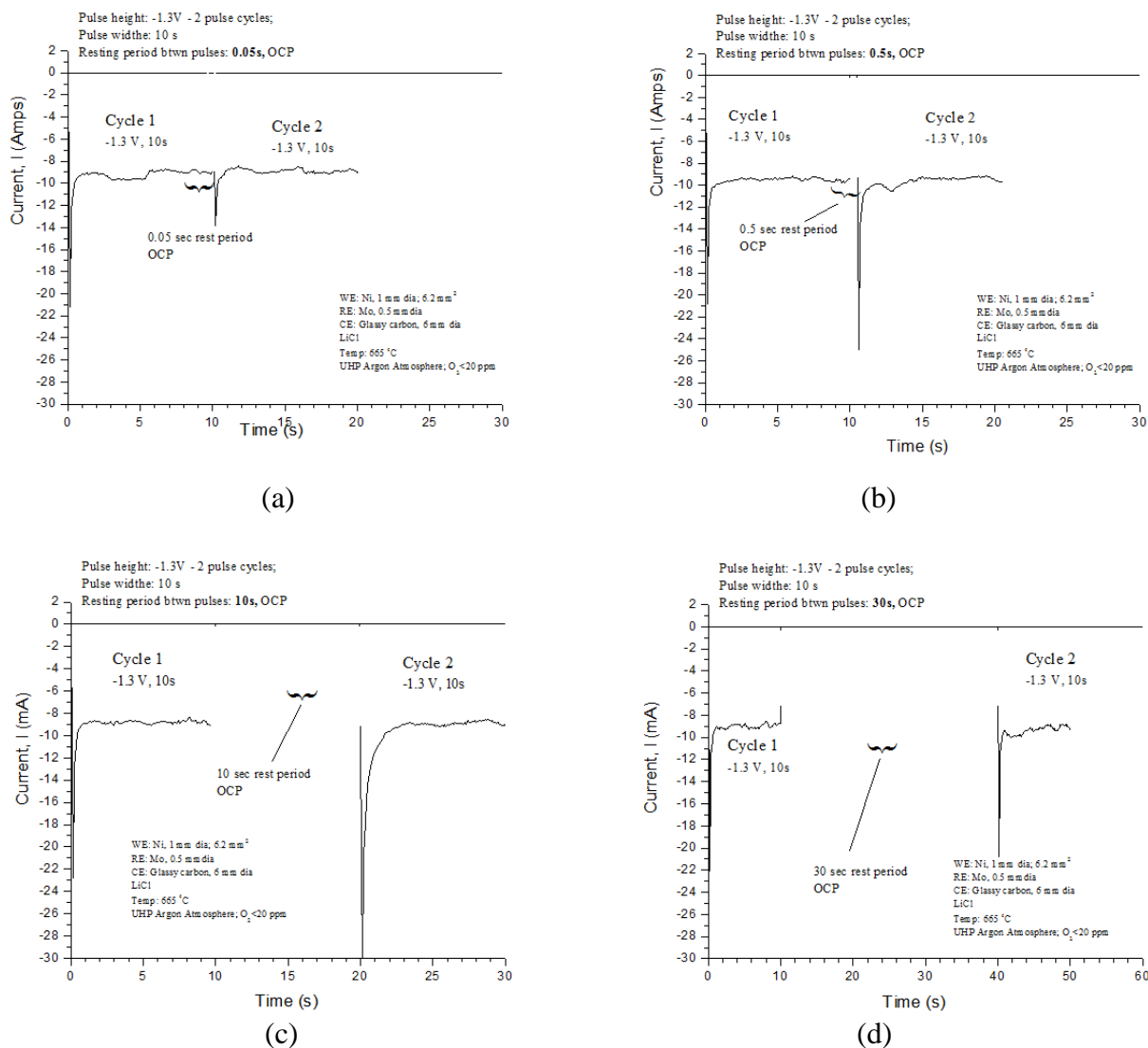
Figure 49. Effect of double cathodic pulse as a function of rest time between pulsing in LiCl.

For a potential of -0.8 V in the LiCl-Li$_2$O system, the current response was measured for 10 seconds; then the potential was stopped for 0.05, 1, 2, and 5 seconds (Figure 50[a-d]).

(a) (b)

(c) (d)
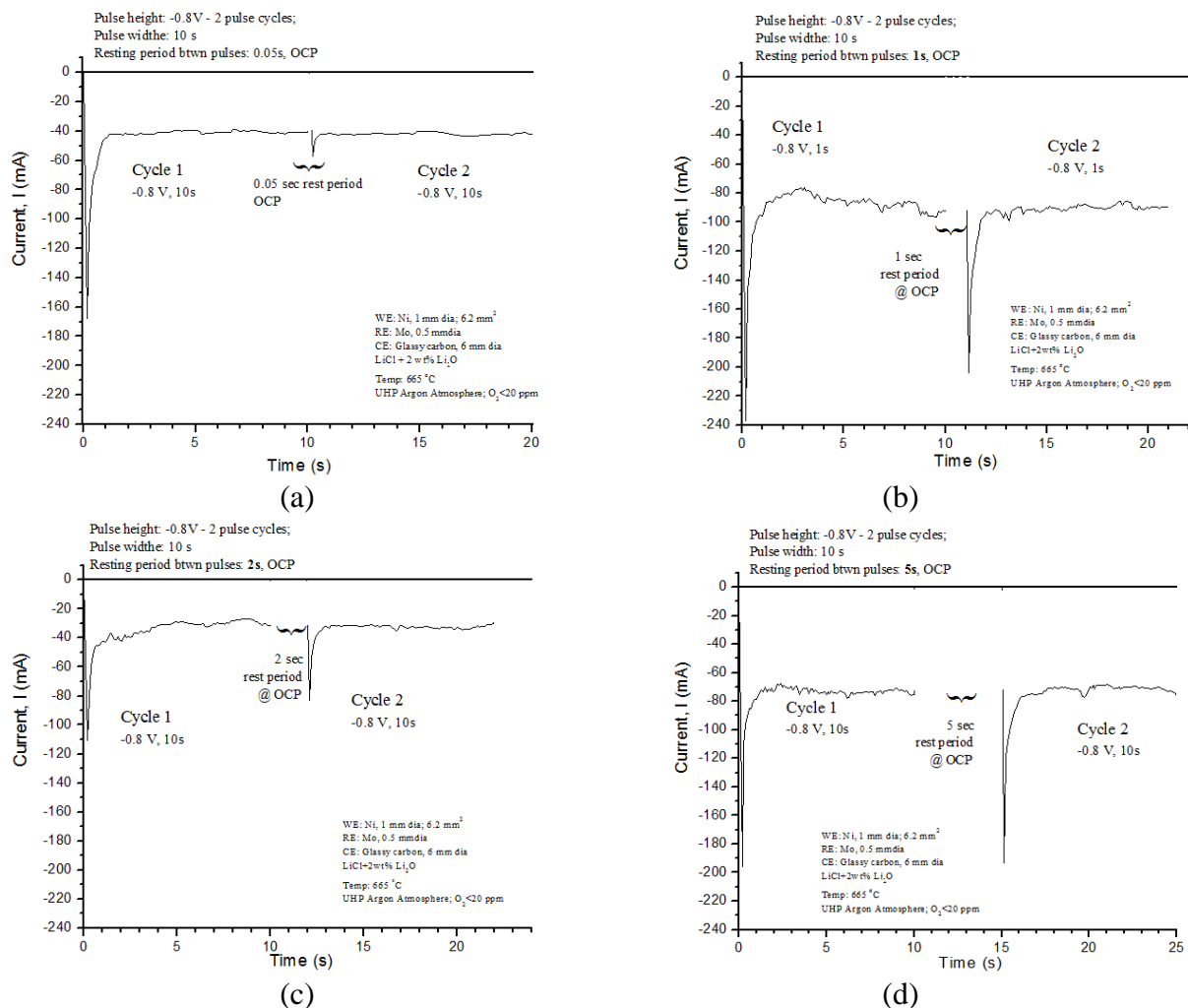
Figure 50. Effect of double cathodic pulse as a function of rest time between pulsing in LiCl-2wt% Li_2O.

For a potential of -0.3 V in the $LiCl-Li_2O-H_2O$ system, the current response was measured for 10 seconds; then the potential was stopped for 0.05, 2, 10 and 30 seconds (Figure 51[a-d]).
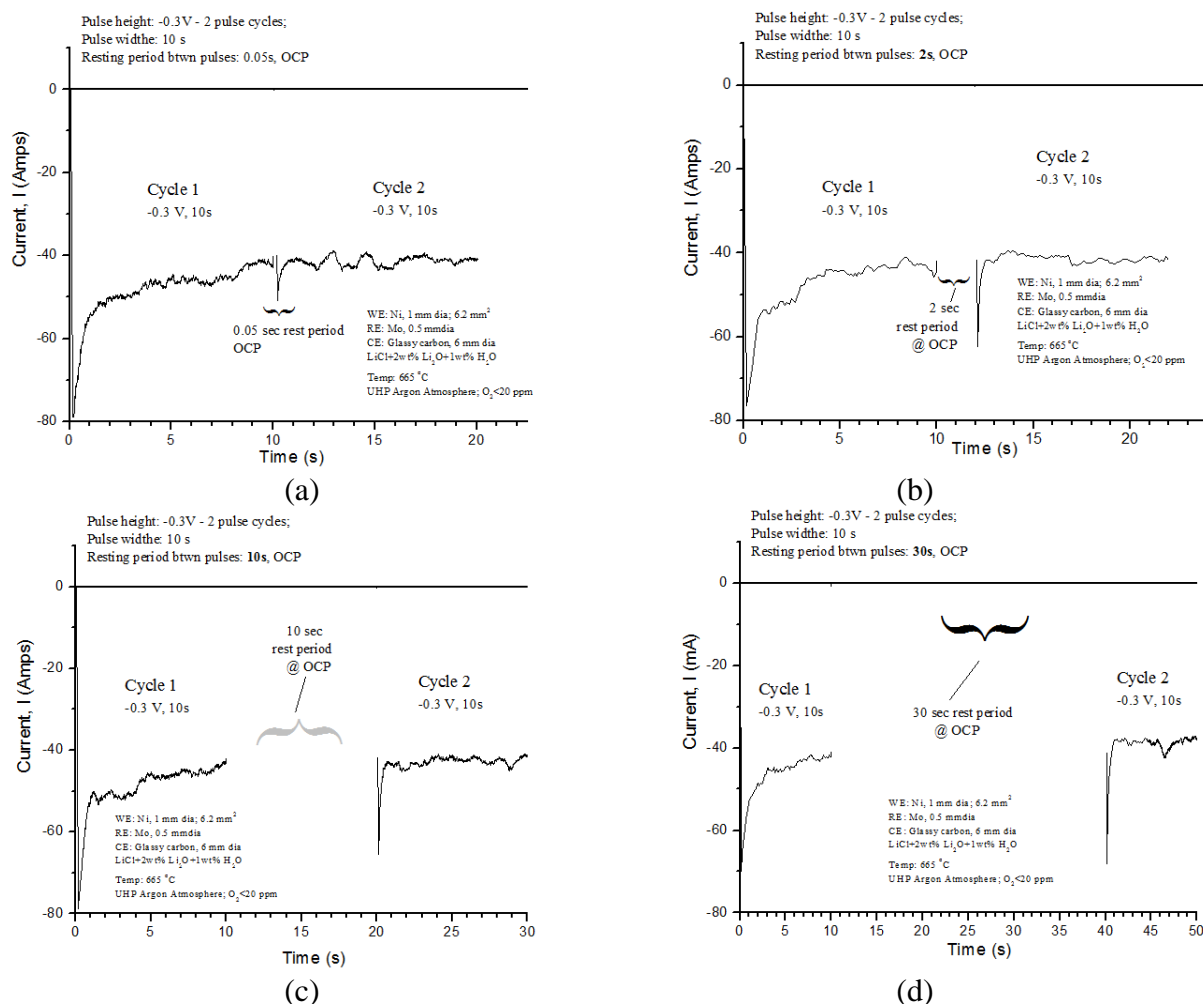
Figure 51. Effect of double cathodic pulse as a function of rest time between pulsing in LiCl-2wt% Li_2O-1wt% H_2O.

A key feature in the plots is that current response is partially recovered if 0.05 sec rest between pulsing is permitted for all three systems, and as the rest time between potential pulses increases, the cathodic-peak current was fully recovered. The idea of underpotential deposition of lithium in all three systems is confirmed here and was also confirmed in fast-scan CV run in these systems in Section 4.4.

The lithium could be adsorbed on the electrode surface, and the recovery of the adsorbed species takes increasingly longer as more constituents are added to the LiCl salt.

4.6   Chronopotentiometry

Chronopotentiometry was carried out in order to further confirm the electrochemical reactions characterized with cyclic voltammetry in the LiCl molten-salt systems. In Figure 52, chronopotentiograms plotted at -100 mA exhibit a single large plateau region at -1.25 V, corresponding to the potential for the reduction of lithium in an LiCl-Li$_2$O system. There is a second plateau that can be observed at approximately -2.0 V, which corresponds to the potential for reduction of lithium from LiCl.
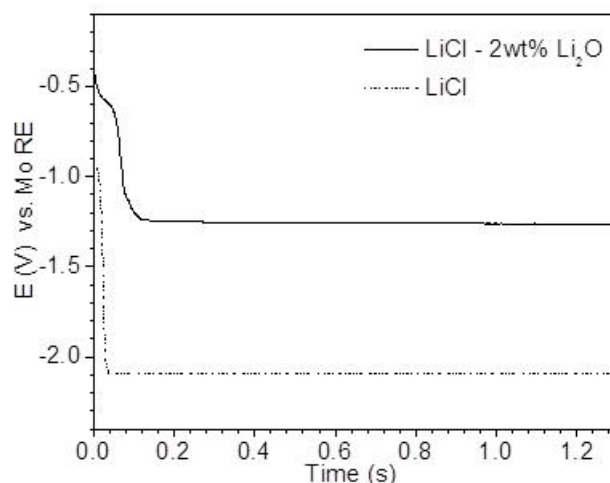
Figure 52. Lithium reduction from LiCl and LiCl-Li$_2$O molten salts at 650°C , characterized by chronopotentiometry at -100 mA imposed current. Conditions: WE(Ni), QRE(Mo), CE(glassy carbon).

It was also observed that the transition time decreased when the applied current increased. These results are typical of the formation of a soluble species on a solid cathode and behave according to the Sand equation[94,95] which is valid for diffusion-controlled reactions (Equation 38).

$$\frac{i\tau^{1/2}}{C_0} = 0.5 \, n \, \pi^{0.5} \, F \, D^{0.5} \tag{38}$$

Equation 38 can be recast to determine the confusion coefficient, according to Equation 39.

$$D = [(2* i*\tau^{0.5})/(nFAC\pi^{0.5}]^2 \qquad (39)$$

where τ is the transition time in seconds; n is the number of electrons exchanged; F, the Faraday constant (96,500 C); D the diffusion coefficient in cm^2 s^{-1}; and C_0 is the solute concentration in mol cm^{-3}. The effect of applied current was more extensively applied in the LiCl-2wt% Li$_2$O because there was a known concentration of solute, $C_0 = 9.8 \times 10^{-4}$ mol cm^{-3}. In the LiCl, there are no diffusion-controlled species, no transition time, so the Sand equation is not valid. With the transition times measured, from Figure 53, the diffusion coefficients could be determined from the Sand equation with all other values known.
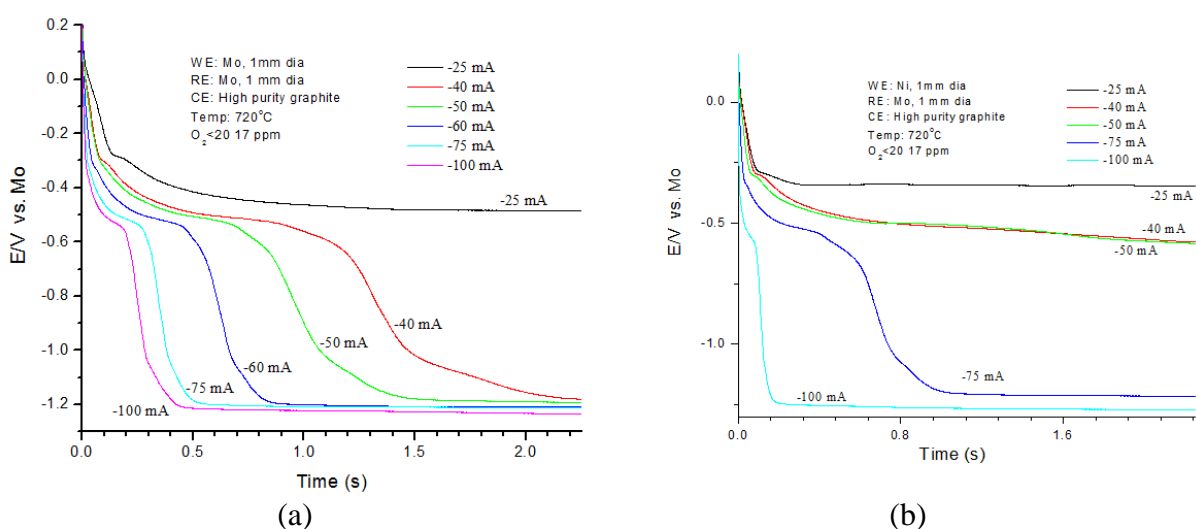
Figure 53. Chronopotentiometry of LiCl-2wt% Li$_2$O as a function of constant applied cathodic current for (a) molybdenum and (b) nickel working-electrode material.

Transition time for Li reduction is induced at -40 mA on molybdenum. If a current more positive than -40 mA is applied, there is no transition for Li$_2$O reduction. The same experiments were run for a Ni WE. Transition time for lithium reduction on nickel was not induced until -75 mA for the 3 sec time interval studied. For the nickel working electrode, current applied that was more positive than -75 mA did not have distinguishable transition times. On the molybdenum electrode, transition time decreased as the intensity of cathodic current applied was increased. The transition time indicates time which corresponds to the complete reduction of the species in the vicinity of the electrode. The transition time is proportional to the concentration of the diffusing species (see the plots in Figure 53[a-b]). For the LiCl-Li$_2$O the diffusion coefficients have been summarized in Table 14.

Table 14. Calculated diffusion coefficients in LiCl-2wt% Li_2O.

Conc (moles/cc)	Transition time τ (s) cathodic	Pulsed Current $|I_{step}, A|$	$D^{1/2}$ (cm/s)	D (cm^2/s)
Molybdenum				
0.00098	0.400	0.040	0.002433	5.92E-06
0.00098	0.230	0.050	0.002307	5.32E-06
0.00098	0.160	0.060	0.002309	5.32E-06
0.00098	0.096	0.075	0.002235	4.99E-06
0.00098	0.062	0.100	0.002403	5.77E-06
Nickel (no transition times below 0.075 A)				
0.00098	0.2	0.075	0.003226252	1.04E-05
0.00098	0.05	0.100	0.002150834	4.63E-06

Transition time on Ni is greater than on Mo. Ni probably alloys with lithium, causing the transition time to be more elongated than for Mo. Molybdenum will be used to calculate transition times in LiCl from this point forward (Figure 54).
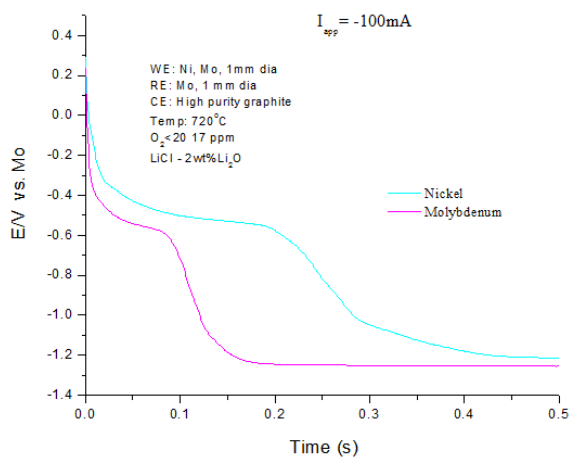
Figure 54. Chronopotentiometry of LiCl-2wt% Li_2O as a function of working electrode material.

The effect of pulsing current as a function of salt composition is shown in Figure 55, Figure 56, and Figure 57. For each system, five pulse cycles were run. Calculations for each system were obtained from the best pulse cycle, as show to the right of each figure. From comparison of the results in Figure 56, and Figure 57 it is clear that there is moisture

contamination in the LiCl-Li$_2$O system. This is clear by the plateau at more anodic potential. This indicates that current will be generated at more anodic potentials due to available LiOH species. In comparing Figure 53 and Figure 56, it also becomes obvious that there is moisture contamination in the case of Figure 56.
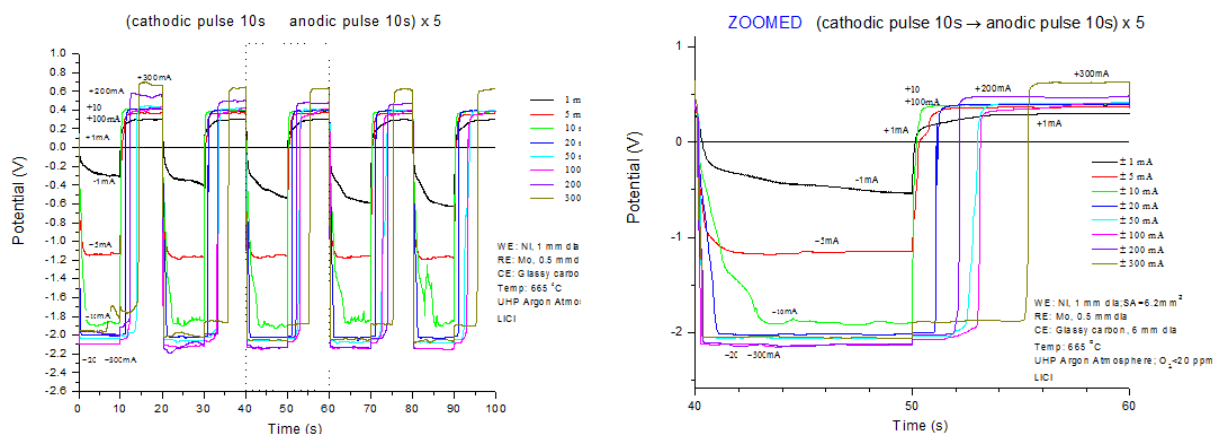
Figure 55. Chronopotentiometry of LiCl as a function of constant applied cathodic current.
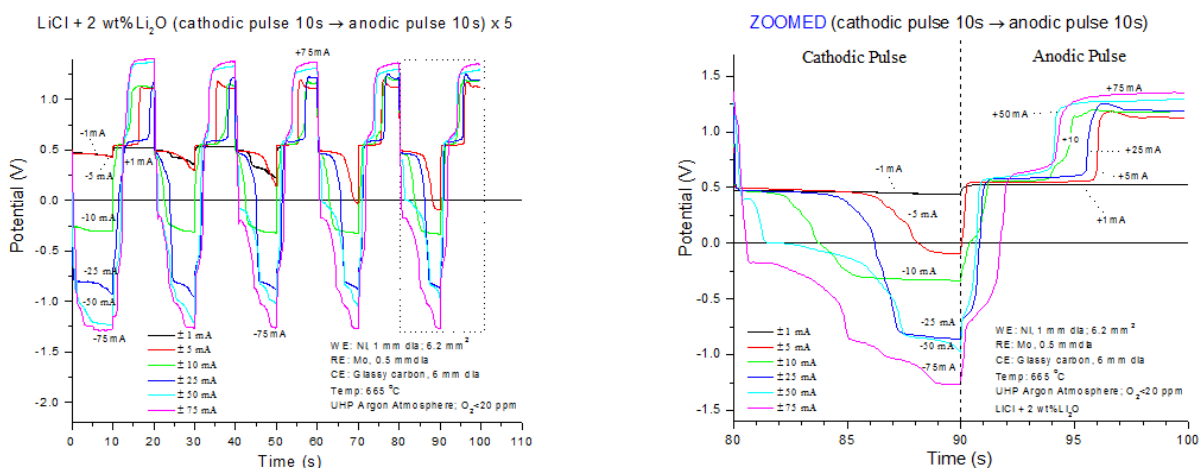
Figure 56. Chronopotentiometry of LiCl-2wt% Li$_2$O as a function of constant applied cathodic current.
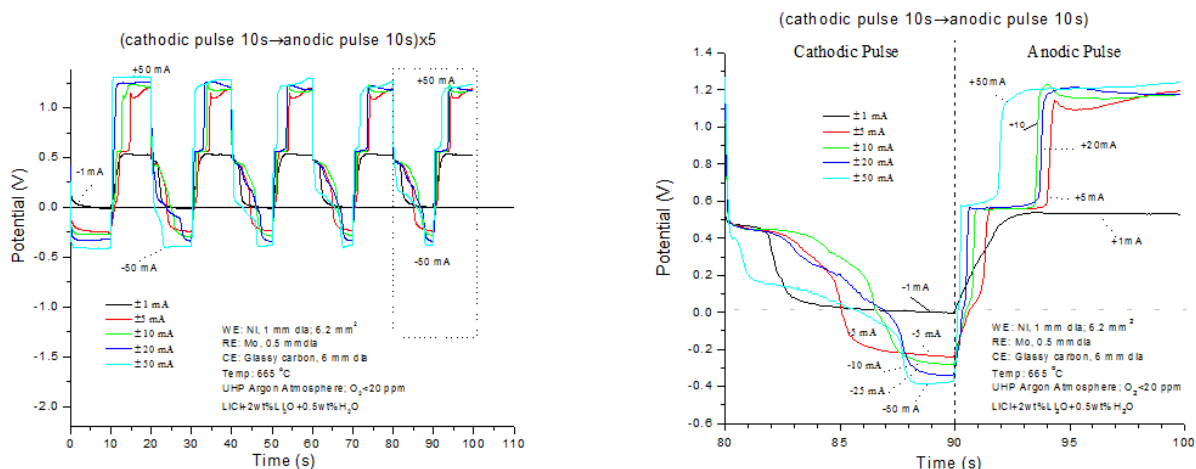
Figure 57. Chronopotentiometry of LiCl-2wt% Li$_2$O-0.5wt%H$_2$O as a function of constant applied cathodic current.

To further show the effect of moisture contamination, CP plots of LiCl-Li2O systems, both contaminated with moisture and not contaminated, are compared in Figure 58. Salt began to electrolyze gas from the cathode after extended use of the same batch of LiCl-Li2O molten salt. This was indication that moisture enters the molten salt and reacts with the lithium oxide in the salt to make LiOH. This reaction suppresses lithium reduction. Lithium in the LiCl-2wt% Li2O system reduces at near -1.2 V, but if contaminated with moisture, the plateau is near -0.5 V due to hydrolysis.
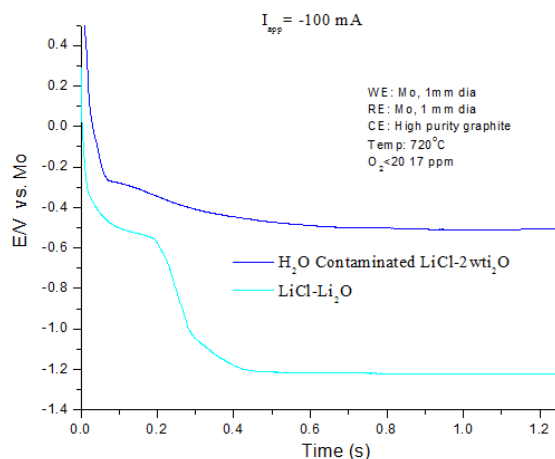
Figure 58. Effect of moisture contamination on CP of LiCl-2wt% Li$_2$O.

Chapter 5: Discussion

The effect of high scan rate was studied in the moisture-containing LiCl-Li$_2$O molten system to determine the effects on the electroactive species in the molten-salt system. An EC mechanism or, also, an adsorption mechanism can be proposed. For scan rates above 1 V/s, there is evidence that another reaction takes place and becomes diffusion-controlled. At slower scan rates, the diffusion-controlled peaks are not observed or are hardly pronounced.

At the slower scan rates, there is a kinetic parameter involved by which the adsorption of hydrogen has time for migration and production of hydrogen gas. If this occurs, then the reaction does not demonstrate reversibility. At very high scan rates (1–50 V/s), only the production of H$_{ad}$ is predominant and forms H$_{2(g)}$ dissolved in solution, and the ratio of anodic- to cathodic-peak current (i_{ap}/i_{cp}) tends toward unity. Therefore, the adsorbed hydrogen reaction could be determined reversible if no hydrogen-gas-bubble production for high scan rates occurs.[96]

Presumably the reduction of hydrogen occurs in two steps. When cyclic voltammetry was run at scan rates below 1 V/s, no reversible behavior was observed for the LiCl-LiOH based system. At high scan rates (between 1–50 V/s), the reaction appears to have reversible or quasi-reversible behavior.[97, 98] For the voltammograms obtained at high scan rates, the ratio of cathodic- to anodic-peak current (i_{cp}/i_{ap}) is nearly unity. On the other hand, for the voltammograms obtained at lower scan rates, i_{cp}/i_{ap} deviates from unity because it is believed to proceed as H$_2$-gas-bubble formation. Gas-chromatography analysis confirmed the production of H$_2$ gas. From these results, OH$^-$ ions are thought to be oxidized to H$_2$ by Equations 40–42.

$$OH^- \rightarrow H_{ads} + O_{ads} + e^- \tag{40}$$

$$H_{ads} + H_{ads} \rightarrow H_2 \tag{41}$$

$$O_{ads} + O_{ads} \rightarrow O_2 \tag{42}$$

For the cathodic reaction, hydrogen may either be in solution or transforming to H$_2$ gas and disappears from the vicinity of the electrode. Before gas bubbles are formed, the reaction may be nearly reversible at high scan rates. If bubbles are formed at slower scan rates, however,

the reaction becomes irreversible. Equations 43 and 44 are the reactions for the reversible and irreversible cases, respectively.

$$H_{ads} + H_{ads} \rightarrow H_{2(g),\ dissolved} \tag{43}$$

$$H_{ads} + H_{ads} \rightarrow H_{2(g),\ bubble} \tag{44}$$

The overall reaction, in both cases, can be regarded as a reversible electrochemical reaction in Equation 43, followed by an irreversible transformation, shown in Equation 44. The thermodynamic basis for these reactions is listed in Table 15. Although the transformation reaction is not a chemical reaction in a rigorous sense, the overall reaction mechanism can be regarded as similar to an $E_r C_i$ mechanism.[99] That is, a cyclic voltammogram of reversible electrochemical reaction followed by a chemical reaction $(E_r C)$ that is irreversible.

Table 15. HSC[100] results for OH reduction reaction at 650°C.

Reaction (720K)	ΔG (Kcal)	E vs. SHE (V)
$OH^- = H_{(g)} + O_{(g)} + e^-$	39.069	-1.695
$H_{(g)} + H_{(g)} = H_{2(g)}$	-81.152	--
$O_{(g)} + O_{(g)} = O_{2(g)}$	-92.098	--

White and Twardoch[101] studied the reduction of water on gold and platinum electrodes in a ternary eutectic molten salt, LiCl-LCl-CsCl, and determined the process observed at in the precurrent potential-voltage range (>-1.5 V vs. Ag/AgCl) correlated to the reduction of water. Their results indicate that the electrochemical pathways are dependent upon the nature of the substrate.[101] In addition, the processes observed at potentials lower than -1.5 V vs. Ag/AgCl were due to the reduction of the hydroxide ion. For the higher voltage range, -0.45 to -1.45 V, the researchers claim the adsorption monovalent hydrogen on the electrode surface occurs. At high concentrations of water and at higher scan rates, they found a follow-up reaction involving adsorbed species (46). The electro-reduction of water in the ternary chloride melt was described by electrochemical reactions (45–48).[101]

$$H_2O + e^- \leftrightarrow H_{ads}{}^s + OH^- \tag{45}$$

$$H_{ads}{}^s \rightarrow H_{ads}{}^w \tag{46}$$

$$2H_{ads}{}^w \leftrightarrow H_{2(g)} \tag{47}$$

$$H_2O + e- \leftrightarrow H_{ads}{}^w + OH^- \tag{48}$$

Reactions 46, 47, and 48 represent the homogenous reaction involving adsorbed hydrogen species when scan rate and water concentrations are high. With high scan rate and low water concentration, there is a homogenous surface follow-up reaction by the adsorbed species with an additional electrochemical step.[101]

The reduction of the hydroxyl anion (OH^-) may be proposed for the reactions observed for the present study. Electrochemical reduction of hydrogen on the cathode has been has been observed visibly and analyzed using gas chromatography. The hydride anion is also of particular interest for this research in LiCl molten salt solutions, as moisture has been found to exist in molten solutions above 923K (650°C). There is also a possibility that a hydride-anion-oxidation reaction occurs.[102] There may indeed be storage of hydrogen in LiH form, which prevents exhaustion of hydrogen. Moisture is known to enter the salt from the atmosphere above the partial pressure of 16 mm Hg.[101] In the present studies, the hydrogen or hydroxide anion is responsible for the production of hydrogen gas on the cathode. Table 16 lists the possible reactions which are taking place on the cathode during reduction of lithium from $LiCl-Li_2O$ systems contaminated with moisture. The associated values for Gibbs free energy of formation have also been listed.

Table 16. Possible electrochemical reactions in $LiCl-Li_2O$ and $LiCl-LiOH$ molten salts.

	Cell Reaction	ΔG(kcal) @ 650°C	Cell Potential (V)
(1)	$LiH + LiOH \rightarrow Li_2O + H_2(g)$	-26.950	1.170
(2)	$Li + \frac{1}{2} H_{2\ (g)} \rightarrow LiH$	-4.112	0.178
(3)	$H_2O_{(l)} = H_{2(g)} + O_{2(g)}$	36.566	-1.590
(4)	$H_2O_{(g)} = H_{2(g)} + O_{2(g)}$	47.070	-2.043
(5)	$Li_2O \rightarrow 2\ Li_{(l)} + \frac{1}{2}\ O_2$	113.70^6	-2.47^6
(6)	$Li_2O(1wt\%\ Li_2O\ in\ LiCl) \rightarrow 2\ Li_{(l)} + \frac{1}{2}\ O_2{}^6$	--	-2.55^6
(7)	$LiOH \rightarrow Li_{(l)} + \frac{1}{2}\ H_2O_{(g)} + \frac{1}{4}\ O_{2(g)}$	59.106	-2.56
(8)	$LiCl \rightarrow Li_{(l)} + \frac{1}{2}\ Cl_{2(g)}$	79.58^6	-3.46^6

The possible decomposition voltage of Li_2O in LiCl (Table 16, Reaction 5) is based on the activity coefficient of 8.4 for Li_2O in LiCl, based on the measured solubility of 11.9 mol% (8.7 wt%) at 650°C.[6] The reduction of lithium as a common ion in $LiCl$-Li_2O can be explained by the Nernst equation:

$$E = E^0 + \frac{RT}{nF} \ln \left(\frac{a_{Li+}}{a_{Li}} \right) \tag{49}$$

Where E^0 is the standard potential of an electrode, R is the gas constants, T is the temperature and F is the Faraday constant. As mentioned in previous sections, the activity of the Li and Li^+ are given as a_{Li} and a_{Li+}, respectively. When more than one monolayer of lithium is deposited on the solid electrode at any given time, the activity for lithium, a_{Li} can be assumed to be equal to 1 and $E = E^0$. However, when there is less than one monolayer of lithium deposited on the surface of the electrode, the activity of lithium, $a_{Li} \neq 1$. For the latter case, lithium deposition will begin at potentials more positive than values at which the deposition of lithium occurs on pre-deposited lithium.[6] Hence, when lithium is reduced and then dissolved into the melt, the electrode surface is continuously in the $a_{Li} \neq 1$ situation, and lithium UPD will always appear as black metal fog in the pre-reduction region for lithium containing molten salts. It has been observed that when lithium is introduced into LiCl molten salt, a black fog is evolved from the surface of the lithium. It is well known that atomized metal will appear as black streams of metal fog in clear molten salts. Therefore, when similar streams of black fog were evolved off of the surface of a solid cathode during electrochemically reducing conditions, they can be attributed to the UPD of Li.

When the hydrogen is dissolved in the molten-salt solution, reduction of hydrogen to hydride is a possibility, as explained by reactions 50 and 51. Ito et al[103] determined that hydrogen, dissolved into a LiCl-KCl melt, behaves as an unusual reactant in the surface redox process; that is, hydrogen molecules diffuse towards the electrode surface and are reduced to hydride ions either by reaction 50 or 51. In addition, the general voltammetric behavior of the hydrogen reduction by cyclic voltammetry showed that the hydrogen ion reduction peak by reaction 46 or 47 was accompanied by a hydride ion oxidation peak (reaction 52) during the reverse scan.

$$H_{2(dissolved)} + 2\ e^- \rightarrow 2\ H^- \qquad (50)$$

$$H + e^- \rightarrow H^- \qquad (51)$$

$$H^- \rightarrow H + e^- \qquad (52)$$

Moisture in the LiCl-Li$_2$O system is a source of hydrogen. There is evidence suggesting the reduction of the subsequently produced hydrogen molecules to the form of a hydride ion. Lithium hydride will then be reduced to form lithium in a region more anodic than that of the reduction of lithium from LiCl-Li$_2$O. Because the concentrations are so low, the lithium produced by lithium-hydride reduction dissolves into the melt. Black fog,[90,91] appearing at the surface of the working electrode, may thus be attributed metallic lithium from the reduction of LiH.

Diffusion coefficients were calculated for the LiCl-Li$_2$O molten-salt system (Table 17). In comparison, the results agree with expected values of diffusion coefficients in liquid system.

Table 17. Diffusion coefficients in LiCl-Li$_2$O system for three different electrochemical techniques. (LiCl-2wt% Li$_2$O, Li$_2$O = 1.96×10-4, mol/cm3.)

Technique	Equation	Parameter		Diffusion Coefficient $\times 10^{-5}$ cm^2/s
Cyclic voltammetry	Levich	0.1–50	V/s	**0.323**
Chronopotentiometry	Sand	-25 -50 -75	mA	- 1.521 1.691
Chronoamperometry	Cottrell	-0.5 -0.8 -1.0 -1.2	V	0.024 0.042 **0.357** 0.182

The following reactions have been proposed in the LiCl-LiOH molten-salt system. It is likely that the reactions being observed at scan rates greater than 10 V/s are OH$^-$ (LiOH) reduction to produce hydrogen (Equation 53), which then proceeds to form LiH (Equation 54). The LiH is very stable at the temperature used for these experiments, and the currents observed in the pre-lithium-reduction range are likely produced by both the reduction of lithium and H$_2$-gas evolution. In addition, LiH and LiOH can react to form Li$_2$O and H$_2$ gas (Equation 55).

$$LiOH + e \rightarrow Li^+ + 1/2H_2 + O^{2-} \tag{53}$$

$$Li^+ + 1/2H_2 + e \rightarrow LiH \tag{54}$$

$$LiH + LiOH \rightarrow Li_2O + H_2 \tag{55}$$
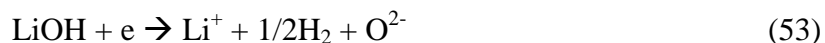
It was observed that when a crucible containing $LiCl$-Li_2O molten salt was left exposed to the atmosphere, moisture was found to react with the Li_2O in the molten salt within one hour of exposure and to cause hydrolysis in place of lithium reduction. On the other hand, as long as the crucible was covered, even in the atmosphere containing moisture, there was no effect of moisture or hydrolysis on the salt. As soon as the salt is exposed to the glovebox atmosphere containing moisture, the moisture interfered with lithium reduction.

In addition, the hydrogen ion can dissolve into the melt (Equations 56 and 57). Once in the melt, hydrogen will be available for electrochemical reduction to yield the hydride ion (Equations 56 and 57). Once in hydride form, the hydride ion may electrochemically oxidize (58) and react with oxygen to form water (Equation 59). Hydrolysis of the salt will thus increase with time and increased concentration of moisture (60).

$$H_{2(in\ LiCl\ +\ Li2O\ molten\ salt)} + 2e = 2H \tag{56}$$

$$H_{(in\ LiCl\ +\ Li2O\ molten\ salt)} + e = 2H^- \tag{57}$$

$$2H^- \rightarrow H^+ + 2\ e \tag{58}$$

$$H^+ + O^{2-}(from\ dissolved\ Li_2O) = H_2O \tag{59}$$

$$H_2O + 2e \rightarrow H_{2(g)} + O^{2-} \tag{60}$$
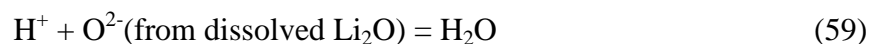
This mechanism for hydrogen production may explain why the moisture in the salt could not be removed electrochemically beyond the theoretical charge for reduction of associated concentration of LiOH in the molten salt.

Chapter 6: Conclusions

Moisture in LiCl, LiCl-Li$_2$O, and LiCl-LiOH molten-salt systems was studied. It was experimentally determined that moisture can be removed from the LiCl and LiCl-LiOH systems by heat-treating the salts above the dehydration temperature of the most thermally stable LiCl hydrate, LiCl·1/2H$_2$O. Hydrolysis of LiCl-Li$_2$O was observed, and an irreversible transformation into LiCl-LiOH occurred. Moisture plays a significant role in LiCl-Li$_2$O molten-salt mixtures, but the effect was not observed in the LiCl and LiCl-LiOH systems. These findings can pose significant interferences with the lithium-oxide reduction process for the efficient reduction of uranium-oxide fuels. At low partial pressures of moisture, hydrolysis of the molten mixture will occur. Thus, it is important to assure measures are taken to monitor moisture concentrations at all times.

The formation of LiOH from reaction of Li$_2$O with H$_2$O in LiCl-Li$_2$O salt was confirmed by running CVs as a function of H$_2$O concentration. Controlled amounts of LiOH were added to LiCl salt to confirm that LiOH forms from interaction of Li$_2$O with LiCl hydrate. Excessive gas production on the working electrode was observed in addition to simultaneous production of black metal fog, indicating that two reactions proceed simultaneously at the cathode. The black metal fog, likely lithium-metal droplets, will react with gases in the salt and eventually disappear. The lithium-metal fog will either form Li$_2$O or LiH. For both the LiCl-Li$_2$O-H$_2$O and LiCl-LiOH systems, bubbling was observed at the counter-electrode; however, it was not observed to the extent that was seen to evolve off the working electrode. The same features were present for both LiCl-Li$_2$O-H$_2$O and LiCl-LiOH systems, thereby demonstrating that the Li$_2$O-containing LiCl salt formed LiOH when contaminated with moisture. The mechanism for moisture interaction with LiCl-Li$_2$O molten salt can then be explained as follows: in the salt, Li$_2$O reacts with H$_2$O to form LiOH (Equation 30), which dissociates to Li$^+$ and OH$^-$ (Equation 31). The hydroxide ion reacts at the working electrode to produce hydrogen gas and oxide ion O^{2-} (Equation 32). Both lithium and oxide ions produced at the working electrode react to regenerate Li$_2$O (Equation 33). And oxide ions that reach the counter-electrode are oxidized to form molecular oxygen (Equation 34). The overall reaction (Equation 35) is dissociation of water into hydrogen gas and oxygen, without any lithium produced.

The following are general conclusion based on moisture studies:

Moisture contamination to the LiCl-Li$_2$O in the form of LiOH comes from (1) Li$_2$O interaction with hydrated LiCl, (2) Li$_2$O interaction with trace LiOH, and (3) the reaction of LiCl-Li$_2$O molten salt with moisture-containing atmosphere.

The potential for reduction of LiOH is more positive than the reduction potential of lithium. Therefore, there will always be currents preceding lithium reduction if moisture impurities are present, complicating the practical application of these salts by overriding all pertinent electrochemical reactions.

In more-cathodic regions, vigorous hydrogen-gas bubbling purges Li metal away from the electrode surface, precluding its detection by anodic oxidation.

The following are conclusions based on the electrochemical studies:

1. Cyclic Voltammetry (Moisture)

   - The presence of moisture affects the LiCl-Li$_2$O melts by forming LiOH.

   - In LiCl melts the presence of moisture is not effective.

   - The presence of LiOH (formed by hydrolysis of Li$_2$O) influences the order of reduction. Hydroxide reduction takes preference to lithium reduction.

2. Cyclic Voltammetry (Li UPD)

   - The observed black fog is related to UPD of Li. The formation of black metallic fog is also an indicator of saturation of that metal in the molten salt and poor wetting properties of the electrode material.

   - UPD of lithium is present in all studied molten salt systems, LiCl, LiCl-Li$_2$O, and LiCl-LiOH.

   - The reversibility of reaction, according to Randles-Ševčík is proven for only high scan rates.

3. Chronopotentiometry

- The applicability of the Sand equation was valid only for LiCl-Li$_2$O. It was not applicable to pure LiCl.

- CA was used to confirm the potential at which lithium reduction occurs, as found by the CV studies.

4. Chronoamperometry

- Cottrell equation was used to determine diffusion coefficients

- Cathodic staircase experiments were used to confirm the potential for lithium reduction from LiCl and LiCl-Li$_2$O molten salts.

Chapter 7: Suggestions for Future Work

Investigation of other salt systems, the effect of moisture, salt pretreatment, atmosphere purification, and electrochemical pretreatment methods of the salt should be the subject for further study. In addition, reference electrodes need to be compared. Separation of the cell in the anode and cathode compartments should be mandatory.

Bromide salt systems would be a good area to study in parallel with the LiCl systems. Bromide salt systems are highly hygroscopic and may help to show more pronounced effects for the interaction with moisture.

A quantitative analysis of salt samples would be very beneficial as an addition to this research. A technique for analysis of Li_2O and LiOH concentration in molten salt, paired with the quantitative analysis of the gas chromatography, would have been valuable information in this research. When the initial chemical composition of molten salt was strictly anhydrous LiCl and Li_2O, the precurrent prior to the onset of lithium reduction was minimal. However, over time, the precurrent increases. If this is due the absorption of moisture impurities in the glovebox atmosphere into the molten salt, then a moisture sensor would have helped to confirm this effect by showing that, indeed, the glovebox atmosphere was contaminated with moisture. Confirming the composition change in the molten salt—i.e., measuring the concentrations of Li_2O, as well as the change in LiCl-Li_2O composition to LiCl-Li_2O-LiOH over time as moisture was absorbed into the molten salt from the impure glovebox atmosphere—would be very useful information in any future study.

During analysis of the cathode off-gas during the electrochemical reduction in moisture-laden LiCl-Li_2O molten salt, a control sample should have been taken to provide a basis for comparison. A better setup should be designed to sample the off-gas from the anodic and cathodic electrode reactions taking place in the electrochemical cell.

Gas sampling was attempted, but not successfully sampled on the anode, although on a carbon-based anode, reduction of the oxide ion was implied to yield CO and CO_2.[104, 105, 106]

A shrouded anode compartment would prevent the parasitic reaction of Li and H_2O, which would, in turn, prevent the production of Li for chemical reduction of UO_2.[107] This would be a design consideration for future experiments

A Ni/NiO reference electrode should be used for electrochemical studies in $LiCl-Li_2O$ system for more stable reference potential.

Appendices

Appendix A: SEM Characterization

All characterizations were performed with a Tescan Vega II LSU SEM at 20 keV accelerating voltage. Elemental anlysis was performed with IXRF Model 550i, E2V Scientific Instruments EDS detector.

Appendix A-1: Black Stain Formation on Mullite RE Sheath

In early experiments, the LiCl-KCl system was used for electrochemical studies. After determining that the solubility of Li_2O was low, research was switched to the LiCl-based system. However, in the LiCl-KCl, a mullite-sheathed Ag/AgCl-based reference electrode was used. It was found that the mullite became stained during the course of experiments when lithium was electrochemically produced in the salt. In future runs, it was determined that, if lithium was being generated to any extent, the use of the mullite-sheathed Ag/AgCl reference electrode was not a good choice from a stability perspective.

Figure 59. Post-testing reference electrode composed of silver wire immersed in LiCl-KCl-2.5 wt% Ag/AgCl inside mullite with fritted end.

The EDS spectrum in Figure 60 was generated from analysis of stained mullite tubing. Elemental maps of the sample were obtained, as shown in Figure 61. The stains were most likely caused from the occlusion of K and Cl. The analysis of these elements was generated from the EDS-X-ray fluorescence (XRF) software. These results leave out Fe, N, Cr, and V because these peaks correspond to the mounting device and do not contain information pertaining to the stained reference electrode; aluminum was quantified even though the inside of the chamber is composed of aluminum components. Thus, the alumina component is artificially high.
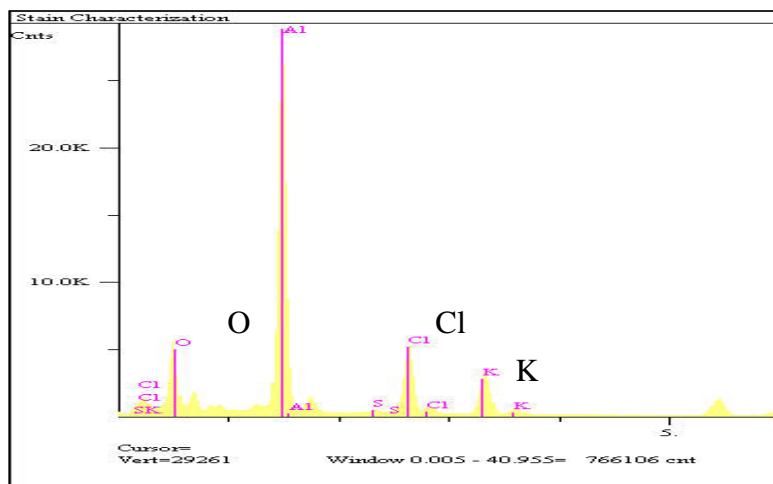
Figure 60. EDS X-ray spectrum map of stained mullite RE sheath specimen.
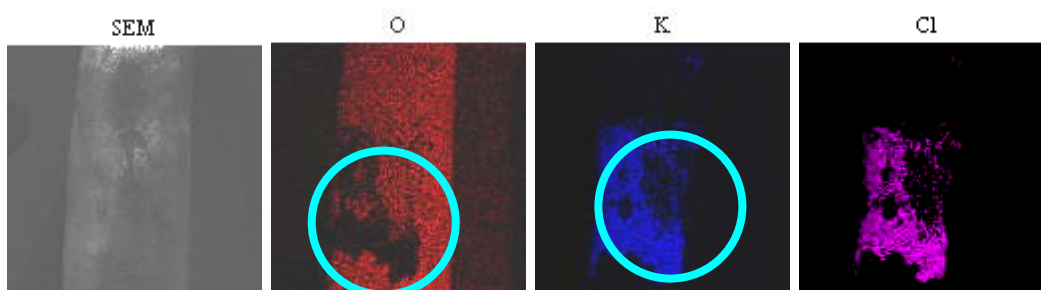
Figure 61. SEM EDS elemental-mapping characterization of O, K, Cl, which were elements that generated the most-intense peaks pertaining to the specimen being analyzed.

The black staining found on the mullite tubing was expected to be from silver; however, it turned out to be more likely from chlorine, potassium, or oxygen or the formation of oxides and compounds containing these constituents.

Appendix A-2: Post-Test Analysis of Molybdenum Coil Counter-Electrode

An SEM secondary electron (SE) image obtained for a portion of molybdenum used as a counter-electrode during lithium generation is shown in Figure 62. Molybdenum was used as a counter-electrode during early experiments; however, due to noticeably severe degradation from oxygen and chlorine its further use was discontinued. Oxygen and chlorine have been characterized in the EDS elemental maps in Figure 62 and a sum spectra from the EDS mapping is provided in Figure 63.
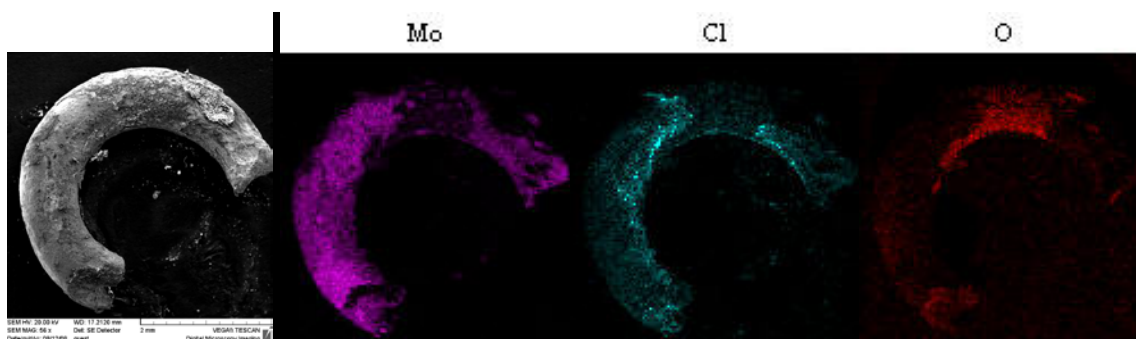
Figure 62. SEM SE image, 20 kV, 56×, of molybdenum post-test electrode portion exposed to the salt and associated EDS elemental mapping indicating chlorine and oxygen.
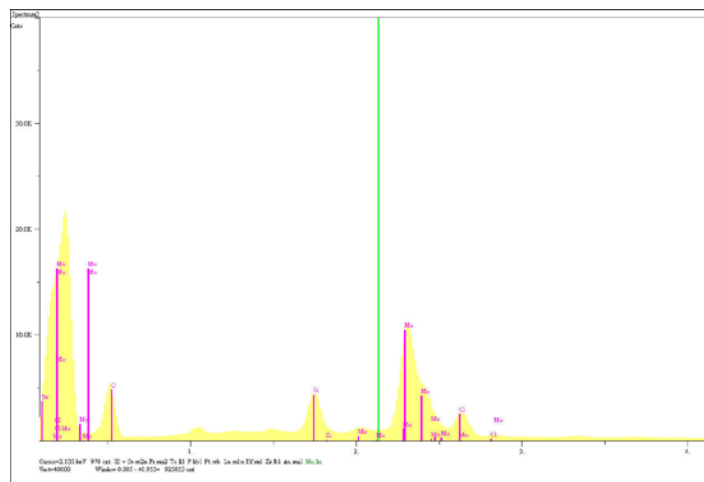
Figure 63. SEM SE sum spectra of molybdenum post-test electrode portion exposed to the salt and associated EDS spectra.

Appendix A-3 Post-Test Analysis of Degraded Tungsten CE Material

During experiments run for the exhaustion of moisture from LiCl-Li$_2$O molten salt, using constant applied potential of -0.65 V for 2 hours, it was noticed that a black reaction product formed or precipitated. The precipitate found on the WE was dissolved and rinsed in DI water with HCl. The solution was siphoned, and remaining black residue was rinsed with acetone 1 time, then suspended in acetone and a drop of this solution was laced on carbon tape. Once acetone was evaporated, the sample was mounted in the SEM chamber. The analysis of this reaction product left on the nickel electrode and the reaction product that dissolved off of the electrode is shown in Figure 64 through Figure 67.

The black-reaction-product precipitate remaining on the Ni WE after soaking in DI-H$_2$O solution was locally polished to reveal the Ni surface. After rinsing thoroughly again with DI and then acetone, the Ni WE, with locally remaining reaction product was loaded in the SEM chamber (Figure 65).
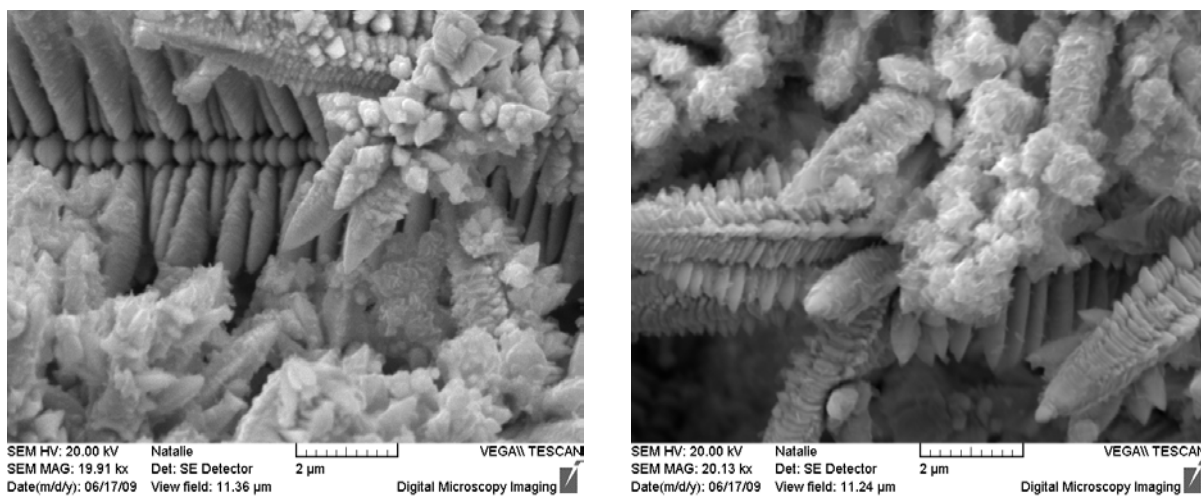
Figure 64. Black reaction product dissolved off Ni WE (Left and right).
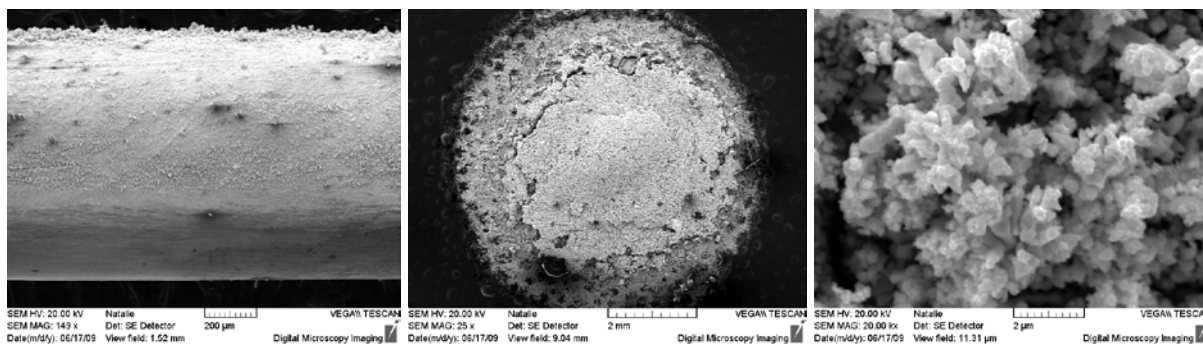
Figure 65. SEM SE images of nickel after 3 min CA, -0.65 V and produced black reaction product. On the left, the precipitate was dissolved off the Ni WE. On the right, the Ni WE was polished off the electrode in the lower area and, in the upper area, the reaction product remaining on the electrode was analyzed.
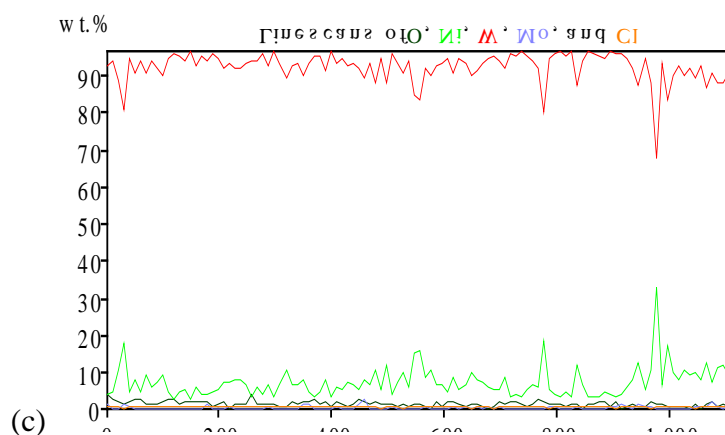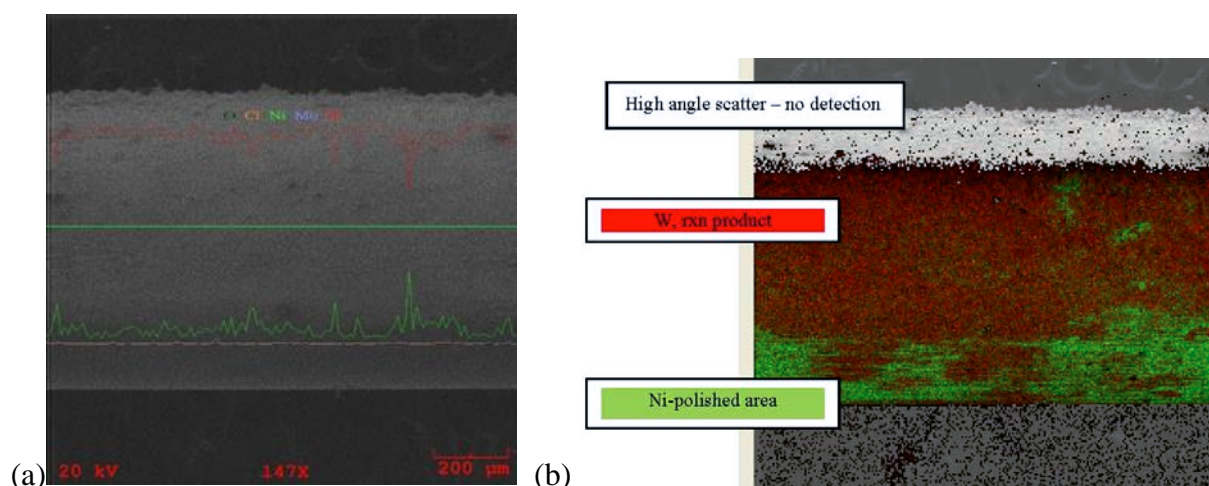
Figure 66. EDS analysis of reaction product remaining on Ni WE following CA experiment run at -0.65 V, for 3 min. Line scan is seen as the straight horizontal line in (a) indicating the region for which the sample was analyzed, and (b) shows particle density analysis for the region of W and Ni. The line scan (c) shows the quantities of Ni. W, Mo, and Cl for the line scan position in (a).

Table 18. Elemental concentration of EDS of Ni WE for region containing black reaction product.

Element	Line	Intensity (c/s)	Conc	Units
O	Ka	52.14	3.746	wt.%
Al	Ka	42.28	1.316	wt.%
Cl	Ka	3.35	0.085	wt.%
Ni(sanded region)	Ka	1,202.98	59.082	wt.%
Mo	La	5.59	0.442	wt.%
W	La	109.18	35.329	wt.%
			100.000	wt.%
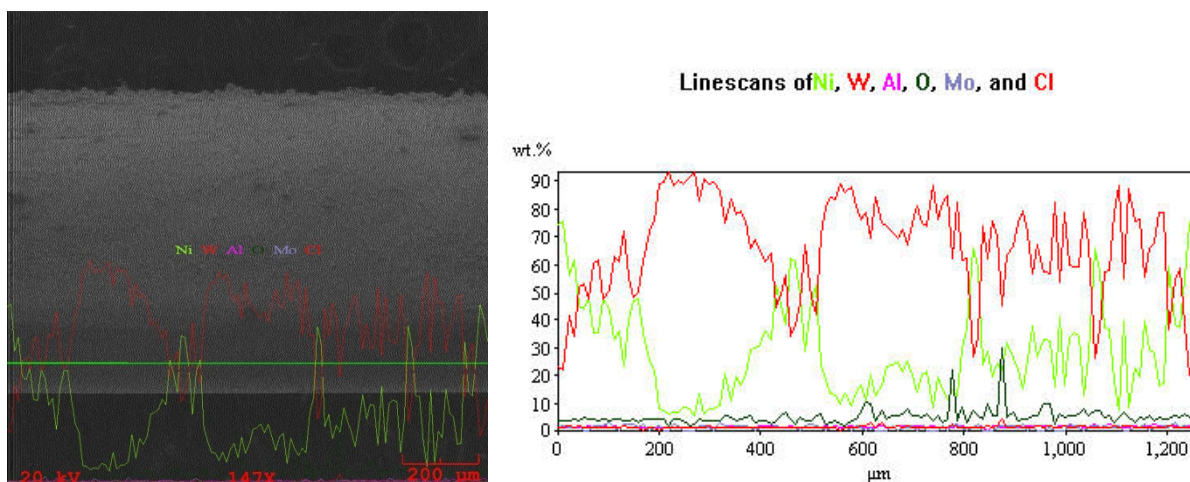
Figure 67. Line-scan position located in the region of the sample where the electrode was polished and the Ni was exposed.
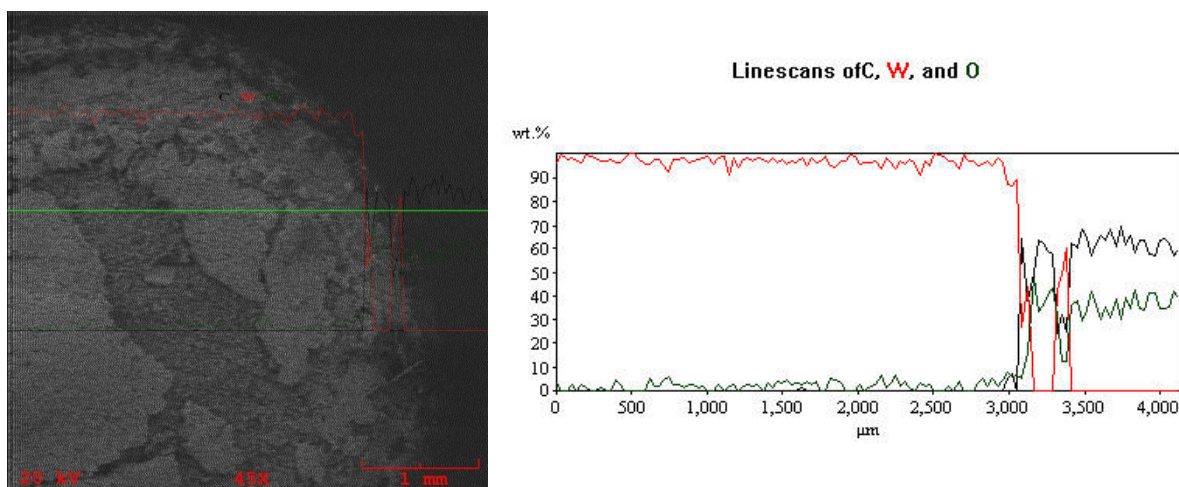
Figure 68. EDS line scan of Ni WE for a region containing black reaction product next to a region where reaction product was sanded to expose the Ni WE surface.

Appendix B: Opened-Ended Graphite Tube with Lithium CE

During early testing in LiCl molten salts, a graphite tube with molten lithium inside was used as a counter-electrode. It was found that the lithium intercalates the graphite material. The use of this type of counter-electrode was observed to shift the onset for the reduction. Lithium-reduction potential is shifted more positively with the lithium intercalated graphite tube used as a CE, as shown in Figure 69. Normally, in LiCl, lithium reduction peaks do not commence until approximately -1.9 V versus a molybdenum reference electrode. In the case here, lithium commences close to -1.3 V. Most likely, this is electrorefining of lithium from the counter-electrode.
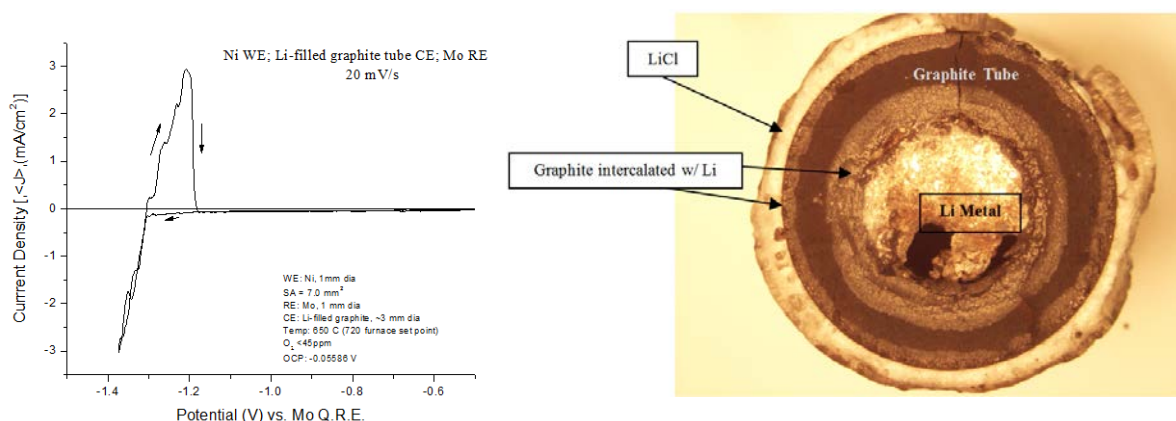
Figure 69. CV of Ni WE with lithiated graphite counter-electrode (left). Fractured high quality graphite tubing counter-electrode loaded with metallic lithium used for CV of Ni in LiCl.

The graphite tube intercalated with lithium was not very robust and could not sustain thermal cycling very well. A fracture in the tube occurred when it was momentarily placed back into the molten salt to melt clumps of lithium from the outer wall of the tubing. Lithium escaped from the inner tube and collected around the outer wall of the tubing while experimenters attempted to resituate the electrode.

Appendix C: Anodic Polarization of Working Electrode Materials

Cyclic voltammetry in LiCl and LiCl-Li$_2$O molten salts were run to determine the anodic limits of each working-electrode material. For the LiCl system, it appears that tungsten was the most stable in the presence of chlorine-gas evolution (Figure 70). For the LiCl-Li$_2$O system, it appears that platinum is the most stable in the presence of oxygen (Figure 70). However, since Pt is relatively expensive and is attacked by lithium, and because tungsten has limited ductility, preventing the ability to make a high-surface-area coil, molybdenum was used as a counter-electrode in some cases, as were graphite and glassy carbon. Data sets obtained for the LiCl-LiOH system Figure 71 include graphite. Also, Figure 71 includes a comparison of graphite anodic polarization in all three salt systems. It is presumed that CO and CO$_2$ gas form in the LiCl-Li$_2$O system, which would explain why the oxidation commences at a lower potential for graphite in that particular system.
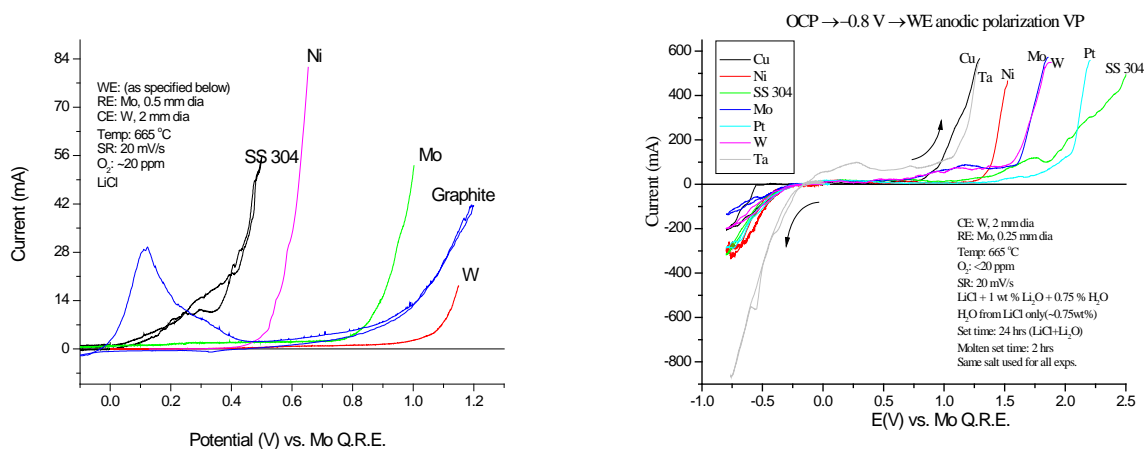
Figure 70. Anodic response for CV of various working-electrode materials in LiCl (left) and LiCl-Li$_2$O-H$_2$O (right) molten-salt systems.
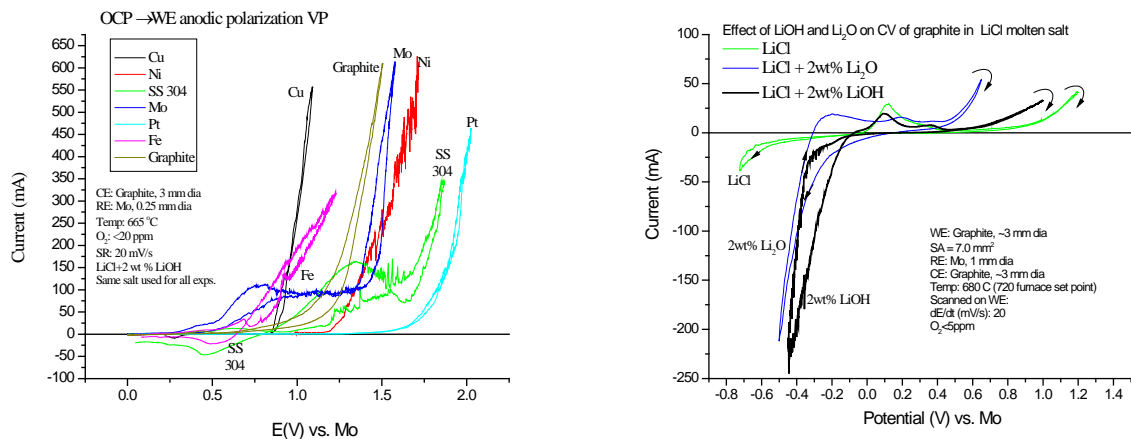
Figure 71. Anodic polarization of electrode materials in LiCl-LiOH (left) and response for graphite in LiCl, LiCl-Li₂O, and LiCl-LiOH molten salt systems (right).

Appendix D: Cyclic Voltammetry Studies with SS 304 Working Electrode

An interesting observation regarding the SS 304 electrode was found in the pre-lithium-reduction range. The electrode exhibited a scan-rate-dependent cathodic-current response, observed to commence at approximately -1.0 V and shown in Figure 72. Prior to running each experiment, the working electrode was cleaned by sanding and sonication in acetone, and dried with an air gun. These CVs were obtained during the first cycle, and subsequent cycles did not show reproducible peak response unless considerable resting time was allowed between cycles. Between the range of 5 and 200 mV/s, the current response followed Randles-Ševčík behavior, indicating possible reversibility. For scan rates greater than 200 mV/s the linearity was less defined, and the slope increased (Figure 73). Table 19 summarizes the OCP and peak-current values prior to each scan rate run.
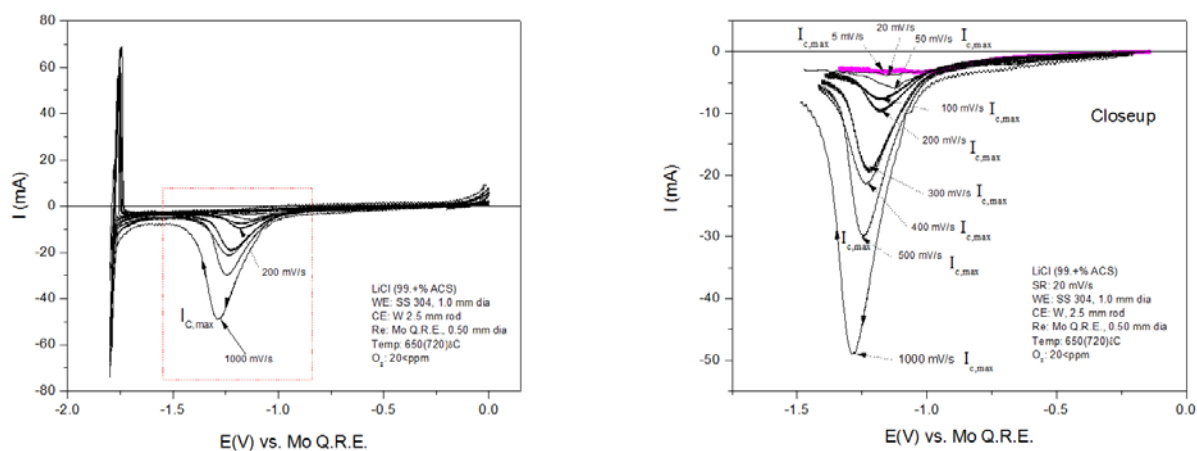
Figure 72. Cyclic voltammetry of SS 304 in a heat-treated LiCl ACS-grade electrolyte, showing effect of scan rate (right). Current response of the first cathodic peak between the potential range of -1.1 and 1.3 V are clearly a function of scan rate. Branches taken from CVs on the right to determine Randles-Ševčík linearity for $I_{c,max}$ values (left).
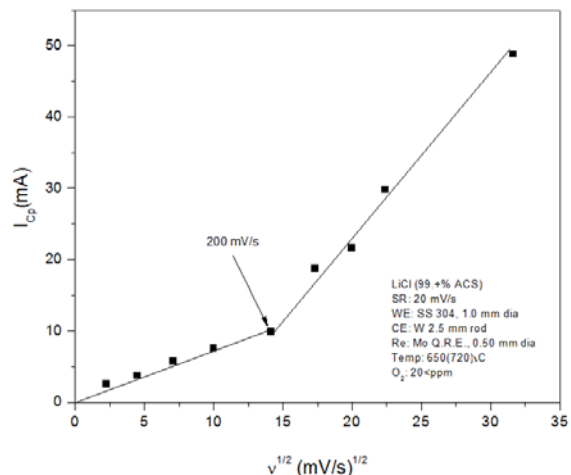
Figure 73. Randles-Ševčík plot for reversibility for CV cathodic-peak current values, $I_{c,max}$, with respect to the square root of the scan rate.

Table 19. OCP and cathodic-peak current ($I_{C,p}$) for CVs run between 5 and 1000 mV/s.

	Scan Rate	OCP (V)	$I_{C,p}$ (mA)
(a)	5 mV/s	-0.143	2.54
(b)	20 mV/s	-0.161	3.77
(c)	50 mV/s	-0.200	5.76
(d)	100 mV/s	-0.195	7.61
(e)	200 mV/s	-0.209	9.816
(f)	300 mV/s	-0.204	18.76
(g)	400 mV/s	-0.203	21.65
(h)	500 mV/s	-0.192	29.81
(i)	1000 mV/s	-0.202	48.76

Appendix E: Corrosion Studies

Appendix E-1: Tafel Extropolation Method

Although using both the anodic and cathodic Tafel regions for determining the corrosion rate, i_{corr}, is preferred, it can be determined by Tafel extropolation of either the cathodic or anodic polarization curves. Anodic polarization may sometimes produce concentration effects, as well as roughening of the surface, which can lead to deviations from Tafel behavior. Thus, extropolation of the cathodic Tafel region back to "zero overvoltage" gives the net rate of the cathodic reaction at the corrosion potential, E_{corr}. This is also the net rate of the anodic reaction at the corrosion potential.

In order to calculate the corrosion rate, β_a, the anodic Tafel constant must be determined. In order to determine β_a, clarification of the following terms are necessary:

i_{app} = the sum of the experimentally observed anodic current and the extropolated cathodic current density

$i_a = 10^{\log(i_a)}$; anodic current density data calculated $(|i_c| - i_{app})$

$\log(i_c)$ = log of the cathodic-current density calculated (Note: this is determined by selecting the linear portion of the cathodic Tafel branch, then running a linear fit and solving in terms of $\log(i_c)$, see definition for $y = mx + b$ below).

$i_c = 10^{\log(i_c)}$; cathodic current density

$i_{app} = 10^{\log(i_{app})}$; log of original cathodic-current data

The cathodic and anodic Tafel region linear fit generated from the selected Tafel portion of the cathodic branch will be of the following forms (i.e., $y = mx + b$):

$$E(V) = (\beta_c) \log(i_c) + b_c \tag{61}$$

$$E(V) = (\beta_a) \log(i_a) + b_a \tag{62}$$

Where $y=mx+b$ format, the following values are related: $y=$ E(V); $m=\beta_c$ or β_a (mV/decade) are the cathodic or anodic Tafel constants (or slope); $x = \log(i_c)$ or $\log(i_a)$ and b_c or b_a are the y intercepts in the respective equations. They are constants.

Step 1: Import original Tafel data into Excel and make a new set of data for the anodic and cathodic branches (for practice assignments this data will be provided)

Step 2: Select linear portion of the cathodic Tafel branch data and past into a new set of columns. This can be done by plotting the cathodic Tafel branch, then going to the data and selecting only the points that are withing the linear Tafel region. Paste these data into a newly labeled column. This section of data can be located from the original cathodic data by clicking on the points of interest in the graph. The coordinates for the points that are clicked will be displayed in a small flag. Also by a rule of thumb the data must be 50-100 mV from E_{corr}.

Step 3: Run a linear fit of this selected data in Excel.

Step 4: Take the linear equation and solve in terms of x (Note: $x= \log[i_c]$)

Step 5: Take the antilog of these values to get $|i_c|$

Step 6: To get i_{app}, take the antilog of the original cathodic branch current density values

Step 7: Calculate i_a by subtractig i_{app} from i_c

$$i_a = |i_c| - i_{app} \tag{63}$$

Step 8: Take the log of i_a

Step 9: Plot E vs. $\log(i_a)$; use the same potential values from the original cathodic branch Tafel data. Linear fit these data by plotting a trendline and displaying the equation on the graph.

Step10: Set E=(β_c) $\log(i_c)$+ b_c and E=(β_a) $\log(i_a)$+ b_a equal to each other to solve for i_{corr}. At E=E_{corr} , i_a and $i_c = i_{corr}$. Therefore, by substituting i_{corr} for the current density values, i_{corr} can be determined. Where β and b are constant values in the following equations.

$$E=(\beta_c) \log(i_c)+ b_c \rightarrow E_{corr} =(\beta_c) \log(i_{corr}) + b_c \qquad (64)$$

$$E=(\beta a) \log(i_a)+ ba \rightarrow Ecorr =(\beta a) \log(i_{corr}) + ba \qquad (65)$$

Step 10: Plot I_{corr} and E_{corr} on the graph (Figure 74).
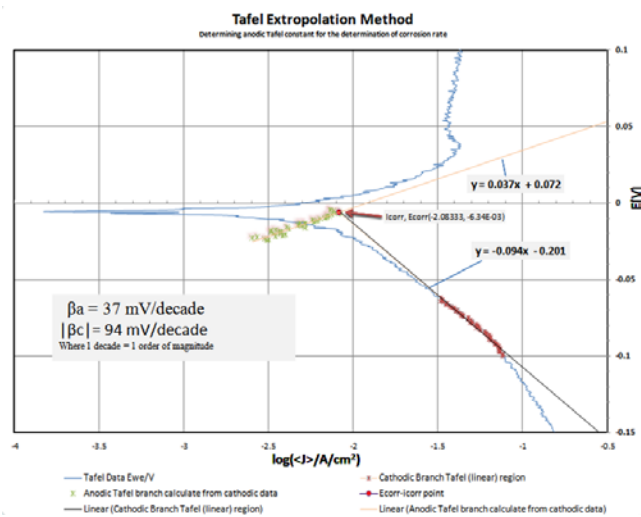
Figure 74. Tafel extrapolation in EC-Lab.

Appendix E-3: Corrosion Behavior of Platinum
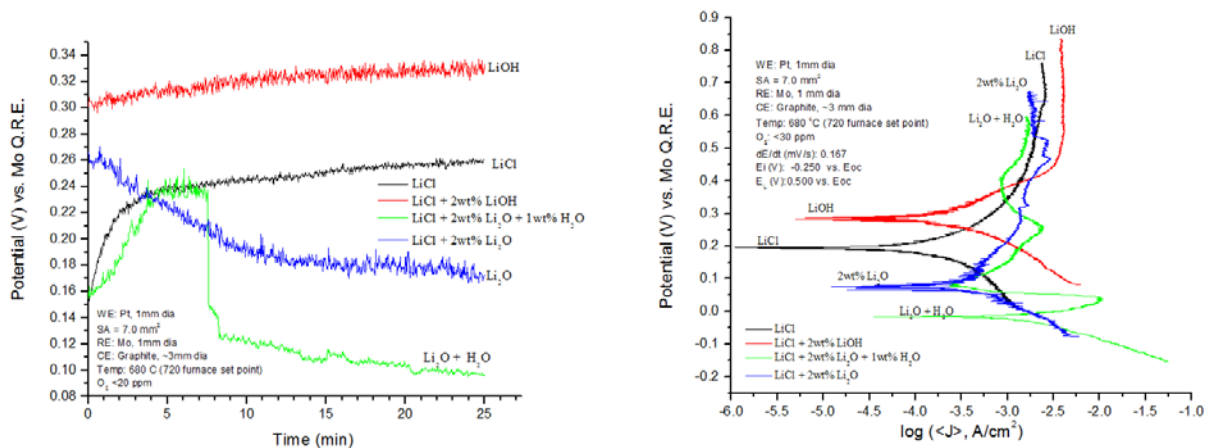
Figure 77. CP vs. time of Pt in LiCl molten salts for equilibration prior to Tafel w/ extended anodic polarization (left). Tafel polarization of Pt in LiCl molten salts (right).

Table 20. Tafel results for Pt in LiCl molten salt.

Salt Composition	E_{corr} (mV)	I_{corr} ($\mu A/cm^2$)	β_c (mV)	β_α (mV)	R_p (Ω)	CR, mpy (mmpy)
LiCl	203.648	227.565	251.1	207.3	3095.87	94(2.388)
LiCl + 2wt% Li_2O + 1wt% Li_2O	-15.848	1 764.938	91.0	51.7	115.895	795(20.2)
LiOH	292.349	186.386	111.6	122.5	1943.89	45.91(1.166)
LiCl + 2wt% Li_2O	78.355	310.754	109.5	275.5	1564.39	91(2.312)

Appendix E-4: Corrosion Behavior of Iron

Iron was completely dissolved in the LiCl system. It was dissolve to the point that contact was lost with the molten salt.
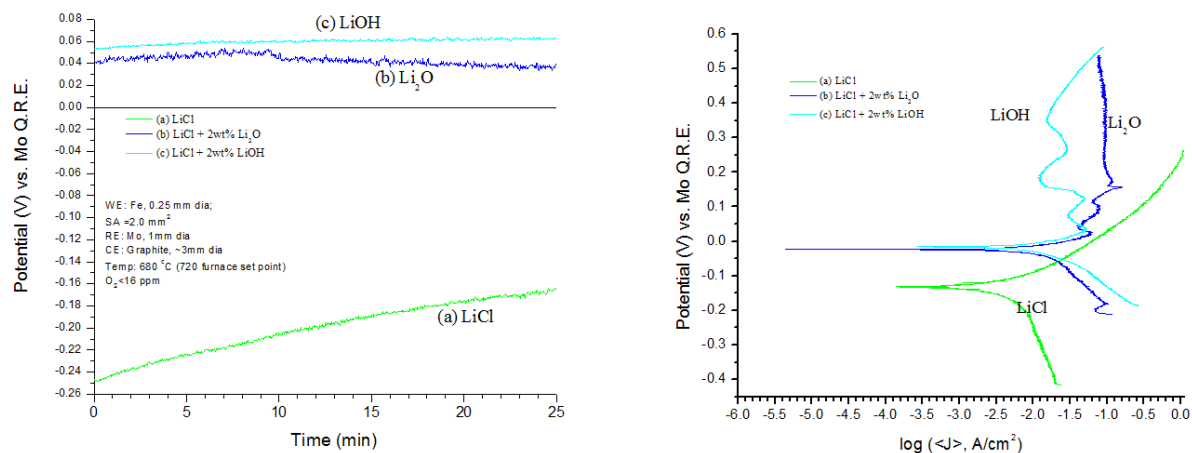
Figure 78. OCP vs. time of Fe in LiCl molten salts for equilibration prior to Tafel w/ extended anodic polarization (left). Tafel polarization of Fe in LiCl molten salts (right).

Table 21. Tafel results for Fe in LiCl molten salt.

Salt composition equivalent weight = 27.925 g/equivalent density = 7.86 g/cm^3 surface area = 0.020 cm²	E_{corr}(mV)	$I_{corr}(\mu A/cm^2)$	β_c (mV/dec)	β_α (mV/dec)	R_p (Ω)	CR, mpy (mmpy)
LiCl	-136.501	5,998	506	135.3	386.487	2744 .47 (69.73)
LiCl+2wt%Li$_2$O	-23.6	14,046	192	0.052	63.24	6427.40 (163.28)
LiCl+2wt%LiOH	-0.0159	19,651	0.160	0.082	59.91	8992.31 (228.44)
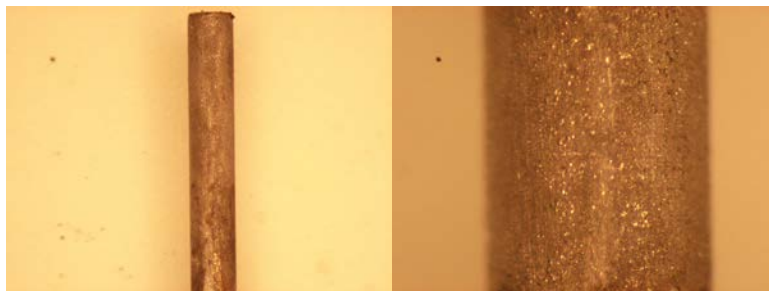
Figure 79. Optical images of pre- (left) and post- (middle and right) Tafel polarization of Fe electrode in LiCl-2wt% LiOH.

Appendix E-5: Iron – Tafel Calculations in LiCl Molten Salts
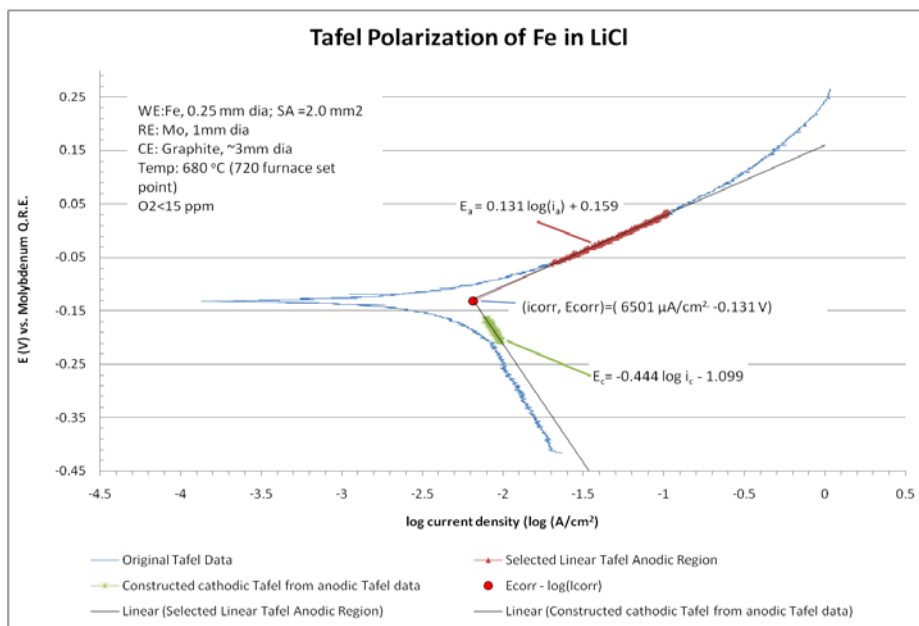
Figure 80. Tafel polarization of iron with extended anodic polarization n LiCl molten salt.
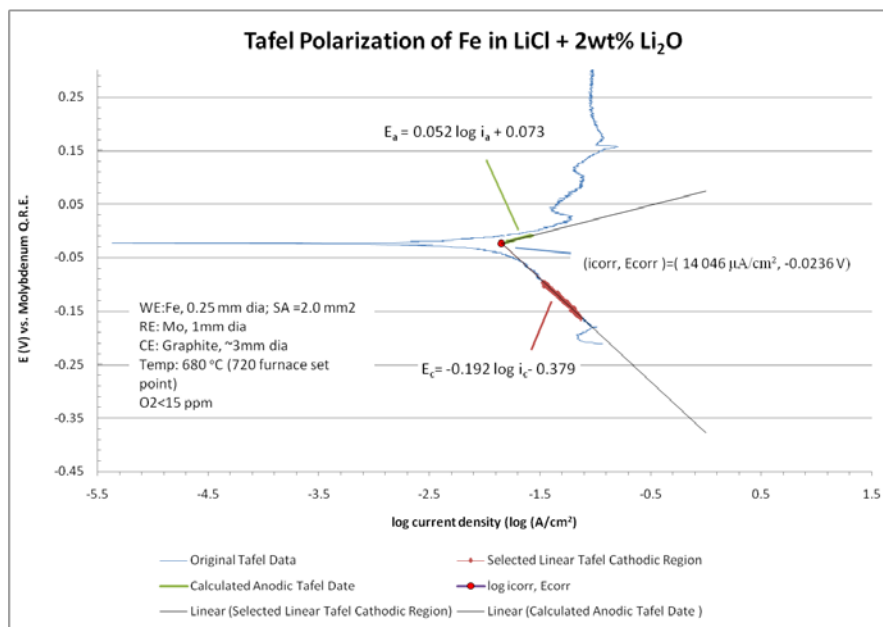
Figure 81. Tafel polarization of iron with extended anodic polarization n LiCl-Li$_2$O molten salt.
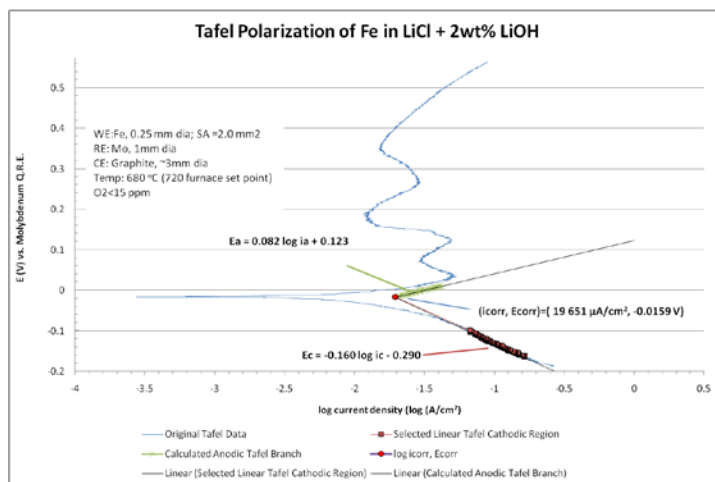
Figure 82. Tafel polarization of iron with extended anodic polarization n LiCl-LiOH molten salt.

Appendix E-6: Corrosion Behavior of Nickel

E_{corr} changes but i_{corr} remains relatively constant for Ni in all salt systems. The change in E_{corr} values is also in good agreement with°CP and Tafel data. The passivation region of the anodic portion of the Tafel polarization curves (c) and (d) in Figure 83.
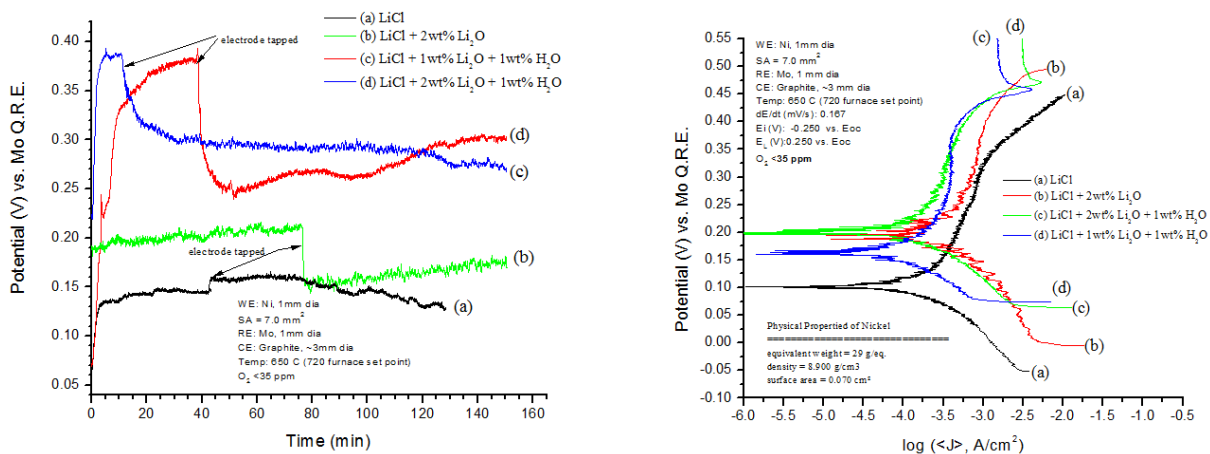
Figure 83. OCP vs. time of nickel in LiCl molten salts for equilibration prior to Tafel w/ extended anodic polarization (left). Tafel polarization of nickel in LiCl molten salts (right).
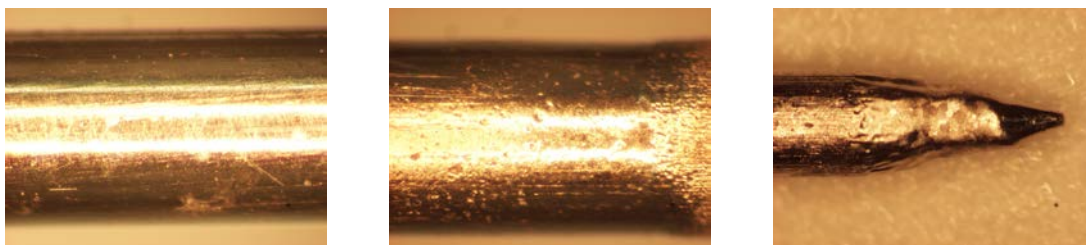
Figure 84. Optical images of pre- (left) and post-Tafel polarization (middle and right) of Ni electrode in LiCl.

Figure 85. Optical images of pre- (left) and post- Tafel polarization (middle and right) of Ni electrode in LiCl-2wt% LiOH.

Table 22. Tafel results for corrosion rated determination of Ni in LiCl molten salts.

Salt Composition	E_{corr}(mV)	$I_{corr}(\mu A/cm^2)$	β_c (mV)	β_α (mV)	R_p (Ω)	CR, mpy (mmpy)
LiCl	78.026	134.398	121.0	189.1	10,338	107 (2.62)
LiCl+2wt%Li_2O	198.023	361.52	153.3	362.0	2,056	140 (3.55)
LiCl+2wt%Li_2O+1wt%H_2O	196.926	11.76	101.7	391.8	1,724	71 (1.79)
LiCl+1wt%Li_2O+1wt%H_2O	167.227	94.886	97.3	132.2	638	40 (1.02)

Appendix E-7: Electrode Materials Corrosion Behavior Comparison

The Tafel behavior of different electrode materials was studied in LiCl molten-salt systems. The graphs in Figure 86 compare all the electrode materials in each of the salt systems. From the electrode materials studied, platinum performed the best and had the lowest average corrosion rates in all the systems studied. One of the most interesting observations is that nickel corrodes very fast in the LiCl system, but passivates fairly well in the other systems.
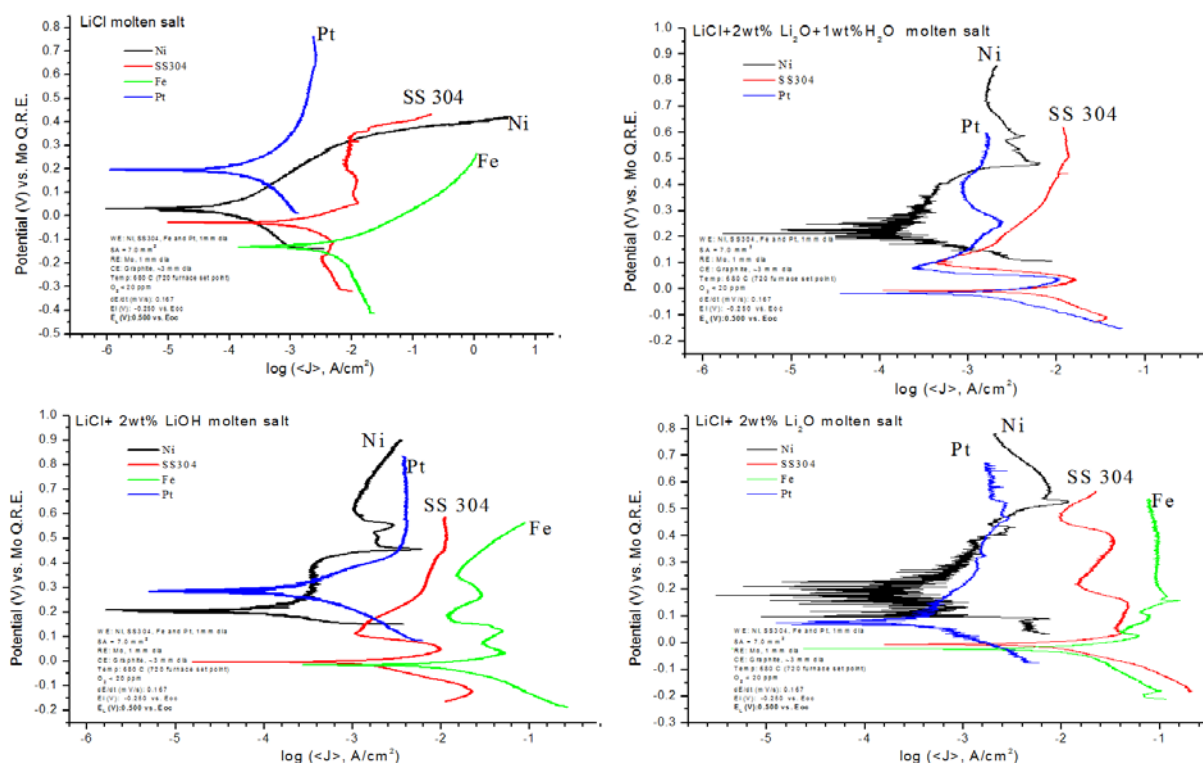
Figure 86. Tafel polarization of WE electrode materials in LiCl molten salts.

References

1.   Goff, K. M. and M. F. Simpson (2009). *Dry Processing of Used Nuclear Fuel*.

2.   Simpson, M. F. (2010). "Nuclear Fuel Reprocessing." *DOE Contract DE-AC07-05ID14517* INL/EXT-10-17753: 31.

3.   Herrmann, S. D. and SX Li (2010). "Separation and Recovery of Uranium Metal from Spent Light Water Reactor Fuel via Electrolytic Reduction and Electrorefining" *Nuclear Technology* 171(3): 247-265.

4.   Herrmann, S. D., et al. (2002). ANS Fifth Topical Meeting. Charleston, S. C.

5.   Jeong, S. M., B. H. Park, et al. (2010). "An Experimental Study on an Electrochemical Reduction of an Oxide Mixture in the Advanced Spent-Fuel Conditioning." *Nuclear Engineering and Technology* 42(2): 183-192.

6.   Hur, J.-M., S. M. Jeong, et al. (2010). "Underpotential deposition of Li in a molten LiCl-Li2O electrolyte for the electrochemical reduction of U from uranium oxides." *Electrochemistry Communications* 12(5): 706-709.

7.   Poignet, J. C. and J. Fouletier (2008). Physico-Chemical Properties of Molten Salts. *Materials Issues for Generation IV Systems*: 523-536.

8.   Orbakh, D. *Nonaqueous Electrochemistry*. New York: Marcel Dekker, 1999.

9.   Kissinger, P. T. and W. R. Heineman (1996). 17 Electroanalytical chemistry in molten salts. *Laboratory Techniques in Electroanalytical Chemistry*. New York, Marcel Dekker, Inc.

10.   Masset, P. and R. A. Guidotti (2007). "Thermal activated (thermal) battery technology: Part II. Molten salt electrolytes." *Journal of Power Sources* 164(1): 397-414.

11.   Voigt, W. and D. Zeng (2002). "Solid-liquid equilibria in mixtures of molten salt hydrates for the design of heat storage materials." *Pure and Applied Chemistry* 74(10): 1909-1920.

12.   Burkhard, W. J. and J. D. Corbett (1957). "The Solubility of Water in Molten Mixtures of LiCl and KCl." Journal of the American Chemical Society 79(24): 6361-6363.

13.   Tetenbaum, M. F., A. K.; Johnson, C. E. (1985). "An Investigation of the Solubility of Lithium Hydroxide in Solid Lithium Oxide." *Fusion Technology* 7(1): 53-56.

14. Karell, E. J., K. V. Gourishankar, et al. (2001). "Separation of Actinides from LWR Spent Fuel using Molten-Salt-Based Electrochemical Processes." *Nuclear Technology* 136(3): 342-353.

15. Steve D. Herrmann, S. X. L., Michael F. Simpson, Dale R. Wahlquist (2002). "Electrolytic Reduction of Spent Oxide Fuel - Bench-Scale Test Preparations." Idaho Falls: 1-7.

16. Nakajima, T., R. Minami, et al. (1974). "Miscibility of Lithium with Lithium-Chloride and Lithium Chloride Potassium Chloride Eutectic Mixture." *Bulletin of the Chemical Society of Japan* 47(8): 2071-2072.

17. Nakanishi, K. (1970). "Thermodynamic Studies of Phase Equilibria in Molten Salt Systems. Prediction of Liquidus and Eutectic Behavior in Mixtures Having a Common Ion." Industrial & Engineering Chemistry Fundamentals 9(3): 449-453.

18. Li, S. X. and S. D. Herrmann (2002). "Experimental Observations of a Thoria Oxide-Ion Sensor in a Molten Salt System." *Journal of The Electrochemical Society* 149(2): H39-H43.

19. Shin, Y., I. Kim, et al. (2000). "Lithium Recovery from Radioactive Molten Salt Wastes by Electrolysis." *Journal of Radioanalytical and Nuclear Chemistry* 243(3): 639-6433.

20. Usami, T., M. Kurata, et al. (2002). "Pyrochemical Reduction of Uranium Dioxide and Plutonium Dioxide by Lithium Metal." *Journal of Nuclear Materials* 300(1): 15-26.

21. Park, B. H. and J. M. Hur (2010). "Behavior of Diffusing Elements from an Integrated Cathode of an Electrochemical Reduction Process." *Korean Journal of Chemical Engineering* 27(4): 1278-1283.

22. Sakamura, Y. (2010). "Solubility of Li2O in Molten LiCl-MClx (M = Na, K, Cs, Ca, Sr, or Ba) Binary Systems." *Journal of The Electrochemical Society* 157(9): E135-E139.

23. Li, S. X., S. D. Herrmann, et al. (2003). "Electrochemical Reduction Of Uranium Oxide Fuel in a Molten $LiCl/Li_2O$ System Electrochemistry," in Mineral and Metal Processing VI: Proceedings of the International Symposium, Paris, France, Pennington, N.J.: Electrochemical Society.

24. OECD (2006). *Physics and Safety of Transmutation Systems: A Status Report*. Issy-les-Moulineaux, France, Nuclear Energy Agency, Organization for Economic Cooperation and Development.

25. Levy, S. (2010). "Need for USA high level waste (HLW) alternate geological repository (AGR) and for a different methodology to enhance its acceptance." *Nuclear Engineering and Design* 240(10): 3665-3668.

26. GAO (2009). "Nuclear Waste Management Key Attributes, Challenges, and Costs for the Yucca Mountain Repository and Two Potential Alternatives: Report to Congressional Requesters." U. S. G.A.O. (Washington, D.C.), U.S. Govt. Accountability Office.

27. Tahraoui, A. and J. H. Morris (1995). "Decomposition of Solvent-Extraction Media During Nuclear Reprocessing—Literature-Review." *Separation Science and Technology* 30(13): 2603-2630.

28. URL: http://www.world-nuclear.org/info/Nuclear-Fuel-Cycle/Uranium-Resources/Supply-of-Uranium/

29. Ullmann F., W. Gerhartz, et al. (1985). "Lithium and Lithium Compounds" in Ullmann's encyclopedia of industrial chemistry. Weinheim, Federal Republic of Germany; Deerfield Beach, FL, USA, VCH. Vol. A15. P393.

30. Kroschwitz, J. I. and A. Seidel (2004). *Kirk-Othmer Encyclopedia of Chemical Technology*. Hoboken, N.J., Wiley-Interscience.

31. Averill, W. A. and D. L. Olson (1978). "A Review of Extractive Processes for Lithium from Ores and Brines." *Energy* 3(3): 305-313.

32. Sadoway, D. (1998). "Toward New Technologies for the Production of Lithium." *JOM Journal of the Minerals, Metals and Materials Society* Retrieved 5, 50, from http://dx.doi.org/10.1007/s11837-998-0027-x.

33. Jaskula, B. W. (2008). Lithium from 2008 Minerals Yearbook, U.S. Department of Interior and U.S. Geological Survey.

34. Koerner, B. I. (2008 3/29/2010). "The Saudi Arabia of Lithium." *Forbes Magazine* from http://www.forbes.com/forbes/2008/1124/034.html.

35. Talison Lithium (2010). "Talison Lithium is a leading global producer of lithium." Retrieved 3/26/2010, 2010, from http://www.talisonlithium.com/home.aspx.

36. (3/25/2010). "Lithium Production Process." From http://www.sqm.com/aspx/about/ProductionProcess.aspx.

37. Wilkomirsky, I. L. C., CL) (1999). "Production of Lithium Carbonate from Brines." United States, Sociedad Minera Salar de Atacama S.A. (Santiago, CL).

38. Wilkomirsky, I. C., CL) (1999). "Process for Removing Boron from Brines." United States, Sociedad Minera Salar de Atacama S.A. (Santiago, CL).

39. Habashi, F. (1999). *A Textbook of Hydrometallurgy*. Quebec City, Canada, Métallurgie Extractive Québec.

40. Brown, P. M. E., PA), Boryta, Daniel A. (Downingtown, PA) (1993). "Production of Low Boron Lithium Carbonate from Lithium-Containing Brine." United States, Cyprus Foote Mineral Company (Malvern, PA).

41. Ellestad, R. B., Milne, Leute Karl (1950). "Method of Extracting Lithium Values from Spodumene Ores." United States, METALLOY CORP.

42. Basin, A., A. Kaplun, et al. (2008). "The LiCl-KCl Binary System." *Russian Journal of Inorganic Chemistry* 53(9): 1509-1511.

43. "Lithium and Sodium - Extraction ", 2010, from http://www.tutorvista.com/content/chemistry/chemistry-iii/s-block-elements/lithium-and-sodium.php.

44. Alchagirov, B., L. Afaunova, et al. (2009). "The Density and Surface Tension of Liquid Lithium at Melting Temperature." *High Temperature* 47(2): 287-291.

45. Osborg, H. (1935). *Lithium; Theoretical Studies and Practical Applications*. New York, Electrochemical Society.

46. Willit, J. L. B., IL, US), Ackerman, John P. (Prescott, AZ, US), Williamson, Mark A. (Naperville, IL, US) (2009). "Uranium Dioxide Electrolysis." United States, The United States of America as represented by the United States Department of Energy (Washington, DC, US).

47. Lide, D. R. (1999). "Density of molten salt elements and representative salts." *Crc Handbook of Chemistry and Physics: A Ready-Reference Book of Chemical and Physical Data*. Boca Raton, CRC Press.

48. Janz, G. J. (1967). *Molten Salts Handbook*. New York; London, Academic Press.

49. Apelblat, A. (1992). "The Vapor Pressures of Water Over Saturated Aqueous Solutions of Barium Chloride, Magnesium Nitrate, Calcium Nitrate, Potassium Carbonate, and Zinc Sulfate, at Temperatures from 283 K to 313 K." *The Journal of Chemical Thermodynamics* 24(6): 619-626.

50. Apelblat, A. and E. Korin (1998). "The Vapor Pressures of Saturated Aqueous Solutions of Sodium Chloride, Sodium Bromide, Sodium Nitrate, Sodium Nitrite, Potassium Iodate, and Rubidium Chloride at Temperatures from 227 K to 323 K." *The Journal of Chemical Thermodynamics* 30(1): 59-71.

51. Andreas, H., N. Jürgen, et al. (2003). "Crystal Structure of the Monohydrates of Lithium Chloride and Lithium Bromide." *Journal of Inorganic and General Chemistry* 629(2): 312-316.

52. Monnin, C., M. Dubois, et al. (2002). "Thermodynamics of the LiCl + H2O System." *Journal of Chemical & Engineering Data* 47(6): 1331-1336.

53. McGreevy et al. (1990). "The Structure of Molten Salts." *Proceedings of the Royal Society of London* 430(1878): 241.

54. Piet, S. J., D. W. Jeppson, et al. (1987). "Liquid Metal Chemical Reaction Safety in Fusion Facilities." *Fusion Engineering and Design* 5(3): 273-298.

55. Hubberstey, P. and T. Sample (1997). "Thermodynamics of the Interactions Between Liquid Breeders and Ceramic Coating Materials." *Journal of Nuclear Materials* 248: 140-146.

56. Machado-Vieira, R., H. K. Manji, et al. (2009). "The Role of Lithium in the Treatment of Bipolar Disorder: Convergent Evidence for Neurotropic Effects as a Unifying Hypothesis." *Bipolar Disorders* 11: 92-109.

57. Bourgeois, M. L. (2001). "Lithium and the Treatment of Mania." *European Neuropsychopharmacology: The Journal of the European College of Neuropsychopharmacology*. 11: S131-S132.

58. Chang, L., L. Feng, et al. "Advanced Materials for Energy Storage." *Advanced Materials* 22(8): E28-E62.

59. Lyublinski, I. E., A. V. Vertkov, et al. (2009). "Application of Lithium in Systems of Fusion Reactors. 1. Physical and Chemical Properties of Lithium." *Plasma Devices & Operations* 17(1): 42-72.

60. Übeyli, M. (2009). "Effect of Lithium Enrichment on the Tritium Breeding Characteristics of Various Breeders in a Fusion Driven Hybrid Reactor." *Journal of Fusion Energy* 28(3): 300-303.

61. Luo, W., X. Li, et al. "Synthesis, Characterization, and Thermal Stability of LiCo[sub 1 - z][MnMg][sub z/2]O[sub 2]." *Journal of The Electrochemical Society* 157(9): A993-A1001.

62. Tarascon, J. M. and M. Armand (2001). "Issues and Challenges Facing Rechargeable Lithium Batteries." *Nature* 414(6861): 359-367.

63. Karditsas, P. J.; Edwards, J. E. G., Blanket and First Wall Conceptual Design Issues of the Spherical Tokamak Power Plant. *Fusion Eng. Des.* 2000, *48* (3-4), 379-387.

64. Gupta, C. K. (2003). "Electrometallurgy." *Chemical Metallurgy: Principles and Practice*. Weinheim, Germany. Wiley-VCH: 650.

65. Laidler, J. J. (1993). "Pyrochemical Recovery of Actinides." *Proceedings of the American Power Conference* 55: 1074.

66.   Wahlquist, D. L.; Bateman, K. J.; Westphal, B. R.; Asme, "Second Generation Experimental Equipment Design to Support Voloxidation Testing at INL." *Amer Soc Mechanical Engineers*: New York, 2008; p 91-97.

67.   Morss, L. R.; Edelstein, N. M.; Fuger, J., "The Chemistry of the Actinide and Transactinide Elements." (Set Vol.1-6): Volume 2; 836. Springer: 2010.

68.   Inoue, T. and L. Koch (2008). "Development of Pyroprocessing and its Future Direction." *Nuclear Engineering and Technology* 40(3): 183-190.

69.   Nagarajan, K. "Pyrochemical Reprocessing of Fast Reactor Fuels." 2010, from http://www.igcar.ernet.in/lis/nl46/igc-29-1(4p).htm.

70.   Till, C. E.; Chang, Y. I., "Plentiful Energy: The Story of the Integral Fast Reactor, the Complex History of a Simple Reactor Technology, with Emphasis on Its Scientific Basis for Non-specialists." Charles E. Till and Yoon Il Chang: 2011.

71.   Vavilov, S.; Kobayashi, T.; Myochin, M., "Principle and Test Experience of the RIAR's Oxide Pyro-Process." *J. Nucl. Sci. Technol.* 2004, *41* (10), 1018-1025.

72.   Kofuji, H.; Sato, F.; Myochin, M.; Nakanishi, S.; Kormilitsyn, M. V.; Ishunin, V. S.; Bychkov, A. V., MOX Co-Deposition Tests at RIAR for SF Reprocessing Optimization." *J. Nucl. Sci. Technol.* 2007, *44* (3), 349-353.

73.   Kofuji, H.; Okamura, N.; Mizuguchi, K.; Myochin, M., "Effect of Pulse Electrolysis on Morphology of Co-Deposited MOX Granules." *J. Nucl. Sci. Technol.* 2008, *45* (9), 942-950.

74.   Subramanian, T., "Pyrochemical Processes: Application in Nuclear Technology."

75.   Madic, C., "Processing of the Nuclear Spent Fuels." *Actual Chim.* 1999, (5), 16-22.

76.   Sadoway, D. R. (1995). "New Opportunities for Metals Extraction and Waste Treatment by Electrochemical Processing in Molten Salts." *Journal of Materials Research –Pittsburgh*. 10(3): 487.

77.   Alvarez, R.; Beyea, J.; Janberg, K.; Kang, J.; Lyman, E.; Macfarlane, A.; Thompson, G.; von Hippel, F. N., "Reducing the Hazards from Stored Spent Power-Reactor Fuel in the United States." *Science & Global Security* 2003, *11* (1), 1-51.

78.   Johnson, Irving. "The Thermodynamics of Pyrochemical Processes for Liquid Metal Reactor Fuel Cycles." *Journal of Nuclear Materials* 154. (1988): 169.

79.   Steve D. Herrmann, S. X. L., Michael F. Simpson, Dale R. Wahlquist (2002). "Electrolytic Reduction of Spent Oxide Fuel - Bench-Scale Test Preparations." Idaho Falls: 1-7.

80.   Kado, Y., T. Goto, et al. (2008). "Dissolution Behavior of Lithium Oxide in Molten LiCl-KCl Systems." *Journal of Chemical & Engineering Data* 53(12): 2816-2819.

81.   Park, B. H., I. W. Lee, et al. (2008). "Electrolytic Reduction Behavior of U3O8 in a Molten LiCl-Li2O Salt." *Chemical Engineering Science* 63(13): 3485-3492.

82.   Laitinen, H. A. (1967). *Polarography in Molten Salts. Pure and Applied Chemistry* 15 (2): 228-238.

83.   Cannon, J. C. and Y. Zhang (1995). "Catalytic and Inhibiting Effects of Lithium Peroxide and Hydroxide on Sodium Chlorate Decomposition." *Industrial & Engineering Chemistry Research* 34(9): 3146-3148.

84.   Noda, S., M. Nishioka, et al. (1999). "Gas-Phase Hydroxyl Radical Emission in the Thermal Decomposition of Lithium Hydroxide." *The Journal of Physical Chemistry B* 103(11): 1954-1959.

85.   Masset, P., Thermogravimetric Study of the Dehydration Reaction of LiCl·H2O." *Journal of Thermal Analysis and Calorimetry* 2009, 96 (2), 439-441.

86.   Compton, R. G.; Banks, C. E., "Understanding Voltammetry." *Imperial College Press*: 2011.

87.   Thomas, F.; Henze, G., *Introduction to Voltammetric Analysis: Theory and Practice*. CSIRO PUBLISHING: 2001.

88.   Zanello, P.; Chemistry, R. S. o., *Inorganic Electrochemistry: Theory, Practice and Applications*. Royal Society of Chemistry: 2003.

89.   Bard, A. J.; Inzelt, G.; Scholz, F., *Electrochemical Dictionary*. Springer Berlin Heidelberg: 2012.

90.   Zhuxian, Q.; Liman, F.; Grjotheim, K.; Kvande, H., "Formation of Metal Fog During Molten Salt Electrolysis Observed in a See-Through Cell." *Journal of Applied Electrochemistry* 1987, 17 (4), 707-714.

91.   Haarberg, G. M., *Formation of Metal Fog and Dissolved Metals During Electrodeposition from Molten Salts*. Electrochemical Society Inc.: Pennington, 2002; Vol. 2002, p 789-796.

92.   Herrmann, S. D., S. X. Li, et al. (2007). "Electrolytic Reduction of Spent Nuclear Oxide Fuel-Effects of Fuel Form and Cathode Containment Materials on Bench-Scale Operations."

93.   Nohira, T. and Y. Ito (2002). *Journal of the Electrochemical Society* 149(5): E159-E165.

94. Jain, R. K., H. C. Gaur, et al. (1977). "Chronopotentiometry: A Review of Theoretical Principles." *Journal of Electroanalytical Chemistry* 79(2): 211-236.

95. Gibilaro, M., L. Massot, et al. (2009). "Electrochemical Preparation of Aluminum-Nickel Alloys by Under-Potential Deposition in Molten Fluorides." *Journal of Alloys and Compounds* 471(1-2): 412-420.

96. Nohira, T. and Y. Ito (2002). "Electrochemical Behavior of Hydride Ion in a LiCl-KCl Eutectic Melt." *Journal of the Electrochemical Society* 149(5): E159-E165.

97. Nicholson, R. S. and I. Shain. (1964). "Theory of Stationary Electrode Polarography. Single Scan and Cyclic Methods Applied to Reversible, Irreversible, and Kinetic Systems." *Analytical Chemistry* 36(4): 706-723.

98. Southampton Electrochemistry Group. (1985). "Instrumental Methods in Electrochemistry."

99. Nohira, T. and Y. Ito (2002). "Electrochemical Behavior of Hydride Ion in a LiCl-KCl Eutectic Melt." *Journal of the Electrochemical Society* 149(5): E159-E165.

100. A. Roine. *Outokumpu HSC Chemistry for Windows* Outokumpu Research Oy, Pori, Finland (2006).

101. White, S. H. and U. M. Twardoch (1987). "The Electrochemistry of Water at Noble Metals in an Ionic Solvent." *Electrochimica Acta* 32(1): 191-194.

102. T. Nohira and Y. Ito. "Electrochemical Behavior of Hydride Ion in a LiCl-KCl Eutectic Melt." *J. Electrochem. Soc*. 14. (2002). E 159. DOI:10.1149/1.1467943.

103. Ito, H. and Y. Hasegawa (2000). "Electrode Behavior of Hydrogen Reduction in LiCl-KCl Melt. Voltammetric Analysis." *Journal of The Electrochemical Society* 147(1): 289-295.

104. Iizuka, M., T. Inoue, et al. (2007). "Electrochemical Reduction of (U,PU)O-2 in Molten LiCl and CaCl2 Electrolytes." *Journal of Nuclear Science and Technology* 44(5): 801-813.

105. Jeong, S. M., H. S. Shin, et al. (2009). "Electrochemical Behavior of a Platinum Anode for Reduction of Uranium Oxide in a LiCl Molten Salt." *Electrochimica Acta* 54(26): 6335-6340.

106. Sakamura, Y., M. Kurata, et al. (2004). *Conversion of Oxide into Metal or Chloride for the Pyrometallurgical Partitioning Process*. Actinide and Fission Product Partitioning & Transmutation, Eighth Information Exchange Meeting, Session II: Partitioning Technology Las Vegas, Nevada, USA, Nuclear Energy Agency.

107. Takeda, O.; Li, M.; Hoshi, M.; Sato, Y., Electrowinning of Lithium from Molten Salt Containing LiOH for Hydrogen Storage and Transportation. ECS Transactions 2010, 33(7), 455-462.